Design and Application of a Water Powered Irrigation Robot

by

Kurt Fairfield

B.Eng., University of Victoria, 2010

A Thesis Submitted in Partial Fulfillment of the Requirements for the Degree of
MASTER OF APPLIED SCIENCE

in the Department of Mechanical Engineering

We acknowledge with respect the Lekwungen peoples on whose traditional territory the university stands and the Songhees, Esquimalt and WSÁNEĆ peoples whose historical relationships with the land continue to this day.

Supervisory Committee

Design and Application of a Water Powered Irrigation Robot

by

Kurt Fairfield

B.Eng., University of Victoria, 2010

Dr. Caterina Valeo, (Department of Mechanical Engineering)

Co-Supervisor

Dr. Daniela Constantinescu, (Department of Mechanical Engineering)

Co-Supervisor

ABSTRACT

This paper reports the findings of conceptual design and application research for a novel use of irrigation fluid power to provide mobility to a legged autonomous, tethered irrigation robot. Systems already exist to convert fluid power to rotary motion to power various irrigation systems. The conceptual designs implement a McKibben actuator to generate linear motion with water as the process fluid and a compact 3DOF spherical joint to create a modular robot leg that can be used to create a legged ambulatory robot. A six-legged robot is proposed from the conceptual design of the modular leg.

Irrigation was selected as the initial leading application, however, once deployed the devices provide a field-ready platform to facilitate a whole suite of agriculturally important activities; seeding, weed suppression, pest management, soil sensing, crop growth assessment, as well as creating a robust research platform. This work is the lead in research to provide a viable mechanism to facilitate control system and dynamic modelling ahead of full-scale prototyping and field testing.

TABLE OF CONTENTS

LIST OF FIGURES

LIST OF TABLES

DEDICATION

To my partner Cindy for her endless patience, support and love throughout the entire process. Without her, this would not have been possible:)

To my parents Marina and Gord, for there relentless support and encouragement throughout my academic career. Their wisdom, guidance and love helped me through tough times during this process and beyond.

To my brother Sean, for putting that first bug in my ear.

To my supervisor Caterina, for guiding me with just the perfect balance of active concern and behind the scenes support.

1 INTRODUCTION

This work addresses, in part, the worsening situation created by our increasing capacity to extract and redistribute water resources. Unfortunately, it seems unlikely that demand for water resources [1] will fall, short of a global catastrophe. It is therefore important to understand and observe the implications of the satiation of this demand. We have an ethical responsibility to address, at a minimum, the efficiency of these use patterns. Engineers are the keepers of efficiency, and therefore the responsibly falls to us to act.

1.1 WATER RESOURCE MANAGEMENT

Water is the most important life supporting substance on the earth. Biswas references Leonardo Da Vinci's observation that water is the prime mover of nature in his chapter in 'Water Management in 2020 and Beyond' [2]. He also discusses how then, as now, humanity continues to recognize only part of this story. While much energy and effort are expended to harness this powerful driver, too little attention is paid to the care and maintenance of our most precious, yet finite, natural resource.

Chenoweth notes that water is critical to social and economic development [3] pushing 'utility' to the forefront of the discussion. This necessarily pushes other attributes, like 'responsibility', to the background. This is apparent when one observes the dwindling global freshwater resources [4] and the predicted outcomes if we maintain of the current global trajectory of ever increasing consumption rates.

This focus on utility is obvious when examining historical irrigation water consumption patterns. This is most evident since the industrial revolution provided the capacity to extract and distribute water with increasing mechanical efficiency.

Wada provides an instructive graphic in his study of the human and climactic impacts on global water resources [5]. This illustrates the dominance and increasing rate of water use by humans and highlights the importance that irrigation plays in overall consumption rates.

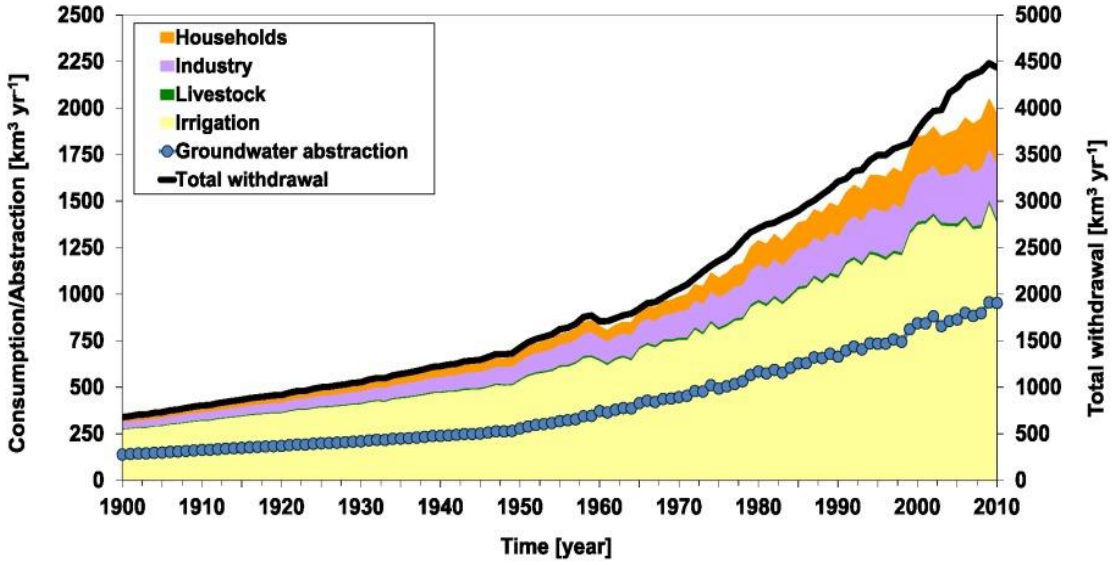

Figure 1 - Global water use by sector. Adapted from Wada et. Al [5]

Sub-optimal soil moisture levels constrain crop development. Without irrigation techniques, soil moisture levels are dictated by the magnitude and frequency of global, regional and local water cycle events. Irrigation allows us to shift the constraints on soil moisture away from naturally occurring events, which may or may not align with our cropping objectives. Instead soil moisture is constrained only by the availability of resources; fresh water, equipment and energy.

There is a connection between the availability of technology and the pattern of increasing consumption. Leng presents the correlation between irrigation technology employed and impacts on key factors such as overall irrigation efficiency, run off and ground water depletion [6].

Field flooding is a simple, passive, gravity-based distribution method and has been used successfully for millennia throughout the world [7]. While a simple and effective method of distribution, it typically does not provide optimal soil moisture levels for crop growth. Pumped water coupled with surface/subsurface piping and sprinklers increase the resolution of control over the spatial and temporal distributions, at the expense of increasing cost and complexity. Irrigation efficiency, a key metric, becomes increasingly important when faced with dwindling freshwater reserves. The table below summarizes the expected efficiencies from various methods of irrigation.

Table 1 - Irrigation Efficiency by Method. Adapted from Trimble [8]

Irrigation Method	Irrigation Efficiency Range
Gravity - Developed	60 – 85 %
Sprinkler - Fixed/Hand Move/Wheel Move	60 - 85 %
Sprinkler - Pivot/Lateral Move	75 - 90 %
Sprinkler - Linear - Low pressure	75 - 95 %
Sprinkler - Volume gun	55 - 75 %
Micro - Spray - Sprinkler	70 - 95 %
Micro - Drip - Trickle	70 - 95 %

It is important to note the range of efficiencies between technologies, but also within a specific subtype. This table illustrates that selecting an appropriate method and refinement of that method, can provide a route to actualizing increased irrigation efficiency. It is towards this goal that this research strives.

Additionally, while these technologies exists, simple gravity based surface irrigation is used on 85% of the land mass under irrigation globally [7]. This leaves significant room for improvement in global irrigation efficiency. However, it is not a lack of irrigation technology choices that limits the global irrigation efficiency. Rather it is an inability to implement existing technologies. One must also consider that these methods, while heavily employed in industrialized areas of the globe, may not meet the overall needs of the majority of global inhabitants. Cost is the key limiting factor, but perhaps a desire to sidestep the resultant environmental outcomes of industrialized farming also impacts individual choices.

Differences in regional socio-economic structure are created by the varying levels of global affluence. These variations have a significant impact on the ability of individuals to adopt advanced agricultural methods and technologies. Graeub et al investigate these structural variations and the impacts to the operation of family farms globally [9]. While they comment on the challenge of defining ‘family farming’ and its implications on developing effective policy, they note that while family farms comprise only 53% of arable land under cultivation, 98% of global operations are family farm units. This highlights the critical role of targeting technologies to the smaller farm operator.

It is easier for industrialized nations to leverage advanced technologies as they have the financial resources and regional systems in place assist operators in the homogenization and industrialization of their operations. However, one must inquire on the impact of enabling industrialized agriculture practices throughout the world. The obvious answer is that we are likely to experience the same social and environmental challenges the industrialized world struggles with, except now at a global scale:

1. Increased demand for supporting/enabling resources
2. Increased environmental degradation from extraction and use of these resources
3. Declines in biodiversity and bio-populations due to habitat destruction
4. Increased destructive climactic events and general disharmony with nature

How do we optimize freshwater irrigation practices globally, while sidestepping the challenges we observe of past and current industrial optimization efforts? Perhaps if we define success metrics and research objectives that directly address the outcomes listed above, while addressing the operational needs of the small-scale operations that dominate the globe we can alter our trajectory.

If one presupposes that resources will be consumed, optimization through synergistic design is one method of reducing the environmental stresses associated with this assumed consumption: simply by improving resource utilization. However, if we also adopt irrigation and cropping modalities that decrease the requirement on homogenization, and the use of petrochemicals this approach mandates, we can begin to address the biodiversity and agricultural pollution issues that proliferate today. Providing intelligent, autonomous agents at the plant scale enables these divergent modalities.

Lastly, if we change our current design paradigm of domination to one of collaboration, we can begin to address the increasingly apparent dis-harmony with our natural surroundings. Biomimicry is an accessible design technique that can be practically employed to harness existing best practices from nature, while at the same time creating a closer connection between the engineer and the environment. These concepts guide the overall design approach of this research.

1.2 RESEARCH OBJECTIVES AND PROCESS

The focus of this research is the investigation of irrigation mechanization that addresses operational requirements while remaining attendant to the social and environmental outcomes of increased mechanization. The primary research objective is to propose and vet the conceptual design of an autonomous device that increases both irrigation and operational efficiencies for small- and large-scale agricultural operations alike.

To support this abstract goal, qualitative design guidelines are proposed and used to support the identification of tangible design constraints. These overarching constraints shape design decisions to ensure they are supportive of the primary goal.

The ideation and conceptualization phases of the project uncovered many design specific technical challenges. The requirement to overcome these challenges framed clear secondary design objectives. These are introduced in subsequent chapters, as they arise. Each is addressed individually, with a range of options examined and vetted, with the leading solution implemented in the final design.

The project followed the development path described below:

1. Literature and general commercial product review
2. Definition and engagement of key personas
3. Review of existing irrigation technology implementation
4. Identification of key requirements and definition of a solution space framework
5. Conceptual design
6. Concept evaluation and refinement
7. Device embodiment
8. Investigate operational use cases

2 PRIOR ART AND FRAMING OF THE DESIGN PROBLEM

An extensive literature review was undertaken to gain an understanding of the demands of agricultural irrigation on water management policy and practice. Topics included hydrology, irrigation methods, agribusiness policy, environmental policy, insect morphology, actuator design and general robotics. This broad ranging review guided the overall research path and illuminated prior art that formed the basis for the overall device. Comprehensive presentation of this review is omitted for brevity with relevant sources referenced where applicable throughout the design presentation. This work focusses on the presentation of design challenges and solutions developed.

Intrinsic in the primary research objective was the creation of a 'viable' device. Viability includes the ability to easily integrate with existing systems, rather than requiring the end user to re-tool or redefine existing processes.

General commercial product review supplies an assessment of the current state of the art from which to advance and propose a workable design. This was fruitful in providing conceptual ideas to exploit and transform, but also provided the framework of existing systems that any device would be required to interact or couple with. This was of importance when assessing the needs of the large-scale application where this coupling proved critical in narrowing the design space to a tractable state.

2.1 PERSONAS DEFINITION

Two primary personas were selected to garner application and design requirements from. The first is the industrial-scale farmer who uses large scale semi-autonomous irrigation systems drawn from private or public water supply systems. The other persona is the small-scale farmer who has access to, at a minimum, a source of freshwater and the ability to pump and pipe this supply across most of the land under cultivation.

To aid in defining these personas, several engagements were made with small- and medium-scale operators. Large-scale operations were easier to asses via online literature and case studies, limited onsite investigation was completed in this domain. Rather, engagement with a large agronomy consultancy (Agritrend) was completed to gain their perspective of

industry practice across their client base. This provided a curated source of information to augment and validate assumptions made via tertiary external assessments.

The industrial farmer is a generalization. No specific geographic location is identified, nor any level of sophistication. For convenience, the local north American industrial model is used in this base line persona. A subset of this overall persona can be defined: those who uses lateral move or center pivot technologies. This reduction was made for two primary reasons; the ubiquity of use of these technologies and the capacity for these systems to provide supporting infrastructure to a mobile device.

The second motivation removed the need to provide the necessary, but complex, irrigation hose handling solutions necessary to support a viable independent device. Focus was kept on the device by defining a design boundary at the irrigation coupling point, and leaving autonomous hose handling as a future task.

As with the simplification for larger scale operations, a typical north American small-scale farmer is used as the basis for this persona and represents the ‘family farm operation’ identified in the introduction. Unlike, large-scale industrial farm operations, which tend to follow a common layout and operation process, dominated by the use of common sub-set of large-scale machinery, small-scale operators showed considerably more variability in equipment choices. As such the decision was made to visit several operators directly to observe and understand their unique operating processes and pain points.

Operations engaged included:

1. Eisenhawer Farms – Metchosin, BC. – 2 acres mixed fruit and vegetables
2. Madonna Farms – Saanich, BC. – 22 acres of mixed vegetables
3. Healing Farms – Saanich, BC. – 18 acres of fruit and poultry husbandry
4. Helmer Farms – Pemberton, BC. – 80 acres of root vegetables

Generally, these operations all had access to a potable irrigation supply, either via municipal connection, onsite wells, or a combination of both. Manual pipe systems and sprinkler placements dominated. The orchardist also had permanent subsurface drip lines and the root

vegetable farmer used semi-automated, water powered, self-rewinding irrigation reels. Without exception, each operation described irrigation as a significant operational challenge, involving frequent compromises in their cropping techniques to accommodate the installed technology as well as the requirement to continually attend to its operation and maintenance.

2.2 REVIEW OF EXISTING TECHNOLOGIES

Agricultural operations typically consist of dedicated areas of arable land and equipment to cultivate that land. The larger the operation, the more the equipment and processes emulated industrial manufacturing processes. A review of irrigation systems and automated farm equipment provides an understanding of the existing processes and boundary conditions.

2.2.1 LATERAL MOVE AND CENTER PIVOT IRRIGATION

Lateral move and center pivot irrigation devices share a common morphology. They are surface mounted devices, structured around a linear irrigation pipe, 40 – 400 m in length, supported periodically along the pipe length by sets of actuated drive wheels. Suspended from the pipe, at tight intervals, are irrigation heads that distribute the water to the crops below.

Figure 2 - A typical center pivot system in operation (*"Irrigation64" by NRCS Montana is licensed under CC PDM 1.0 - https://farm5.staticflickr.com/4577/38829325052_1aba72def6_b.jpg*)

The powered sets of wheels intermittently progress the supported irrigation heads at slow speeds: a center pivot covering a ¼ section of land takes 12-20 hours to complete a full cycle. Maximum speeds of the drive motors range from 1 – 4 m/s, with application rates in the 5 – 15 mm per 24 hours required to replace evapotranspiration rates and account for system losses (wind, run-off, etc.) This is areal irrigation device inflow rate of $0.65 - 1.6 \frac{\mathrm{L/s}}{\mathrm{ha}}$ [10]. Repositioning of the system to accommodate other mobile equipment requires the ability to move without irrigation. However, some systems use water pressure to operate the wheels, requiring an irrigation event to move. Due to this unwanted coupling, auxiliary power systems (electric motor or combustion engine) are more commonly employed. The need to move without irrigation flow provides a key constraint impacting the final design of the proposed device.

Center pivots rotate about a fixed point, usually serviced by subsurface piping for ease of operations. They are suited for large square field installations due to the limited ability to change the radius of coverage or path of travel. They can pivot freely about 360 degrees or operate on smaller segments for odd shaped fields.

While similar in purpose and construction, motion patterns differentiate lateral move systems from central pivots. Rather than constantly pivoting about a central point, they move laterally drawing water from a specially created irrigation ditch or are serviced via flexible hoses. Their operation is often more complex and used for irregular shaped fields. While they predominantly move laterally, they can also be pivoted at either end to change directions. This flexibility in travel direction and the resultant complexities of supply necessitate increased observation and control versus a center pivot system.

Local aquifers or surface sources provide the required irrigation supply. Centralized pumping stations, powered by electrical motors or fossil fuel-based engines, provide the required power to deliver the water from source to the irrigation platform. These pumping stations and pipe networks can be utility supplied, privately operated, or a combination of both. Midstream booster pumping directly on the platform is also employed and provides a localized increase in distribution capacity.

It is common for both types of irrigation platforms to be fully autonomous, computer controlled and remote-monitored to reduce the burden of constant attendance during use. This often includes operational coupling of pumping stations and the serviced platforms.

2.2.2 HOSE REEL IRRIGATORS

Hose reel irrigators are semi-autonomous linear travel irrigation systems. They consist of a large trailer-mounted reel of irrigation pipe ranging from 30 – 300 mm in diameter with a large sprinkler nozzle(s) mounted a travelling cart. The device is maneuvered by a tractor or truck into position, connected to an irrigation supply, then the cart is manually towed to unwind the piping from the reel. Once in the final position, the device is turned on and under its own power, winds the cart back in, returning to the original position, irrigating the entire return trip. Then the device is repositioned, and the cycle repeated.

Figure 3 - Hose reel irrigator with self contained pump (*"Irrigation Hose Reel" by David Wright is licensed under CC BY-SA 2.0* - http://www.geograph.org.uk/photo/3084826)

These systems require much less installed infrastructure than lateral move or center pivots, however they require more operator intervention and auxiliary equipment to setup and reposition. Flexibility of operation is a key benefit of these systems. Additionally, some devices can utilize irrigation fluid power to achieve the rewind operation, sourcing hydraulic power from central pumping infrastructure rather than an onboard combustion-based power supply.

2.2.3 SOLID SET GROUND LAID PIPE NETWORKS

Solid set irrigation systems, commonly used in small-scale operations, are created by temporarily laying lightweight irrigation hoses and piping, from which sprinkler heads or other irrigation device can be directly coupled.

Flexibility is the key attribute of this type of irrigation system. The trade off is the significant amount of manually labour required to configure and the operator supervision required to ensure correct operation of an itinerate and easily disrupted systems. Often the surface installation of the piping networks prevents other key activities from taking place due to their placement or operation.

There are many other, more permanent subsurface embodiments of this concept. These systems require additional planning and installation resources but provide the advantage of dedicated irrigation assets and increased operational flexibility as the piping system is no longer surface mounted restricting vehicle traffic.

2.2.4 EXISTING AGRICULTURAL ROBOTS

They are many similarities between the industrial agriculture sector and the manufacturing sector. They both fit the of ‘dull, dirty and dangerous’ paradigm that is well addressed by robots. However, they have yet to see the adoption rates seen in the manufacturing sector. The tightly controlled operating environment and availability of power and supervisory systems found in manufacturing is distinct from the widely variable and remote nature of the agricultural sector. The unstructured and geographically dispersed nature of agriculture has contributed to limited wide scale adoption.

While the partial autonomy of hose reels, lateral moves and center pivots is acknowledged, their level of autonomy is limited compared to the advanced capabilities of autonomous vehicles or legged robots like the Spot robot from Boston Dynamics. However, auto-steer functionality is one area where autonomy is increasingly common in the agricultural domain.

These systems mount on standard farm tractors or other mobile equipment and, using GPS signals and mechanical actuators, control the steering, direction and speed of the

outfitted equipment. The machine and implement still require continuous operator presence to must monitor the performance of the machine and implement, as well as take over completely for complex tasks. However, steady technological advances are moving this system to increasingly higher levels of autonomy

Many applications have developed specialized equipment types that provide a dedicated transportation mechanism directly integrated into the implement. Combines, threshers, and liquid fertilizer sprayers are common examples.

Taking this cue, specialized autonomous devices are also entering the marketplace, targeted at automating specific applications. These types of systems abandon the ability to use existing conventional towed implements. They instead leverage the specificity and efficiency of a single purposed device, removing many of the automation complexities of the tractor-implement paradigm. Autonomous sprayers and physical soil samplers are commercially available.

Another category of autonomous agricultural device is the multi-purpose, custom implement device. Rather than building an autonomous power train designed to tow existing implements, or rework an all-in-one purpose build vehicle, this concept abandons these modalities entirely.

Instead a custom power train and custom implements are designed that leverage the unique capacities of fully autonomous systems. This allows the system to be optimized for the application use cases, rather than remain coupled to the operator directed/assisted paradigm. This divergence from past paradigms frees designers to develop new innovations for yet undetermined operating practices. One leading example is the Canadian designed Dot system that employs a modified seed head and a conventional seed bin.

One UK firm, Small Robot Company, has embraced this divergent approach a created several unique devices, across a range of physical device scales, to supply a variety of in-field agricultural services. Their four-wheeled prototype, Harry, was particularly instructive for this project. It combines electric actuators, with electrically driven wheels mounted on a platform bio-inspired by long-legged spiders.

Another key area of autonomous agriculture device development is harvesting. This labor-intensive process often requires a large but itinerate labor force, which creates additional societal complexities and intersections. As such, it is an appealing area of development from an economic perspective, despite the significant technical challenges.

The list of commercially available devices, prototype equipment and research projects continue to expand. Two critical areas of design constrain implementation; adapting current processes (digging, planting, weeding, harvesting, irrigating, etc.) to create autonomous agricultural tools, and practical systems to automate the platforms that carry these autonomous tools.

The task of full autonomy is a daunting undertaking in itself. However, extensive long-term investments by the automotive industry have lowered the activation energy to achieve full autonomy for a generalized device in a generalized environment. Autonomy packages are now commercially available, and the roboticist can offload this complex control task and focus on implementing agricultural applications.

This work does not directly address the autonomy needs of the proposed device, instead externalizing it as a challenging, but tractable future task. To simplify this future task, provisions are made for the necessary equipment and resources, namely controllable sensors and actuators as well as the onboard electrical and computational resources required to operate them.

2.3 REQUIREMENTS AND SOLUTION SPACE FRAMEWORK

Engineers and designers have an ethical responsibility to address the social and environmental challenges associated with the increasing mechanization we can enable. We must identify and maintain a cognitive connection between our actions and their outcomes, regardless of how abstract or removed they may seem. But how to accomplish this during the mundane and isolated exercise of mechanical design?

Tangible design guidelines that specifically address our current pressing societal concerns are necessary to translate principle into practice. To be effective, guidelines must be simple yet instructive, constraining yet enabling at the same time. The design process engaged

promotes the recursive review of implemented concepts. Every concept must meet the application requirements, but also meet the often-overlooked subtler ethical interactions. A set of ethical design guidelines is proposed, and these are presented below.

Table 2 - Ethically Motivated Design Guidelines

Societal Challenge	Supporting Design Guideline
Resource over use	• Simplicity over complexity • Optimize material usage • Prefer passive to active processes • Synergistic system design
Environmental degradation	• Specify low impact materials • Specify highly recyclable materials • Decrease petrochemical dependency • Maximize device longevity
Biodiversity and habitat destruction	• Low impact devices • Leverage existing eco-system services • Leverage existing irrigation systems
Disharmony with nature and climate resiliency	• Leverage biomimicry • Operate at the plant scale • Design for future expected conditions

With a guiding ethical framework established and actualized in the form of design guidelines, the collection of the irrigation application specific requirements can commence.

There are two distinct use cases each possessing a set of common requirements: coupling to existing large-scale semi-autonomous irrigation platforms, and the stand-alone coupling to static, small-scale irrigation networks. While presenting distinct needs in many areas, there are several common features found in both applications.

- Ability to self-locomote in an agricultural setting
- Low capital cost

- Low operations and maintenance requirements
- Fully autonomous for majority of operating conditions

From these overarching application requirements and the ethical paradigm, I propose a set of additional, self-imposed constraints to narrow the design scope and strengthen the focus on elements that support the design guidelines.

Table 3 - Design Constraints and Motivations

Design Constraint	Motivation
Human scale device	• Low impact devices • Operate at plant scale
Actuated using irrigation pressure	• Synergistic system design • Specify low impact materials • Simplicity
Legged morphology	• Leverage biomimicry • Ability to handle agricultural terrain • Low impact device
Tethered robot	• Simplicity • Low impact device • Synergistic system design
Prefer aluminum and HDPE	• Specify highly recyclable materials

Human and plant scales are similar in magnitude. The intent is a device conforming to the environment, rather than requiring the conformance, and therefore remaking, of the natural environment. The homogenization and mechanization of industrialized farming is optimized by monoculture cropping. This mechanically efficient approach is a stark contrast to the successes observed in the polycultures that predominate in nature. Shiva observes that monoculture cropping has a consequent negative correlation to biodiversity and positive correlation to petrochemical usage [11].

The scale of the proposed device was constrained to generate a low impact device that would be easily adapted to existing plant ecosystems. The human scale device easily adapts

to existing human-scale interactions the dominate the small-scale operation. A modular implementation strategy sees multiple devices working in parallel, in contrast to the construction and use of a single, larger device. The focus on increasingly large-scale devices is predicated on the short supply of sentient machine operators. With a smaller scale, modular automation modality, new cropping processes that leverage polyculture and bio-diversity as powerful forces can emerge.

Utilization of irrigation water pressure is employed to power existing irrigation equipment. The simplest example is the self-advancing, rotary sprinkler head with it easily identifiable intermittent noise. Here the momentum of the water indexes the nozzle of the sprinkler, automating the redirection of water over a larger area than a static nozzle.

The widely deployed Zimmatic 7500WD pivot, manufactured by Lindsay, is an example of a semi-autonomous mobile irrigation system that uses water pressure to transport the platform itself. This unit is relatively small compared to other commercially available pivot systems. However, its commercial success confirms the efficacy of using irrigation pressure to self-locomote the distribution system. The necessity of an optimally sparse design provided valuable insights towards achievement of many of the design guidelines; simplicity of design and synergistic use of resources.

The selection of irrigation fluid to operate the device actuators, rather than the more commonly employed electric motors, potentially reducing the demand for specialty metals often employed in electrical motors desirable for actuation. Hydraulic operation also allows the joints to be locked without consuming energy, whereas electrical actuators often require input energy to achieve the joint locking torque. Additionally, a less complex actuation methodologies can be explored, outside the traditional motor gearbox paradigm.

The preponderance of arthropods in the agricultural environment motivated the choice of a legged morphology. Insects perform a wide variety of agro-ecological services and are well suited to the unstructured topographic environment, albeit a reduced physical scale. The desire to allow form to follow function was key in this selection.

A wheeled design, the obvious contraposed design morphology, constrains cropping to conventional row systems. The desire to limit the crushing of crops motivates the

constraining of wheeled systems to travel the same dedicated wheel track. The resulting repetitive driving over the same location creates compaction issues. This results in negative impacts on nutrient retention and uptake [12]. However, a wheeled option may ultimately be a requirement to achieve many of the operational efficiencies required.

Alakukku et al. indicate in their review that increasing soil moisture content, applied ground pressure and frequency of localized force application positively corelate to soil compaction [13]. The requirement of the irrigation devices to be on-field during irrigation events amplifies this challenge as the soil moisture content increases during these events.

A legged morphology can aid in minimizing compaction. The ability to select and recall specific ground contact points, enables a device that can limit repeated compaction events, as well as avoid crushing crops underfoot. While a legged morphology aides in minimizing repeat compaction events, one must attempt to minimize *all* compaction to achieve a truly low impact device. Low ground contact pressure is therefore added as a parametric constraint to address the low impact design guideline. The lowest ground contact pressure recommended by Alakukku, for the highest soil moisture content was selected as our target ground pressure ~ 50 kPa.

A tethered system can simplify an overall design as external systems provide necessary services, eliminating the mass and complexity of the serviced device. For an irrigation device, onboard water storage has a crippling impact on overall mass. Excessive mass negatively impacts compaction and also significantly constrains design options.

Tether length can vary depending on the application and the irrigation platform extended. A simple overhead tethering system has a short and well supported tether. A device that wishes to stray far from the coupling point, must contend with the extra mass and complexity of a long, heavy hose as well as that of the hose handling mechanisms.

Mass of the tether, and the supporting systems can quickly consume the available payload of a mobile device. Reduction in hose diameter results in reduced mass at the expense of increased pipe network losses. The area covered, the method of provision of irrigation supply strongly affect the utility and the challenges of implementing a tethered system. For larger-scale operation, the distances required from source to point of application is in the

10^3 m range versus the 10^2 m range small-scale application. In both cases the flow demands of the device govern the magnitude of the challenges to be overcome.

Finally, the design is constrained to preferentially utilize aluminum for structural components and HDPE for low friction components, which make up a significant proportion of the overall mass of the system. These materials are highly recyclable and provide suitable material characteristics and longevity in the agricultural environment.

The additional self-imposed operating parameters were added to create plausible design boundaries and are presented together in the following table.

Table 4 - Required and Self-imposed Operational Constraints

Constraining Operational Parameter	Nominal or Target Values
Inlet pressure	2 – 6 bar
Target ground contact pressure	50 kPa
Nominal irrigation rate	0.65 - 1.6 L/s/ha
Ground clearance range	300 – 600 mm
Device mass	< 300 kg
Minimum number of legs	6
Bounding dimensions	2.0 m cube

2.4 DESIGN PROBLEM DECOMPOSITION

This research examined several cascading design problems, stemming from the overarching desire to create more efficient irrigation solutions. As design hypotheses were advanced, additional design challenges emerged and were explored. This opened with the primary challenge that there are limited devices currently available that provide site-specific irrigation. Rather most systems are only able to deliver generalized irrigation due to a lack of ability to sense and intervene at the plant scale.

The following flow chart presents the decomposition of the design problems and offers a roadmap of the remainder of this document.

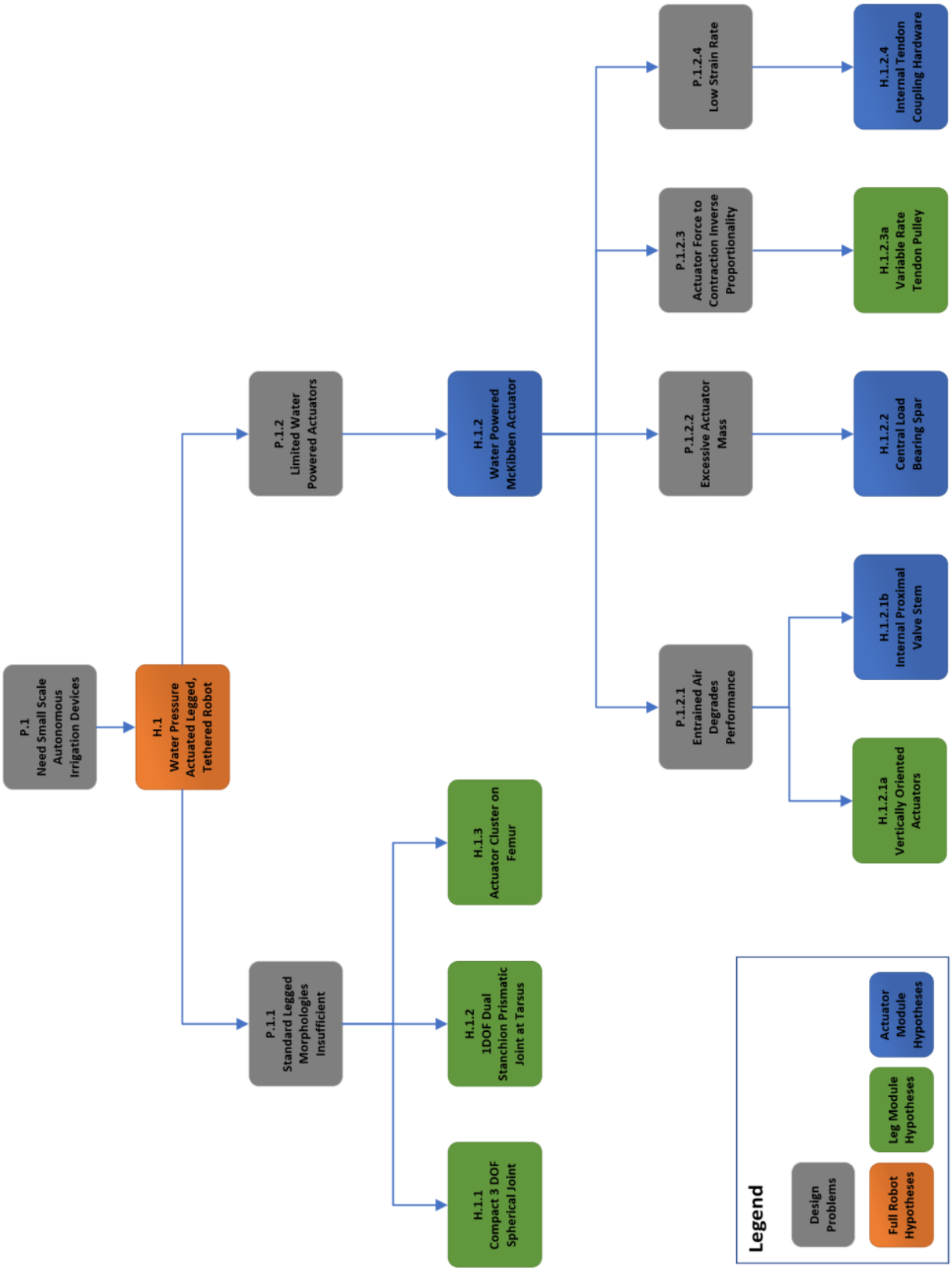

Figure 4 - Design Problem Decomposition

From the initial need for a small-scale autonomous irrigation device, I propose a water-pressure-actuated, tethered, irrigation robot. The overall robot design must address the environmental and operational challenges highlighted above. As various potential solutions to meet these requirements were envisioned and embodied, more design challenges came to light. Once identified, important design challenges were isolated, solutions proposed and validated against the design guidelines and ability to meet the operating requirements.

The ability to avoid damaging crops during normal operations is critical. This requires a compact, yet dextrous joint configuration and the ability to change nominal ground clearance to accommodate for crop growth. Three design hypotheses are presented to address these design challenges:

1. A compact 3 DOF spherical hip joint.
2. A dual-stanchion, 1 DOF prismatic joint as the tibia segment of the modular leg.
3. Clustering of all revolute joint actuators on the femur segment of the modular leg.

Another area of significant design challenge was the limited availability of water powered linear actuators. While there are many hydraulic linear actuators in use in existing legged robots, most harness the power density of high-pressure mineral oils. For this project, it is preferred to leverage the existing installed capacity of low-pressure irrigation as the power supply.

A McKibben style actuator or pneumatically/hydraulically actuated muscle (PAM/HAM) is proposed to address this specific design challenge. While typically operated pneumatically, the design instead uses water, at nominal irrigation pressures, as the working fluid. While this actuator has many valuable attributes, it also has several significant detractions to address, particularly when used with liquid water.

The key challenges of the HAM are actuator performance issues associated with entrained air, excessive mass, inverse proportionality between actuator force and contraction, and a relatively low strain rate.

Five design hypotheses are presented to address these actuator specific issues:

1. Vertical orientation of all actuators.
2. An internal valve stem proximally located to the active actuator volume.
3. A centrally located, load-bearing spar displacing wetted volume.
4. Variable rate tendon pulley.
5. Internally locating the tendon coupling hardware and actuator sensors.

3 A WATER PRESSURE ACTUATED, LEGGED, TETHERED ROBOT

To address the overarching need for a dextrous, efficient, human/plant scaled device, a water-pressure actuated, legged and tethered robot is proposed. Cues from the insect world are taken to leverage biomimetic principles. They are transporters of materials, consumers of waste products, creators of natural structures and emitters of raw materials necessary for the cycle of growth we wish to positively influence.

The common ant is observed to carry many times its own weight and demonstrates an elegant distribution of mass that provides for its primary function, transport. This is also the primary function of the proposed device; to transport water directly to the point of application, synergistically exploiting the contained flow energy, while minimizing negative impact on soil and plant health.

The overall morphology of the ant instructed the device design. Multi-segment legs, emanating from a compact torso or thorax. Simple joints with limited range of motion combine to provide the necessary workspace. Tarsus segments provide a natural 3 DOF contact joint with the ground. Using six legs provides a redundancy of support, where static equilibrium minimally requires only three.

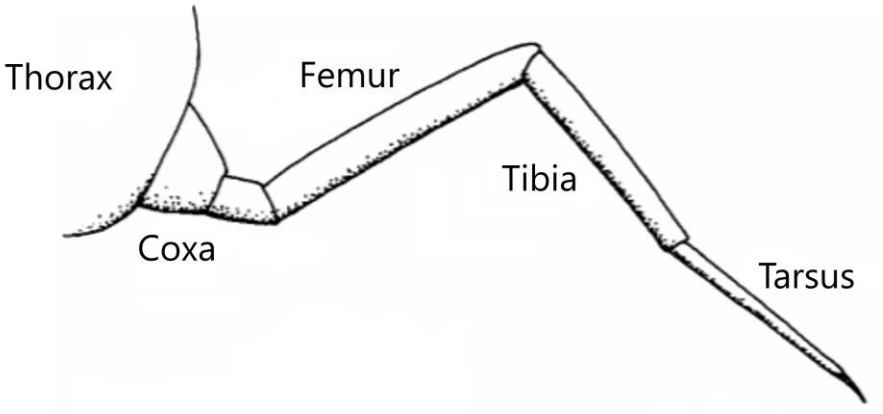

Figure 5 - Invertebrate paraxial locomotory appendage anatomy (adapted from Wootton [14])

The appendage terminology of arthropods is adopted to create a common taxonomy for discussion as well as evoking the overall appendage design. There is a thorax with a rigid leg segments or (podomeres), with joints supplying a single dominant rotational axis to facilitate bending motions between segments.

Many appendage morphologies include a large number single degree of freedom joints, see figure below, stacked in series to allow motion in various directions. Often arthropods have many small low mobility joints in the tarsus region to passively match the ground contact contours. Combining several joints with limited angular deflection to achieve an overall dextrous appendage is effectively employed in nature.

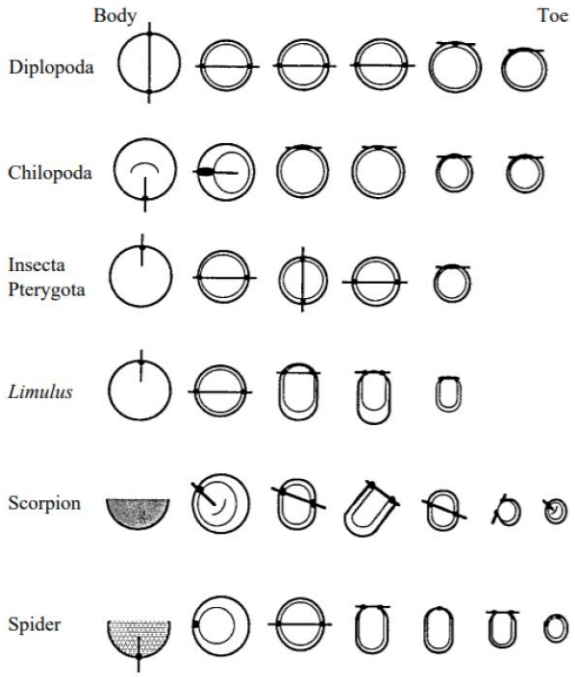

Figure 6 - Schematic representation of various arthropod group sequence of joint types. The straight-line segments indicate the joint axis. With proximal to distal joints represented from left to right. Modified after Manton [15]

This approach was considered but discarded once the issue of entrained air was identified. To achieve optimal motion, many actuators located on various podomeres, or complex tendon routing paths to group actuators would be required. This presented a challenge in achieving actuator placements and orientations that passively addressed venting of entrained air. This challenge was exacerbated by the high aspect ratio of PAM/HAMs. Long thin actuators limit the placement options when contrasted to compact rotational motors and gearboxes.

Series application of single DOF joints is a common approach for hexapod robots, motivated by the commercial availability and ease of implementation of electric actuators with integrated revolute joints. To achieve flexibility in actuator placement and orientation, a joint structure with overlapping degrees of freedom was implemented. This also allowed the clustering of actuators so that support structure and services could be synergistically shared.

3.1 PROPOSED OVERALL MORPHOLOGY

Once the device scale, morphology and operating environment were constrained, open-ended conceptual design was undertaken. Hand sketching, CAD modeling, parameter estimation and numerical validation exercises were completed in recursive cycles. From this formative work, an early proposed morphology was envisioned, and is presented below.

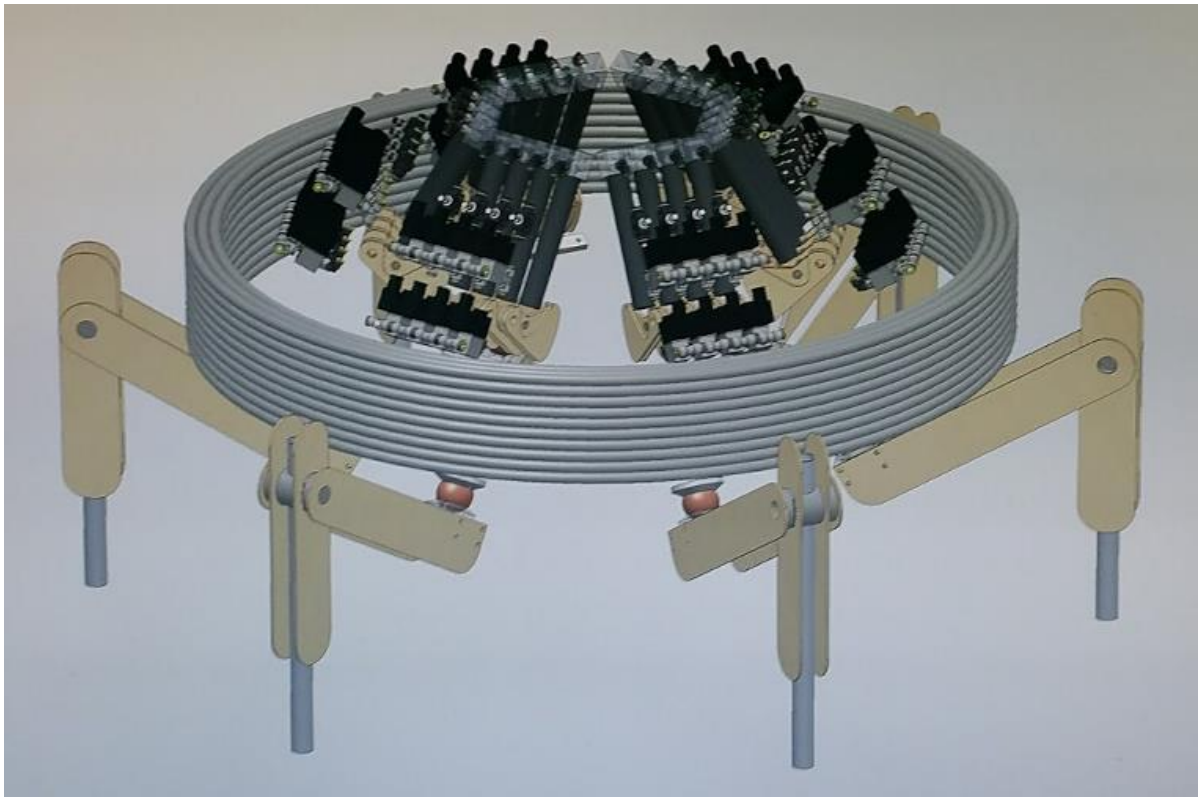

Figure 7 - Early conceptual model, showing externally carried hose reel

This was a simplistic design, intended to capture the overall design intent, while also attempting to provide for easy prototyping processes. Flat structural members were used to allow rapid fabrication and assembly from low-cost, stock materials. A simple actuator design, using commercially available pneumatic components was arranged in a modular leg design. Modularization of the leg components and actuators supports a progressive testing regime. First actuator, then leg module and finally the overall device could be progressively analyzed, prototyped and physically evaluated. This early stage conceptual layout allowed early estimations of mass and volume, as well as creating a structure for functional decomposition.

Table 5 - System Module Function and Proposed Location

Module	Function	Location
Main Body	• Mount leg modules • Mount support equipment • Mount tooling and sensors	• Central thorax
Leg	• Support actuators • Position joints • Monitor and control joint actuators • Mount tooling and sensors	• Distal to thorax • Radially mounted
Fluid Power	• Couple to supply system • Distribute to leg modules • Onboard fluid accumulation	• Distributed on thorax
Electrical Power	• Distribute electrical power • Manage onboard storage	• Mounted on thorax
Command and Control	• Communicate with supervisory system • Communicate with leg modules • Analysis and decision making • Sensor control and data acquisition • Tool control and monitoring	• Mounted on thorax

These base modules serve to segment the system components for design and implementation purposes. They represent the abstract systems required for either the small- or large-scale use cases. Depending on the specific operational requirements, some functions may be implemented in different ways, or not at all. For example, onboard fluid retention requirements will vary widely depending on application, as will sensor, tooling and support equipment requirements.

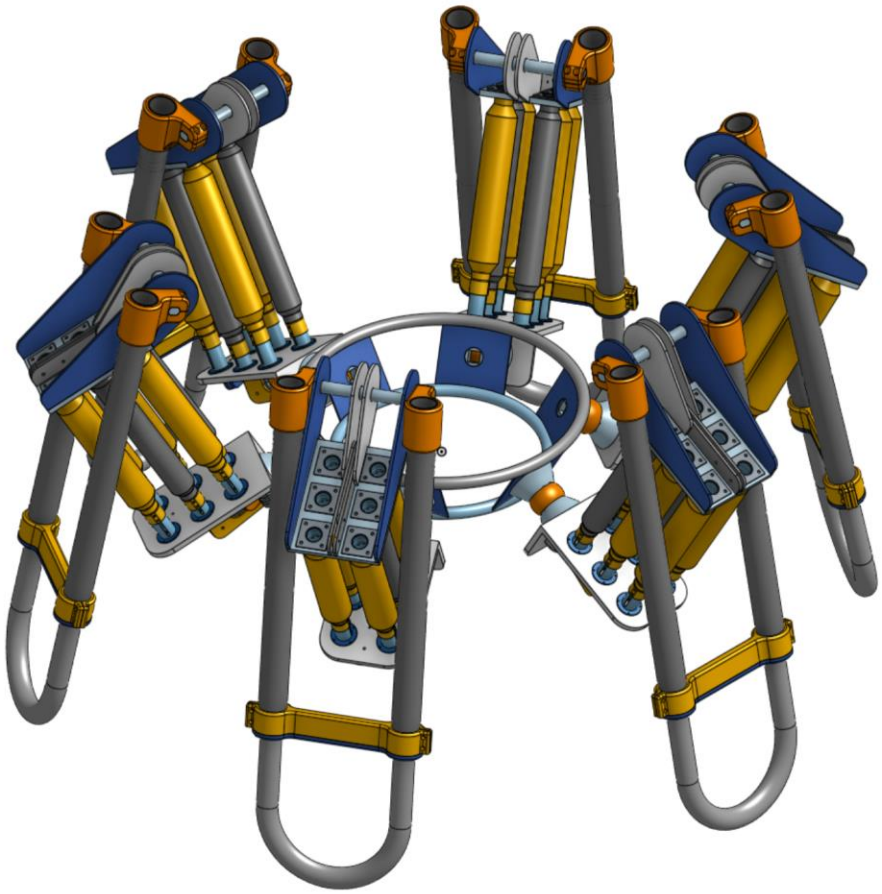

Figure 8 - Proposed overall morphology, showing a six-leg configuration, with a small central thorax

This overall morphology allows for significant customization, while maintaining the overall system composition. Configurable items include:

- Number of legs
- Joint ranges and supported gaits
- Device scaling – device scale or relative component scaling
- Sensor and tool configuration

3.1.1 CONTROL SYSTEM ASSESSMENT

An early conceptual assessment of the control structure was undertaken to identify any control system couplings to other key design elements. The desire to vary the number of legs of a device motivated a distributed control approach.

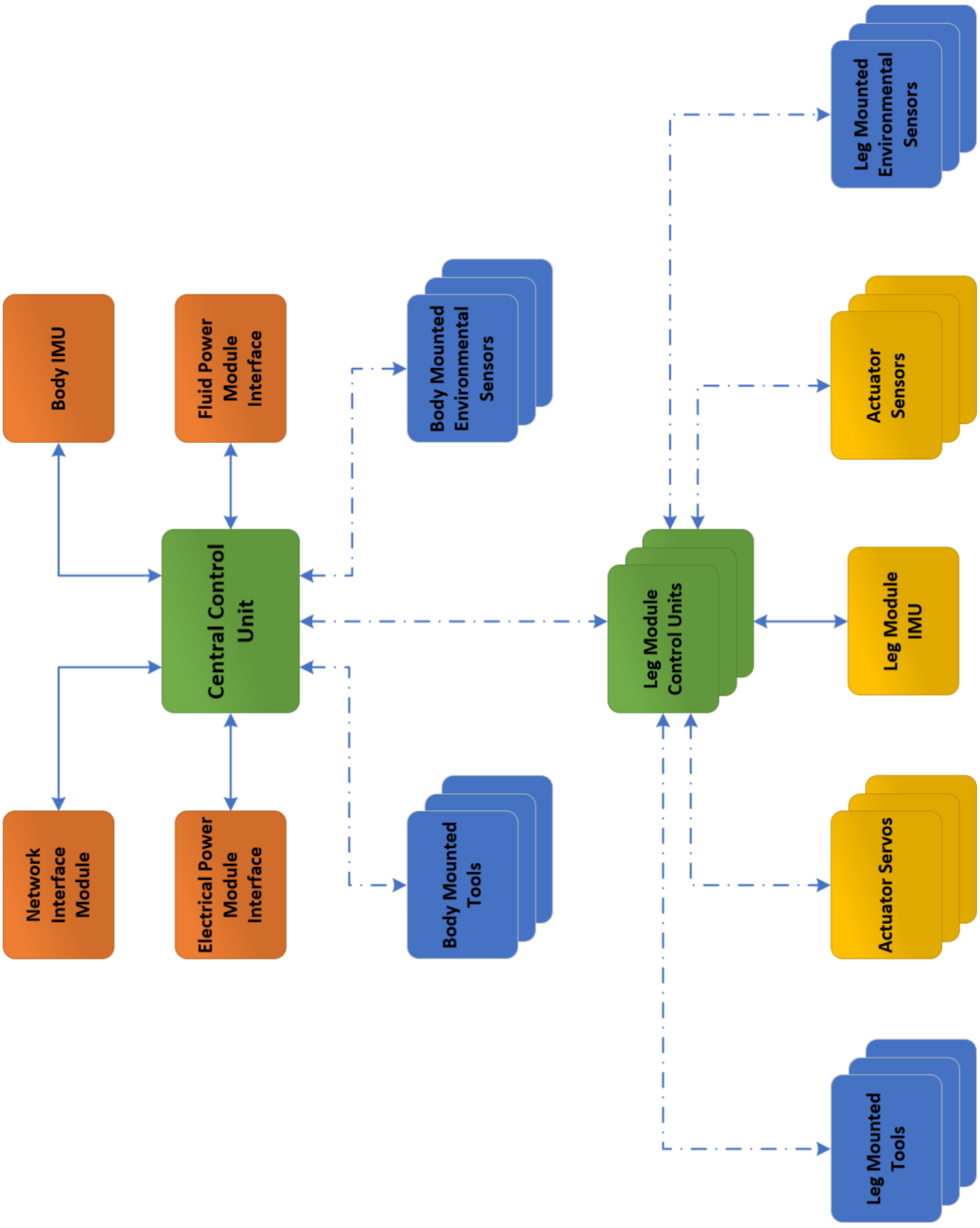

Figure 9 - Proposed high level control system structure

Centrally monitoring and controlling unique actuators to achieve desired overall body poses and gaits creates significant overhead. Independent control channels from the central command unit to each unique control and monitoring element increases complexity, cost and number of potential failure points. A decision to encapsulate and delegate these functions to distinct controllers on each leg module reduced the implementation complexity. When leg count and I/O channel requirements of the central command unit are decoupled, a single version of the base controller is possible. This challenge is duplicated when addressing body versus leg mounted tools and environmental sensors

In the distributed approach, the central controller would monitor the robot body position and orientation, commanding leg poses that each leg module would interpret and execute. Information about the specific joint position, actuator state and leg segment orientation would be federated and processed locally, and only the leg pose would be reported to the central command module. Tool and environmental sensors would also federate at the leg controller and be passed, via a central bus, to the central control unit.

3.2 P.1.1 STANDARD LEGGED MORPHOLOGY

Many legged robot joint morphologies found in the literature mimic the joint morphology found in simple stick insects. These have three independent, primary joints per leg, each actuating an independent axis of rotation, via a set of independent actuators. This facilitates a lifting and swinging motion as shown below.

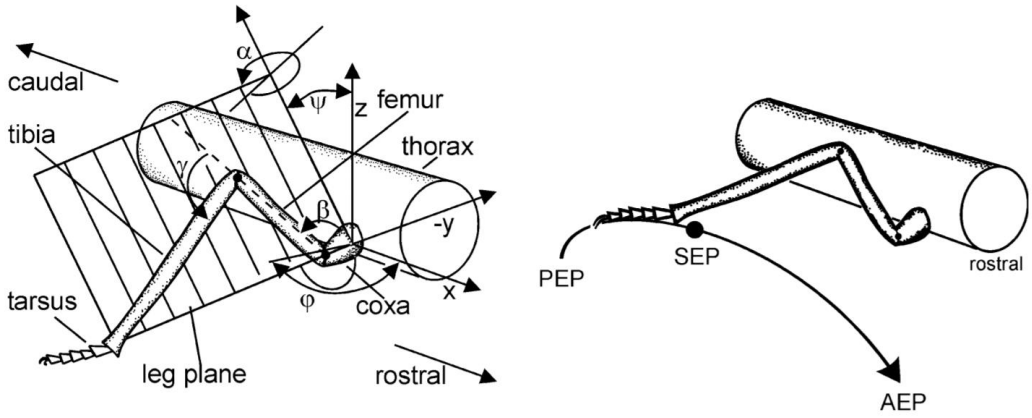

Figure 10 - Schematic diagram of a stick insect leg showing joint angles with respect the body fixed co-ordinate system (left) and diagram of affected swing motion (right). Adapted from Schumm [16]

This configuration provides limited flexibility of the angle of incidence in the *xz* plane of the tibia as it progresses along its swing path. This limits ability to adjust the insertion angle to avoid unwanted contact with crops. A joint configuration that provides improved tibia mobility was sought to address this challenge. Specifically increase dexterity and a vertical insertion angle for the tibia.

Furthermore, the actuator configuration of the stick insect uses two counterposed contracting elements, to flex and extend each distinct joint on the leg segment proximal to the body with respect to the actuated joint. This presents a challenge that is unique to water filled actuators. Internally accumulated entrained air negatively impacts hydraulic actuator performance. A passive system to address this endemic challenge would be very desirable. With the actuators mounted on each leg segment, the ability to control passive venting via actuator orientation becomes increasingly complex. An actuator configuration was sought to enable passive venting and potential co-locate actuators to share common services as well as distribute bending and torsional loads across the modular leg.

Finally, the operational requirement to provide a range of ground clearances is not commonly observed in the stick insect domain. One method to achieve this is to provide for enough range of joint motion in the coxa-femur joint to facilitate a change in 'ride height' by rotating the femur from a vertical alignment to a more horizontal one. The spider morphology is well adapted to this method.

However, this necessarily places additional requirement on the joints and actuators, requiring an increased joint torques to support the body in this configuration. Additionally, this would not be an itinerant pose, rather a pose used indefinitely for certain use cases. The design guideline to prefer passive solutions versus active solutions was invoked and a solution to passively provide a range of ground clearances was sought.

3.2.1 PROPOSED LEG MORPHOLOGY

The basic bio-inspired stick-bug leg morphology was found to be lacking in several areas; leg dexterity, challenges in venting with actuators distributed across all leg segments and the inability to vary ground clearance without excessive large joint rotations.

By selecting a compact 3DOF spherical joint, the overall mechanism is simplified while supplying increased dexterity and gait options. The clustering of all the actuators, for the revolute and spherical joints in a common bank, simplifies service provision to the actuators, including passive venting of both actuators and manifolds. Additionally, it co-locates underutilized structural members to collaboratively carry the variable axial, bending and torsional loads communicated across the femur.

An extendible prismatic joint at the tibia, improves the mobility of the tarsus while providing the capability to vary overall ground clearance without increasing torques at the knee and hip joints. The dual stanchion design creates a simple and robust lower limb that allows the tibia to travel over the femur, facilitating the vertical stacking of these two joints. This permits neutral stances with near-zero joint torques, at rest, across a variety of general load conditions. The implemented leg design is shown below.

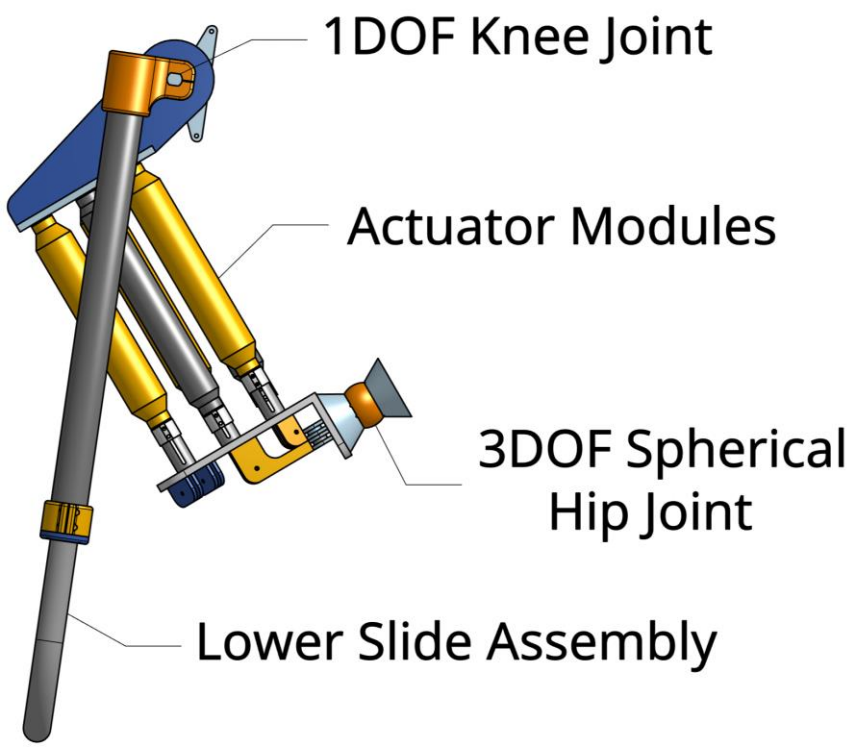

Figure 11 - Side view of proposed leg morphology, showing 1DOF dual stanchion prismatic extension tibia joint, 1DOF revolute tibia/femur joint and 3DOF femur/thorax joint with foot pad removed

When connected to the thorax via a spherical joint, a multi-leg device has many independent degrees of freedom. The ground contact point is modelled as a 3DOF joint as well as the hip joint. The knee joint is a 1DOF pin joint. If one considers the 1DOF

prismatic joint fixed, for simplified motion, one can examine a symmetrical planar mechanism for its mobility, m, using Gasthof's equation. In this case, the ground contact and hip joints are both modelled as 1DOF turning pair joints.

$$m = 3(n-1) - 2j_1 - j_2 \qquad [1]$$

Where, n is the number of links and j_1 is the number of 1DOF pairs, and j_2 is the number of 2DOF pairs. The simplified planar motion 6 bar closed loop linkage, shown below, has a mobility of $m = 3$. Only three distinct parameters are required to specify the mechanism pose. If another constraint is added via a 'virtual' geared coupling between the two femur joints, such that γ at C and E are always equal, the mechanism is further restricted and its position can be controlled via a single parameter. Constraining the mechanism to symmetrical poses by commanding knee angles to remain synchronized keeps the thorax link horizontal and supplies the 'virtual' joint coupling.

In this simplified control regime the torques required to support the thorax mass can be provided from either of the two actuated joints in the leg modules, provided that the applied moments remain balanced between the legs so as to maintain the horizontal thorax constraint.

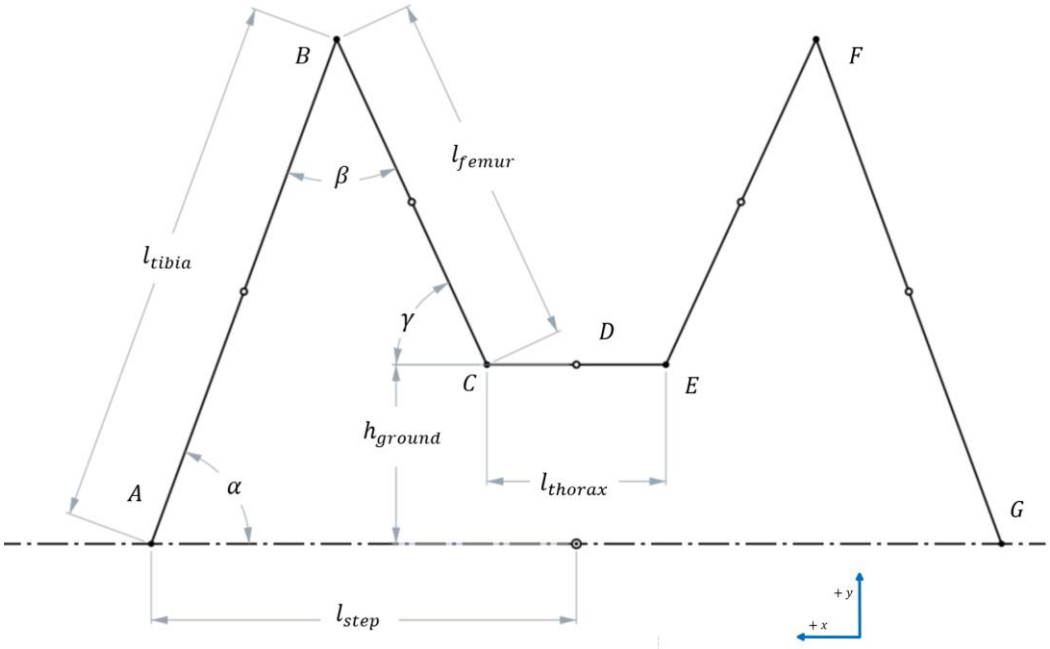

Figure 12 - Planar representation of the 6-bar parallel linkage (two-leg pair)

The parallel nature of the mechanism, and the over actuation allows optimization of actuator usage by distributing the application of torque to the joint with optimal actuator positions, for any given pose and external load profile. For example, the position of the leg could be such that the available actuator forces available at the hip are low compared to joint torque demand, whereas the knee actuators could be in a position where significant force is available to provide the required torque to the closed parallel linkage.

To simplify the conceptual design, the knee actuator is to be specified so as to provide sufficient torque to support the dead weight of the entire device, without the requirement of the hip joint actuators to provide any static mass-supporting torques. The hip actuators require enough strength to support the full weight of an extended leg, and when not supporting a lifted leg, would provide the stabilizing torques to keep the thorax horizontal as well as limit rotation about the center of the device.

3.2.2 H.1.1.1 – COMPACT 3DOF SPHERICAL JOINT

The challenge to provide increased mobility of the distal tibia segment of the leg motivated the search for a joint configuration that would provide an additional DOF to the leg. The simple, and frequently implemented, series arrangement of multiple revolute joints was briefly considered. This would involve stacking of another joint at the coxa. This would create more joint offsets, creating control and stiffness complexities. Additionally, more controlling actuators would need to be oriented and supported, amplifying the issues found earlier. This creates additional venting challenges or necessitates complex tendon routings to provide for more advantageous actuator orientations.

A universal joint is a common method to combine two unique revolute joints to form a composite 2DOF joint. Tanaka et al. developed two types of universal joints that were driven by two pairs of agonistic/antagonistic pneumatic muscles [17]. They noted that controlling joint stiffness was challenging in the joint design having an offset between the two orthogonal axes of rotation. They achieved better stiffness control when they eliminated the offset between the axes via a creative arrangement of pulleys. The convergence of the two joint axes created a 2DOF spherical joint, with two orthogonal joint structures superimposed.

Shimamoto et al. proposed a tendon driven spherical joint that uses a spherical ball and socket, controlled by a set of 3 contraposed pneumatic actuators [18] that has 2 actuated DOF. This reduces the mechanical complexity required to implement the spherical joint, a key design guideline of this research. Both these approaches reduce complexity and eliminate the bending moments introduced by offset axes and but are unable to actuate the third rotational DOF of the joint. The ball and socket joint mechanism of Shimamoto would allow for rotation in the third DOF, however there was no scheme implemented to actuate it.

Many 3DOF tendon actuated designs have been proposed [19][20][21] which provide the necessary third DOF actuation. However, they typically require significant uninterrupted volume surrounding the joint to position tendon routing components and actuators. These configurations, while functional, do not address the need to optimize support structure or provide for high mobility about the actuated 3DOF. Guckert and Naish proposed a novel compact 3DOF spherical joint that address these concerns [22]. This design uses four counter-opposed tendons spanning across the ball and socket joint providing a compact joint design and permitting the clustering of all actuators on one side of the joint and is presented in the diagram below.

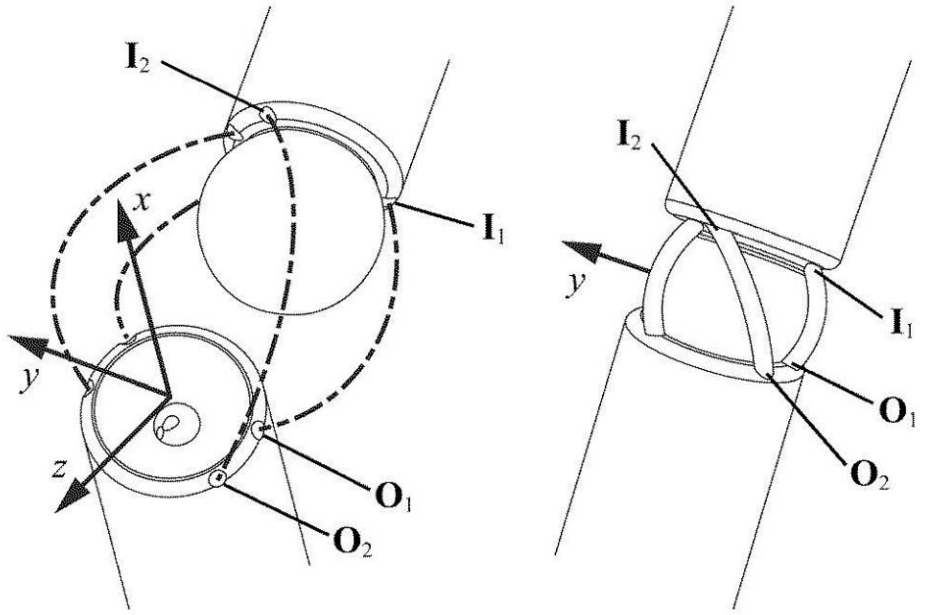

Figure 13 - Compact 3DOF ball and socket joint showing 4 tendons with insertion and origin points. Adapted from Guckert [23]

This design had full force closure across the ball socket for joint angles of +/- 70 degrees about both the y and z axis shown above, and +/- 20 degrees about the x axis. Positions on the fringes of workspace in the y and z axes negatively impact the ability to achieve full 20-degree rotation. This fully actuated spherical joint eliminates the singularities found in the wrist type universal joints presented earlier. Additionally, this configuration shares the tensile loads to generate the required joint torques across all four actuators. This decreases the overall power required from each unique actuator in the typical pair of counter-opposed actuators that drive single axis joints. This coupling introduces control complexities.

This joint type was selected and implemented in the proposed device. To ensure effective workspace access, the joint is limited to operate with only +/- 45 degrees of swing motion, allowing the 20 degree of roll angle to be available over most of this workspace envelope. Guckert and Naish noted that the ability to effectively access the full range of the third degree of freedom was dependent the other two joint angles, as well as the tendon placement. Their optimized tendon placement for a 3 mm ball was scaled up for use with a 50 mm ball.

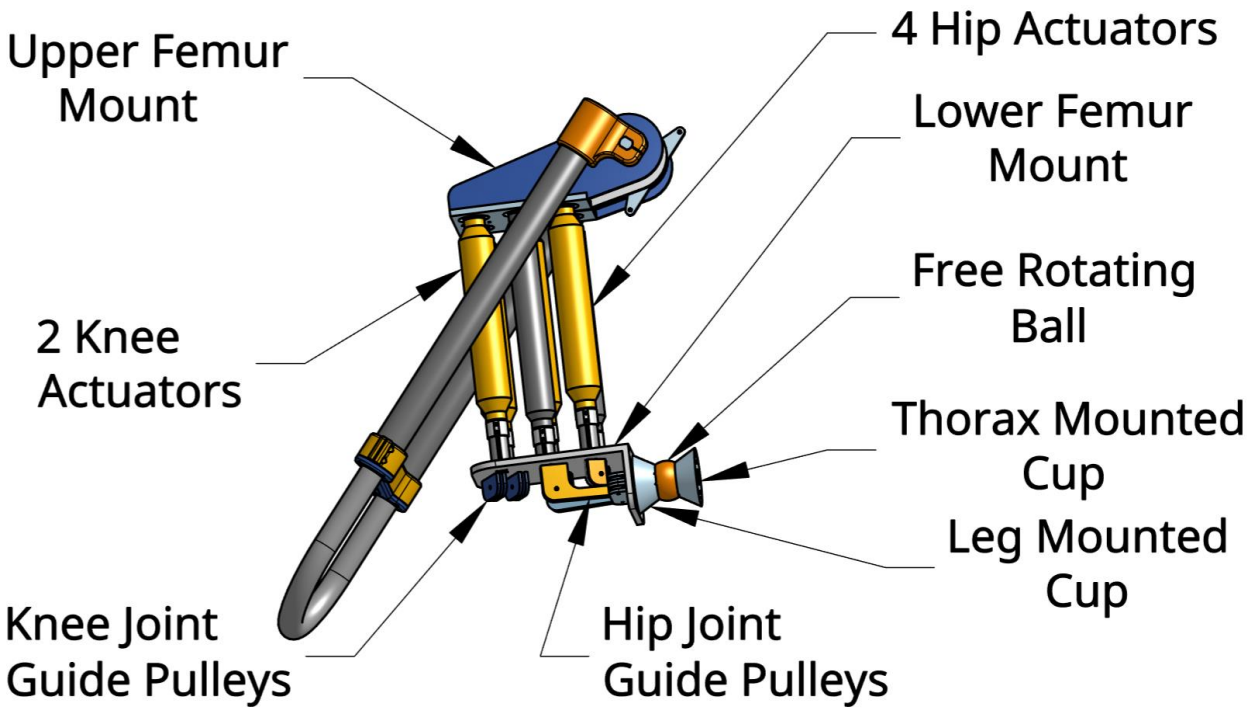

Figure 14 - View of implemented compact 3DOF joint and actuators – tendons not shown

The exposed length between the origin and insertion points of a given tendon is calculated for a given joint geometry and position a shown below. By comparing relative lengths at various positions, the tendon length change, and the resultant actuator displacements can be determined for any joint posture. These values can be used to determine volume flow for a given joint transformation for a given actuator linear displacement. The following geometric relationships follow the results of Guckert and Naish [22].

$$L_n = r \arccos\left(\frac{\boldsymbol{RI}_n}{r} \cdot \frac{\boldsymbol{O}_n}{r}\right) \quad [2]$$

Where L_n is the length of a tendon running across the sphere surface, r is the radius of the sphere, $\boldsymbol{I}_n$ and $\boldsymbol{O}_n$ are the Cartesian co-ordinates on the sphere of the moving (distal) and fixed (proximal) frames respectively. $\boldsymbol{R}$ is a zyx fixed-angle rotation matrix representing the 3DOF rotation of the moving frame with respect to the fixed frame, where the *x*-axis is aligned with central axis of the fixed frame with the angles of rotation around *z*, *y* and *x* are given by θ_1, θ_2 and θ_3 respectively.

The proximal motion, h_n, of the n^{th} tendon away from the fixed frame, for a given initial and final orientation of the joint, is described by the following expression.

$$h_n = L_{n,initial} - L_{n,final} \quad [3]$$

Additionally, the vector of torques, $\boldsymbol{\tau}_n$, generated by tendon *n* about the fixed frame can be determined as follows.

$$\boldsymbol{\tau}_n = \frac{t_n\,(\boldsymbol{RI}_n \times \boldsymbol{O}_n)}{r} \quad [4]$$

Where, t_n is the tension in the n^{th} tendon, and $\boldsymbol{\tau}_n$ is the vector of torques generated by tendon *n* about the fixed frame.

3.2.3 H.1.1.2 – ACTUATOR CLUSTERING ON FEMUR

The unique challenge of entrained air retention inside the active actuator volume was identified early on. Focchi et al note in that even 1% of entrained air can reduce the bulk modulus of water by up to 80% [24]. To passively manage this issue, orientation of fluid

holding components can be used to collect the accumulated air in known locations that will allow it to be released downstream during normal flow conditions. This is particularly important for the actuators where varying bulk modulus makes controlling joint stiffness more challenging. However, pooling of air in other passages of the system also negatively impacts flow conditions, adversely affecting operating performance.

The orientation of the actuators was addressed by reviewing the location of the actuators on the device, then examining the motion of those locations to see ensure that the collection points identified could be effectively vented, either via normal flow conditions, or via a venting valve.

Actuators need to control the knee and hip joints, and placement of the selected actuators needed to be aligned with body and leg structures to ensure synergistic use of the structures for both supporting the compressive loads from the actuator and also carrying the loads from the device weight. These include axial, bending and torsional loads.

The overall system morphology and potential locations for the actuators, which have a high length to width aspect ratio, was examined. Alignment with the femur or tibia structures or that of the structural elements of the thorax allow these load bearing structures to also carry the compressive loads of the selected tendon-based actuators.

Various location combinations were reviewed and evaluated for their impact on several attributes that impact the overall performance of the device. Specifically, is passive venting facilitated, are unwanted thorax morphology and size constraints created, are joint torques in the neutral pose increased, and does the design allow the tibia and femur to overlap resulting in the stacking of the knee and hip joints, vertically, in the neutral pose?

Table 6 - Actuator Location and Orientation Comparison Matrix

Name	Block Diagram	Passive Venting	Constrains Thorax Morphology	Passive Balance	Permits Femur-Tibia Overlap
All Femur	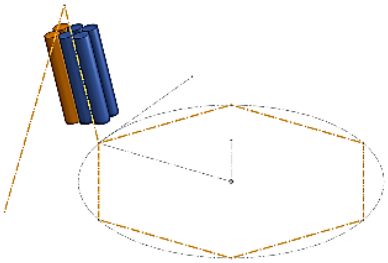	**Excellent**	**No**	**Good**	**Yes**
Femur Tibia Split	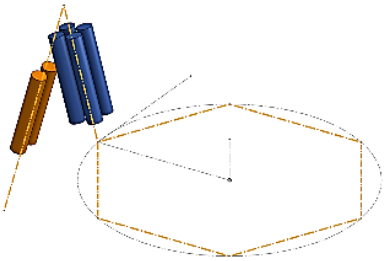	Excellent	No	Good	No
Thorax Angled - Tibia	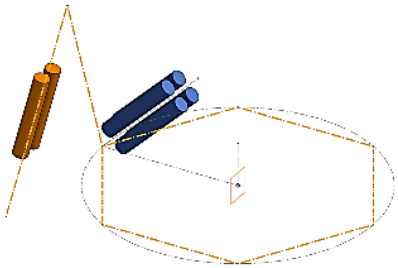	Good	Yes	Poor	Yes
Thorax Angled - Femur	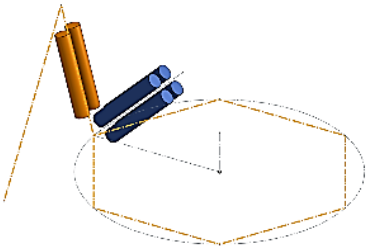	Good	Yes	Poor	Yes

Thorax Ring - Tibia	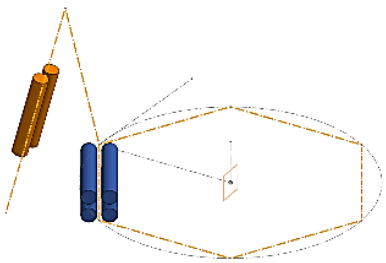	Poor	Yes	Poor	Yes
Thorax Ring - Femur	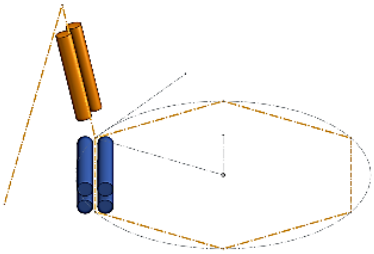	Poor	Yes	Poor	Yes
Thorax Spoke - Tibia	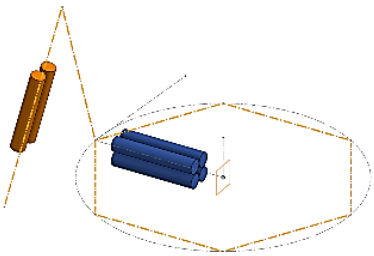	Poor	Yes	Poor	Yes
Thorax Spoke - Femur	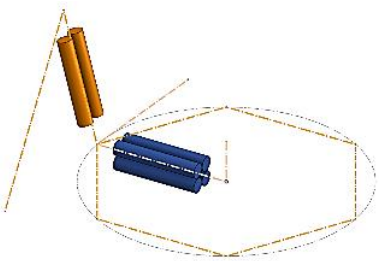	Poor	Yes	Poor	Yes

As the horizontal distance from the ground contact point to the center of mass of the actuator mass increases, larger supporting moments must be carried across the joint. As the mass of the actuators is a significant contributor to the overall device mass, locating these components directly on the leg segments reduces induced joint torques. Locating actuators further away on the thorax increases joint torques further and also increases the minimum possible thorax diameter.

If actuators are oriented vertically to avoid impacting thorax size, structural members that do not contribute to thorax rigidity are required to support the actuators. This configuration violates the design guideline of synergistic use of materials. With increased thorax dimensions, comes increased mass, worsening the joint torque problem. Mounting the actuators entirely on the leg decreased joint torques as well as decouples the body and leg design. This modular design allows the entertaining of many body styles, like varying relative orientation and the number of legs.

The placement of actuators on the tibia, directly over the ground contact point, minimizes the overhung mass acting on the knee and hip joints. However, the complexity of routing tendons across the knee joint, and along the femur to the hip joint, goes against the design guideline of simplicity over complexity. Additionally, joint torques can be minimized by vertically stacking the knee and hip joints in the neutral pose. To achieve this the tibia and femur must overlap. An asymmetric side-by-side configuration requires a very robust knee joint. A symmetrical configuration can be employed with one segment constructed from two structural members and the other segment allowed to pass between these two members. This is a common arrangement in many industrial robots and eliminates overhung bearing loads, between rotating segments. The symmetry of this configuration was appealing given the high tendon loads expected and the resultant bending moments the asymmetrical design introduces.

If the tibia is selected as the two-member segment, the femur should be narrow to minimize the assembly size. To create a space for the femur to pass, the actuators are mounted outboard from the principle axis of the tibia, increasing bending moments and complicating tendon routing. However, the femur will carry higher net bending and torsional loads than the tibia and narrowness is a disadvantageous characteristic for this requirement. Relocating the actuators to the femur allows the bulk of the required structural members to carry these expected increased loads. This is a more plausible approach to achieve the synergies in material usage.

A compromise is struck by placing the knee joint actuators on the tibia and the hip actuators on the femur. Mounting more mass directly above the ground contact point is the advantage of this approach. However, clustering all the knee and hip actuators allows the co-location

and synergistic provision of services (flow, control and support) for the similar actuators. With so many actuators required, this simplification was desirable from a cost, assembly and maintainability perspective. It dominated the marginal structural performance gains of mounting actuators on the tibia.

When the knee and hip actuators are clustered together, in the same orientation, a common actuator design could be employed that collected the entrained air at the top of the actuator, clearing each time the ports were opened. This would pass the trapped air into the LP rail on actuator emptying, and even potentially back into the HP rail should two fill events occur sequentially. This identified two other pooling locations that would also need to be cleared to maintain satisfactory system performance.

The neutral pose of the leg would orient the actuators at near vertical, and the active pose range would pitch the actuators outward from the body. This creates a natural high point in the actuator manifolds to collect entrained air which is also at the highest point on the entire device. With all the actuators collocated here, a single venting valve per service line could be employed to vent air in the manifold piping collected from all actuators in the cluster. This met the both the passive system and simplicity design guidelines; all actuators passively transfer entrained air into a common header with one actively controlled vent port, for each pressure rail, on each modular leg. This vent point consistently remains the highest point possible throughout the workspace envelope of the leg.

This configuration also allows the prismatic joint pressure lines of the tibia to couple directly to these same service manifolds passively transferring entrained air to a single point for active venting and is discussed in more detail in following sections.

The cluster of actuators was also situated outboard of the centerline joining the knee and hip joints, when vertically stacked in the neutral pose. The overhung mass of the femur actuator cluster creates a thorax supporting moment about the hip joint. This is a desirable passive configuration because it reduces the joint torques that would normally be required to support the central thorax mass. The ability to reposition the ground contact point at the base of the tibia directly underneath the hip joint, or possibly even further underneath the body, enables the robot to adjust its pose to achieve a truly neutral stance regardless of

variances in mass distribution. Joint torques would only be required for stability rather than load support.

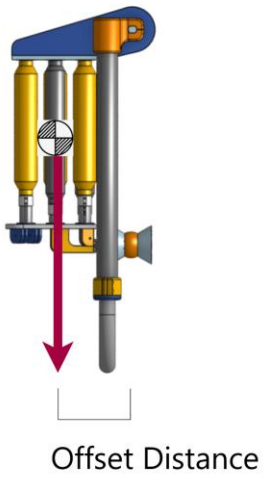

Figure 15 - Cluster center of mass offset, side view of leg module, foot pad removed

3.2.4 H.1.1.3 – 1DOF DUAL STANCHION PRISMATIC JOINT AT TIBIA

The proposed design includes a 1DOF prismatic joint at the tibia. The purpose of this joint is two-fold. It provides additional posture flexibility of the robot on uneven terrain. Without this extra DOF, the hip angle would increase to reach below grade. With an extendible tibia joint, a smaller hip angle, and therefore lower joint torque can be employed. Extendible lower leg segments also enable variation in ground clearance without requiring the knee and hip joints to provide high rotation angles. Ideally, the angle range of the joints should be kept as close to neutral as possible while still facilitating an efficient gate. Torques increases as joints deviate from the neutral pose. Wider stances apply larger moments necessitating higher supporting joint torques. Joint angles from 0 to 45 favor lateral position change of the ground contact point, whereas joint angles from 45 to 90 degrees favor body height increases at the expense of high joint torques.

Inclusion of a prismatic joint allows the joints to operate in the lower range while providing a low-energy, quasi-passive method of achieving increased ground clearance. Once the prismatic joint is extended and the cylinder port closed, no added hydraulic forces are required to support the joint and it can be modelled as a rigid leg segment.

The proposed design clusters the knee and joint actuators on the femur and includes a two-member symmetric tibia design. A dual-stanchion prismatic joint creates a robust lower leg segment and provides a wide and stiff knee joint. As the tibia is significantly longer than the femur, a cross-member connects the lower stanchion tube-ends together, stiffening the entire leg assembly. This approach emulates the time-tested box frame configuration commonly employed in motorcycle front suspensions mechanisms.

Unlike these mechanisms, which experience significant torsional rotation, the simple lower segment has negligible capacity for ground engagement that would generate torsion about the longitudinal axis of the tibia. This reduces the need for robustness in cross members and internal sliding interfaces as the load regime is primarily constrained to the axis of extension.

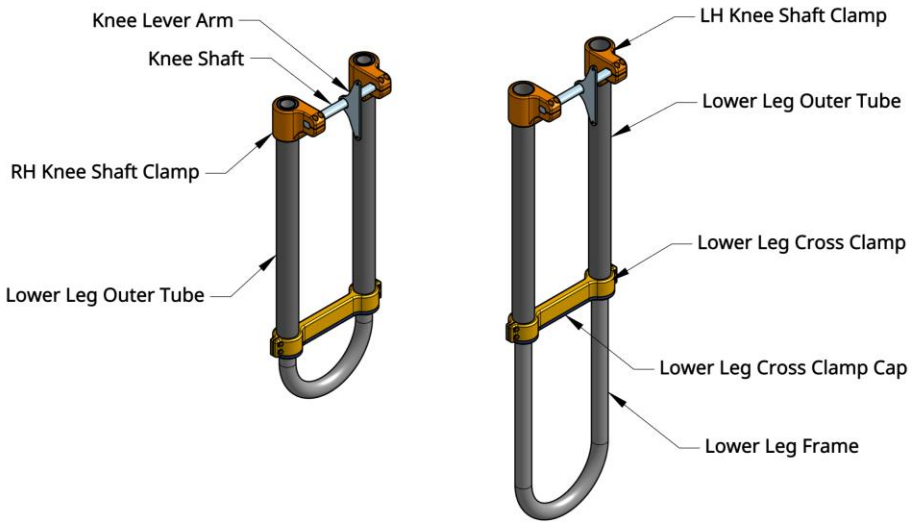

Figure 16 - Dual stanchion 1DOF prismatic joint at tibia - retracted (left), extended (right), foot pad removed

The one-piece stanchion is fabricated from a single tube, bent 180 degrees to form the dual stanchion trombone-like shape. This creates a robust, one-piece fully sealed lower extension member that is simple to manufacture. The open ends have tube-sealing elements rigidly affixed, which insert into the outer barrels to create a cylindrical seal. By varying the volume and pressure in the enclosed chambers, linear motion is enabled. A capping assembly prevent separation at end of stroke.

Insect morphology often use a series of passive tarsus joints to achieve compliance and superior ground contact. The proposed u-shaped design creates an elegant and passively

variable-cross-section ground contact solution with a rounded engagement surface. The rounded surface assist in liberating the degree of freedom added at the hip joint. This allows exploration of a hybrid gate with a rocking foot motion versus a basic lift-and-swing leg motion. A pointed type foot would introduce added torques at the ground contact point introducing added compaction and the creation of open holes in the soil.

Additionally, a pointed or constant cross-sectional profile foot penetrates the soil until enough soil compaction occurs below the foot to supply the restoring force that prevents further penetration. While effective at supplying support, this approach increases sub-soil compaction and is inefficient as the compaction process is non-conservative.

Unlike a peg foot, the proposed u-shaped design increases the contact patch surface area with increasing penetration depth, spreading the load over a larger soil surface area, reducing subsoil compaction. The results of a study of the variation in penetration depth with tube diameter shows that for the base 300 kg mass distributed evenly over four of the six legs, the proposed tube diameter of 50 mm does not meet the base requirements until 85 mm of penetration has occurred.

Data for various tube diameters as well as a rounded ball shaped foot pad is presented below.

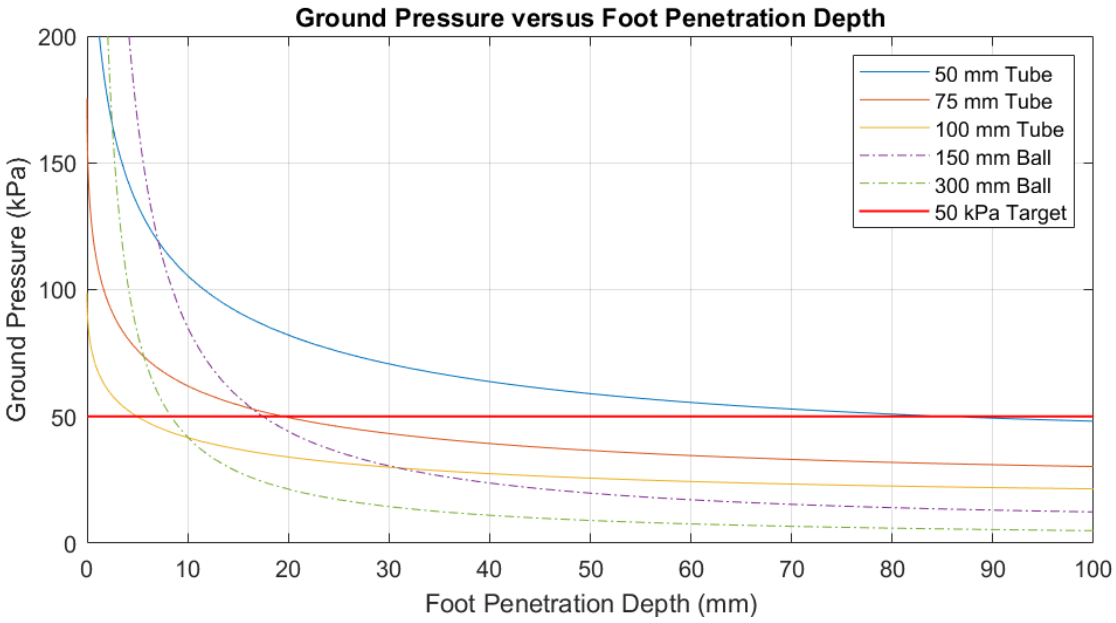

Figure 17 - Variation in ground pressure for various pad profiles, for a max device load of 300 kg, spread over 4 legs

However, increasing tube diameter negatively affects tibia mass. An alternative solution is to wrap or enclose the tube base in a larger diameter foot pad, increasing the surface area, while keeping the variable profile design and rounded contact surface.

Removable pads of differing shape, size and material allows the device to adapt to suit the traction and ground pressure requirements of any particular use case. Specifying a rounded ball shaped pad that increases surface area at more than twice the rate of the u-shaped design achieves ultra low ground pressure with minimal depth.

Figure 18 - Side and isometric view of the optional molded foot pad - 300 mm diameter profile

HDPE as the preferred pad fabrication material owing to its durability and recyclability. In hard packed surface conditions significant shock load shock load during leg placements negatively affects device longevity. Specifying a softer material with elastomeric properties provides the necessary cushioning, at the expense of decreased durability.

If foot pad selection does not provide sufficient cushioning, shock load attenuation is also achievable by modulating the entrained air accumulation inside the active portion of the cylinder chambers. This reduces the effective bulk modulus. Xiang et al. investigate a variable stiffness actuator that leverages both hydraulic and pneumatic operating modes [25]. This air spring mechanism is achieved by the insertion of two flexible, sealed air bladders, one inside each cylinder chamber of a given leg module.

Pre-setting the volume and pressure of the compressible bladders achieves a predictable compression rate. This reduces the shock loads experienced during ground contact, passively reducing wear across the entire device. Development of this subsystem is left as future work to be undertaken with the overall leg module dynamic analysis.

3.3 P.1.2 APPROPRIATE SELECTION OF WATER BASED HYDRAULIC ACTUATORS

The application specifies water as the process fluid, which presents unique challenges and opportunities. A review of potential actuator types suitable for use with water addressed the design guidelines of reduced complexity and mass, versus the standard hydraulic cylinder.

Many applications use hydraulic oil as a power transfer fluid. The dominating motivation for the selection of water as the power transfer fluid was the to synergistically use the readily available pressurized irrigation networks that already exist in the agricultural domain. However, there are many other benefits to using water in place of mineral oils, some which directly address additional key design guidelines.

- Environmentally benign
- Non-flammable
- Low cost (currently)
- Ubiquitously available in the agriculture domain (currently, but declining)
- Easily stored and disposed of
- Multi-purpose in agriculture
    - Irrigation
    - High pressure jets used for weed suppression and soil penetration
    - Steam for weed suppression
    - Icing (used for crop protection – citrus fruit)
    - Power transmission fluid (irrigation pivots and reels)
- High bulk modulus – 38% greater than mineral oils
- Low viscosity – 1/3 that of mineral oil at 50 C
- High specific heat capacity

However, there are some challenges to using water as a power transfer fluid as well.

- Poor lubrication properties
- Freezes under common environmental conditions

- Expands when frozen – causing damage if rigidly constrained
- Water hammer effect – result of high bulk modulus

The investigation into a suitable actuator to leverage the advantages of water started with the simplest and most common of hydraulic actuators and due to a mismatch in characteristics, examination of several types of non-rigid actuators was also considered.

The design converged to use a simple prismatic cylinder for one application and a McKibben style actuator for others. The prismatic joint was ideally suited for the lower tibia extension joint, providing a mechanism to change the overall ground clearance. Whereas, the PAM/HAM device was selected for actuation of the knee and hip joints due to its simplicity and ability to deliver high tensile loads directly to the joints.

3.3.1 SIMPLE PRISMATIC HYDRAULIC CYLINDER

One of the simplest and most common fluid driven actuators is the two-part cylinder, extensively used in both pneumatic and hydraulic applications. Given the design constraint of using the liquid water from irrigation systems, the focus will be on hydraulic applications.

The simple hydraulic cylinder consists of two main parts, the outer pressure constraining barrel and the inner translating rod, together forming a cylindrical prismatic joint. Fluid under pressure is introduced inside the barrel on one side of the piston and exerts a force on the piston face proportional to the face surface area and fluid pressure, which in turn drives the rod out of the barrel, affecting a linear motion. Fluid is prevented from bypassing the piston face by a close fit between the translating parts and supporting piston seals. The maximum force F_{rod}, produced by this type of actuator is determined by the operating pressure $P_{cylinder}$, of the hydraulic fluid and the wetted surface area $A_{plunger}$, of the cylinder plunger.

$$F_{rod} = P_{cylinder} \cdot A_{plunger} \quad [5]$$

Frequently, a return spring is mounted inside the barrel on the non-wetted side of the piston to enable the return stroke. The spring force between the non-wetted barrel end and the backside of the piston face, reverses the direction of travel. Or alternatively, a double-

acting cylinder can be used. In this more complex device, fluid pressure can also be introduced inside the barrel on the opposite side of the piston face, reversing the direction of force application.

The lower limb tarsus joint uses the simpler, single-acting design, oriented vertically, with the rod positioned below the barrel. When the port opens to the high-pressure manifold, water flows into the chamber and drives the twin rods out of the twin barrels, downwards, lifting the robot away from the ground. Retraction occurs when the port to the low-pressure manifold opens, releasing the fluid pressure inside the cylinder. The weight of the robot presses the rod back into the barrel, reversing the fluid flow. When the valve is in the closed position, a hydraulic lock exists, restricting fluid flow and therefore rod motion, not withstanding the compressibility of the fluid and any entrained air.

This gravity-based retraction method removes the need for a return spring or the implementation of a double-acting cylinder. Springs add unnecessary mass and double-acting cylinders require tighter fabrication tolerances, added seals and flow control devices. The single-acting, gravity retraction configuration meets two overarching design guidelines; minimize mass and complexity.

The dual stanchion design with an inner diameter of 50 mm creates a net surface area of 3927 mm^2 per leg. At the lowest operation pressure of 2 bar, this generates a lifting force of 785 N, per leg. The limiting case occurs when four legs are in contact with the ground, supporting a mass of 300 kg, evenly distributed over the four legs. For this case, the force required from each leg is only 736N. This joint design provides sufficient lifting forces across the application pressure range.

This actuator type suits the lower tibia joint as the forces required are in the 10^3 N range and are low compared to those required to work the tendon-controlled joints of the knee and hip. Here, the tendon loads required are in the 10^4 N range. These joints would require significantly larger diameter cylinders to achieve suitable performance, with increases in mass from the additional cylinder materials and process fluids required.

Lastly, the simple single-acting cylinder generates compressive axial forces, while tendon driven joints required tensile forces. If a reverse-acting cylinder is specified, the issues of

increased mass are worsened by the reduction in the effective wetted surface area caused by the presence of rod in the backside of the chamber. Owing to these shortcomings, the common hydraulic cylinder is poorly suited to the tendon-based joints and other actuator types were investigated.

3.3.2 OTHER HYDRAULIC ACTUATOR TYPES

The hydraulic cylinder is common actuation device used in industrial and robotic equipment across a wide range of applications and scales. However, a new class of flexible actuators has seen increasing development in recent years. Yan et al provide an excellent review of the variety of flexible actuators where they also propose a novel high-displacement embodiment [26].

They differentiate flexible actuators by their operation mode and pressurization state, where operation mode is either contraction or expansion and pressurization state is either vacuum or positive pressure, as shown below.

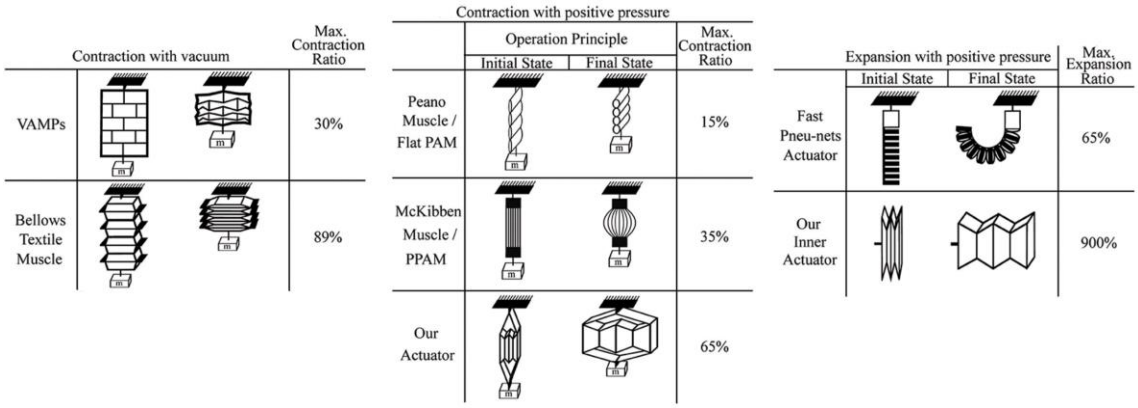

Figure 19 - Types of flexible hydraulic actuators. Adapted from Yang [26]

This review highlighted the range of actuator types to investigate. Many of the actuators listed are not suitable for the current application. Expansion type actuators do not match our tendon driven approach and vacuum based actuators do not match the irrigation pressure-based application at hand. This leaves the three sub-classes of actuators using positive pressure that generate a contractile force.

The Peano muscle [27] has an unsuitably low contraction rate and relies on 3D printing techniques to simplify its manufacture also unsuitable for the expected pressure regime.

The high contraction rate of Yang's novel high-displacement actuator is appealing, however, the complexity of design and the large final volume of the contracted shape results in large masses when used with liquid phase fluids. The remaining design choice, the McKibben actuator, offers a compact morphology and is widely studied and applied and was selected for further research and refinement.

3.3.3 MCKIBBEN TYPE ACTUATOR – SIMPLE STATIC MODELLING

The invention of the McKibben type actuator is credited to Richard H. Gaylord (1958) but was made popular by physicist Dr. Joseph McKibben. He envisioned the concept as a lightweight actuator to aid his disabled daughter afflicted by polio. Commonly referred to as the McKibben Artificial Muscle, Braided Pneumatic Actuator (BPA) or more recently as the Pneumatically/Hydraulically Actuated Muscle (PAM/HAM) in the literature. Non-pneumatic applications are increasingly more common in robotic applications and HAM will be used to reference a McKibben type actuator for the remainder of this document.

The concept and construction are simple and is composed of two key elements; a flexible bladder contained inside a double-helix braided sheath. When the inner bladder inflates, it expands circumferentially which also causes the braided sheath to expand radially, however, the braid also causes it to contract axially. The diagram below illustrates the mechanism of contraction which occurs as a result of the fixed length of the helical braid threads and the change in angle with respect to the central axis upon inflation to a larger outside tube diameter.

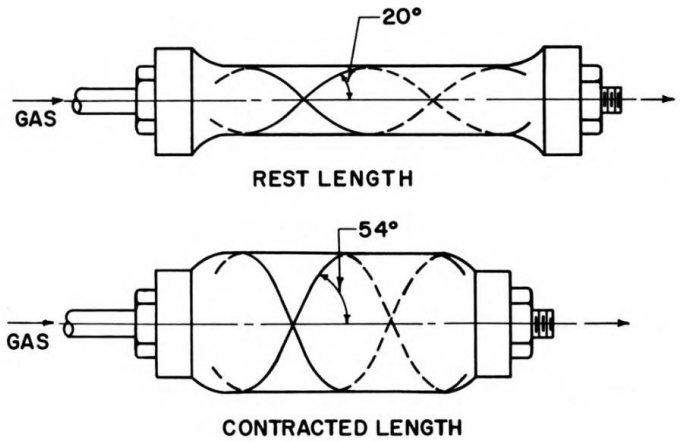

Figure 20 - McKibben type actuator operating concept. Adapted from Schulte [28]

While a variety of high-fidelity actuator response models exist for the HAM, a simplified model is sufficient for concept design validation. Additionally, Robinson et al. note that accuracy of most physical models is poor at lower pressures owing to the pressure deadband effect [29]. As the irrigation pressure domain is quite low, improved models of overall actuator performance will be developed in future work.

While HAM's are a compact, flexible actuators that are simple to construct and implement, the complexity of modelling their highly non-linear behaviour must also be considered. The challenge in developing exact models that predict behaviour makes control system design critical. Much work has been completed to consider the tapering of the terminus [30], the non-zero thickness of actuator layers [31], hysteresis [31]–[33] , sheath fibre elongation [34] and fatigue life [35], [36]. These works will be instructive to refine static and dynamic modelling ahead of control systems research. As the device is constrained to operate at very slow speed initially, a strictly static mechanical analysis is used during this initial conceptual design phase.

The actuator is geometrically modelled following the work of Chou and Hannaford [31] as a cylinder of length L and diameter D. In our simplified model, wall thickness is assumed to be zero and the outer braided threads inextensible. With these constraints in place, the system constants are the thread length b, the number of turns a single thread makes about the cylinder and θ, the interweave angle between the thread and the primary cylinder axis. This relationship is presented below.

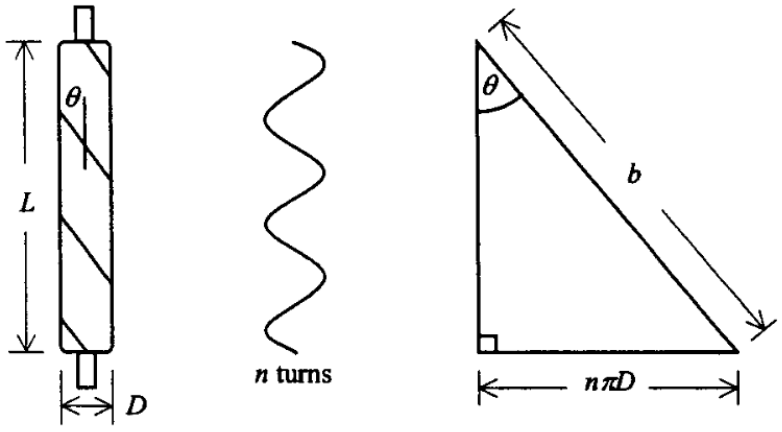

Figure 21 - Geometric relationship of a simple McKibben type actuator. Adapted from Colbrunn [37]

The relationships between the geometric parameters is as follows:

$$L = b\cos\theta \quad [6]$$

$$D = \frac{b\sin\theta}{n\pi} \quad [7]$$

Chou and Hannaford developed an equation that relates the actuator force F, as a function of the geometric parameters and P, the internal pressure. In addition to the assumptions presented above, this model also assumes no tapering at the cylinder end points, neglects any potential energy effects of the stretching of the inner bladder and neglects any Coulomb friction between actuator materials.

$$F = \frac{Pb^2(3\cos^2\theta - 1)}{4\pi n^2} \quad [8]$$

In this simplified model, tension is linearly proportional to pressure and in a monotonic function of θ. This angle can theoretically range from 0 to 90°, however in practice the smallest angle of 20° is common in commercially available weaves, and that F reaches a minimum when $\theta = 54.7°$. This limits the usable range of the actuator.

As θ is often challenging to measure, this is the available force is also expressed as a function of P, b, n and L as follows:

$$F = \frac{Pb^2}{4\pi n^2}\left(\frac{3L^2}{b^2} - 1\right) \quad [9]$$

A strain rate, ε is defined for the actuator as follows, where L_0 is the initial cylinder length and L is the contracted length:

$$\varepsilon = \frac{L_0 - L}{L_0} \quad [10]$$

With this relationship, one can examine the force potential of a given actuator construction and geometry, across the operation pressure range. In his review of PAM/HAM actuator modelling, Tondu [38] presents a relationship that expresses force as a function of initial diameter d_0, and thread angle θ_0, as geometric constants, for a given pressure and strain rate.

$$F_{ideal}(d_0, P, \theta_0, \varepsilon) = \left(\frac{\pi}{4} \cdot d_0^2\right) \cdot P \cdot \left(\left(\frac{3}{tan{\theta_0}^2}\right) \cdot (1-\varepsilon)^2 - \left(\frac{1}{sin\ {\theta_0}^2}\right)\right) \quad [11]$$

The actuator length can instead be determined by the required actuation moments for a given joint geometry. The relevance of this relationship to the overall design is explored in later sections.

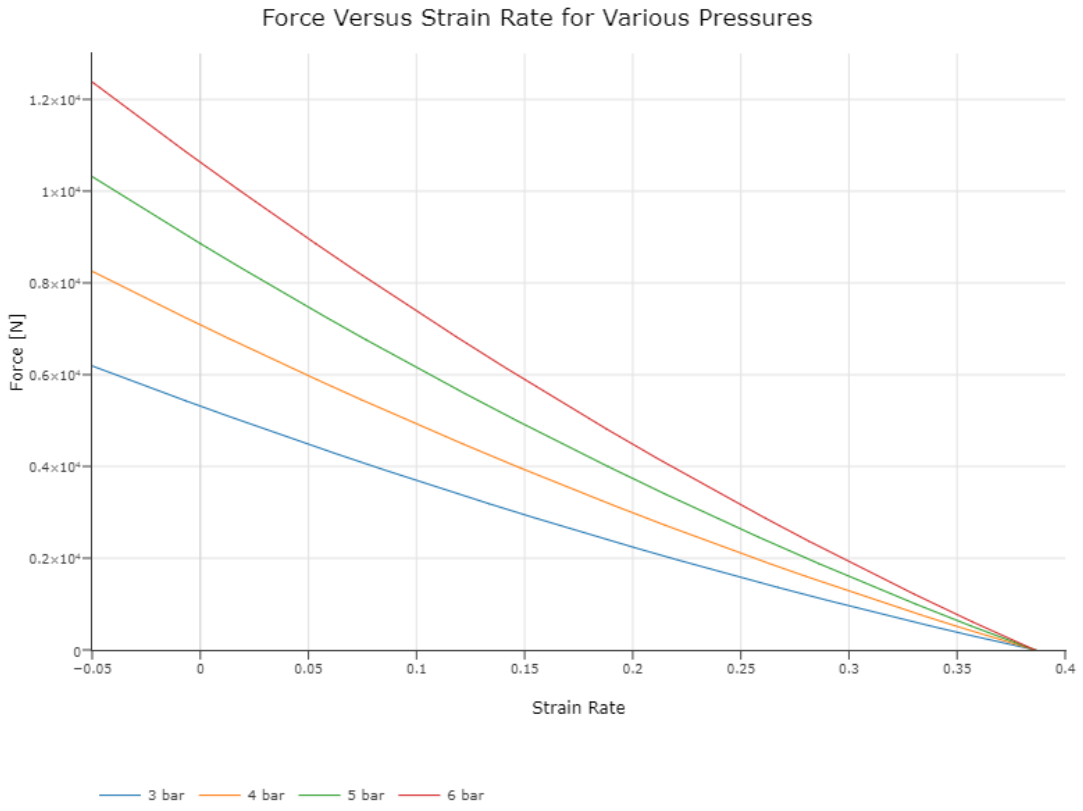

Figure 22 - Exploring the force potential across the strain rate of a nominal 40mm diameter actuator with a relaxed thread angle of 20 degrees for pressures ranging from 3 to 6 bar

For the nominal actuator design parameters of $d_0 = 40mm$, $\theta_0 = 20°$ and a range of expected irrigation system pressures, P from 3 to 6 bar, are plotted in the above chart for the force versus strain rates, ε, independent of actuator length.

3.3.4 MCKIBBEN TYPE ACTUATOR – CONSTRUCTION AND OPERATION

The McKibben type design was explored at length along with orthopaedic applications by Schulte, Adamski and Pearson in their 1961 book on the topic [28]. In its simplest form, the actuator is constructed by mounting a flexible tube inside a braided tube and adding a

plug at either end to create a closed volume. The plugs close the tube volume but also provide mechanical mounting and convenient locations for ports to introduce compressed fluids. Rubber is commonly used for the inner tube owing to its low modulus of elasticity, whereas the double-helix braided tube is often constructed from nylon fibres, or other materials selected for their high strength and low strain rates.

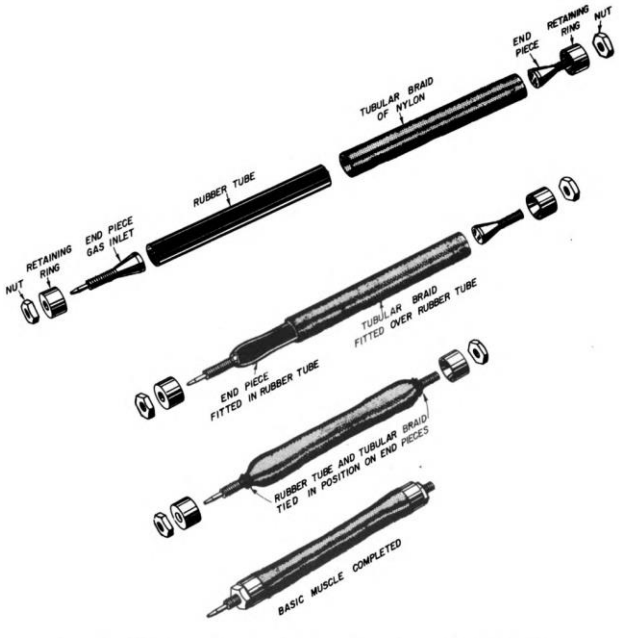

Figure 23 - Construction of a simple actuator. Adapted from Schulte [28]

One other recent development deserves mention. Yi et al. propose a novel class of actuator that uses an origamically folded inner bladder [39]. This device removes the elastic tensile hose from the center of the HAM and replaces it with a folded structure that expands radially and contracts axially when pressurized. This has the advantage of removing the pressure exerted axially outward on the end caps, which reduces the overall tensile forces developed. This, along with the work required to inflate an elastic bladder, results in strain rates of 50% with significantly less internal pressure to develop a similar tensile load. The 3D printed structures are, unfortunately, not able to contain the pressures that are required, nor was any research found using them as a HAM. While promising, this HAM actuator was not considered for application here.

Early PAM concepts had longevity issues. Primarily coming from two sources; inter layer friction and stress concentrations at their terminuses. Both of these challenges have now

been suitably addressed and maximum lifetimes of 1.2 x 10^8 cycles have been reported in the literature [36].

Interlayer friction, primarily the braid effects, are well studied. Davis [40] notes that controlling the contact between braid elements is critical. He found that by halving the number of strands improvements in both contractile range and peak force were achieved. Durability enhancements are also attained by embedding the sheath fibres directly in the flexible membrane matrix, eliminating both the friction between threads but also the friction between the bladder and the threads. This technology is widely available and commercially produced from Festo Corp.

The second significant technological advancement (also employed in the FESTO range of products) is swaging of the terminuses. This advancement provided for a more homogenous distribution of forces at the boundary between flexible and rigid components [36]. The techniques employed by Woods are commercially available, and actuators using this approach can also be uniquely fabricated to meet any given application.

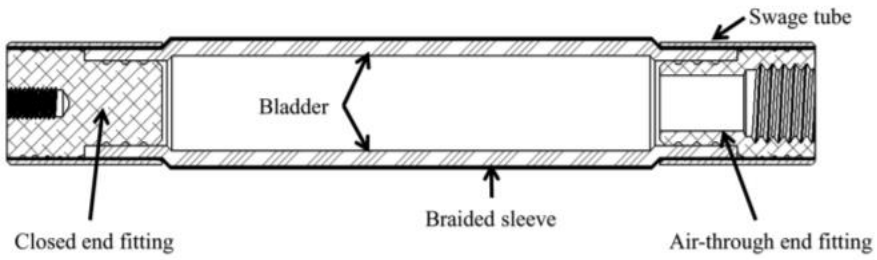

Figure 24 - Cross section view of swaged end fittings. Adapted from Woods [36]

One frequent implementation of the HAM, and one that is proposed in this work, is as antagonistic pairs. This arrangement follows our design guideline of leveraging bio-memetics. This configuration is found across a wide range of biological systems. A common example of this agonist-antagonist pairing is the human biceps/triceps muscles which actuate the elbow, a simple revolute joint, achieving a range of angular displacement exceeding 160°.

The HAM is well suited to the antagonistic pair application. Backlash is zero as both actuators stay in constant tension. The torque applied to the joint is the summation of the moments applied by each counterposed actuator. These applied moments are the product

of radius of the joint and the tensile force developed in each actuator. This principle is also applicable to the 3DOF compact spherical joint, except that the 3D joint torque is a vector sum of the four applied tensile forces acting tangent to the surface of the constant radius ball at insertion and origin points.

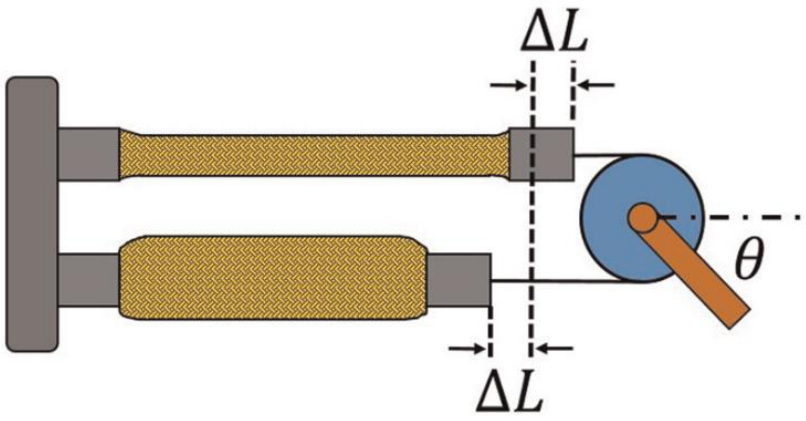

Figure 25 - A tendon driven revolute joint actuated by an antagonistic pair of McKibben type actuators, where a reciprocal linear displacement of ΔL in each actuator results in an angular displacement θ at the pulley. Adapted from Robinson et al.[29]

Although there is a strong match between HAMs and the proposed application, some challenges exist. Some apply to the HAM overall, where other challenges are specific to the irrigation application.

HAMs have two key shortcomings. Force and contraction are inversely proportional, and they have a low overall strain rate, typically below 30%. Variable rate pulleys can be employed to compensate for the inverse proportionality. However, unlike many other actuators, where force is near constant across the range of motion, HAM tensile force decreases to zero as strain rate approaches 40%. This does not mesh well with the force requirements of many applications. As a result, the usable range of the actuator must be reduced to ensure that the actuator provides at least some load carrying capacity across the entire range of motion.

The use of irrigation water causes some specific challenges to the application of HAMs. Namely, the issue of entrained air degrading performance, where bulk modulus is strongly affected by even small volumes of entrained air. This actuator was envisioned as a pneumatic (PAM) where this is simply not an issue, however, the intention in this work is to use it hydraulically (HAM).

Additionally, the mass differential between air and water is significant. This affects static as well as dynamic loads. Even before assessing these, it makes sense to try to reduce the mass systemically, rather than provide structure and control methods to mitigate the impact. Design was directed to find methods to reduce and mitigate the excessive mass challenge of a HAM. These challenges and proposed solutions are presented in the following sections.

The final actuator configuration, used for all six of the joint actuators is shown below. A section view showing the internal components is also provided.

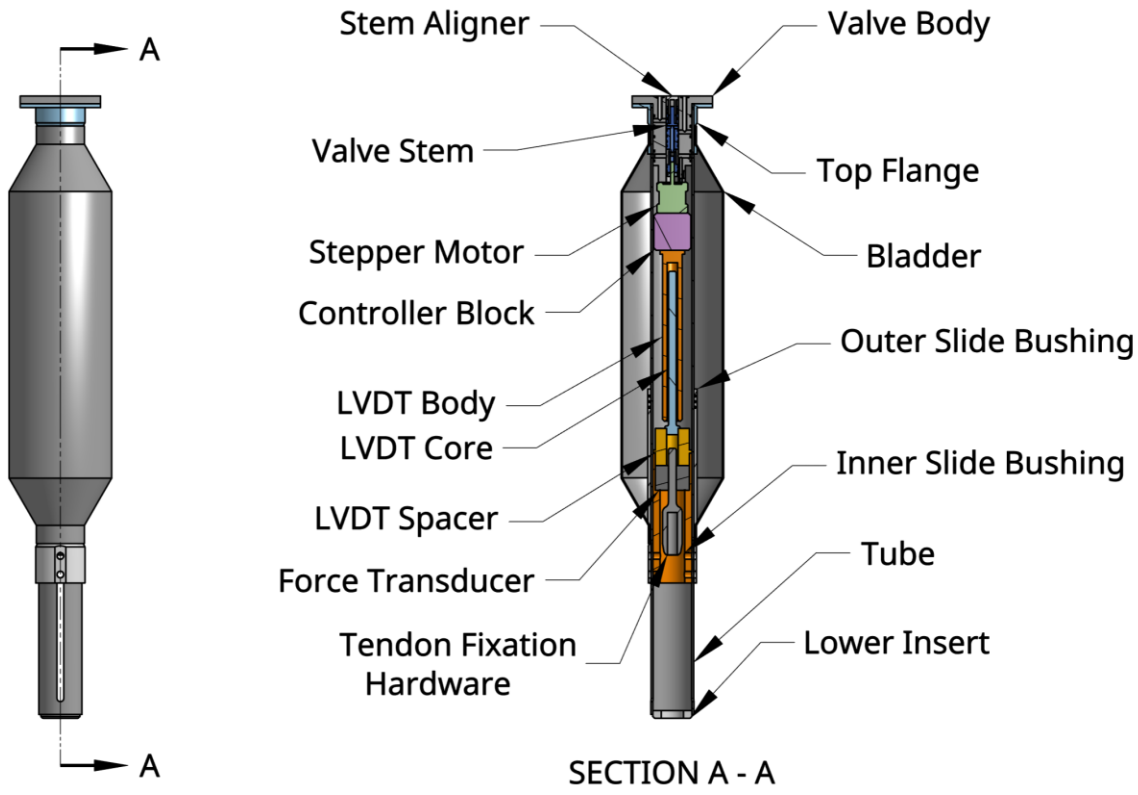

Figure 26 - Final actuator configuration showing internally mounted components. Tendon not shown.

3.3.5 P.1.2.1 – ENTRAINED AIR DEGRADES PERFORMANCE

There will inevitably be entrained air in any closed system that uses water as a process fluid. Irrigation water systems are susceptible to build up of pockets of air that negatively effect flow conditions. NRCS Conservation Practice Standard on Irrigation Pipelines recommend air release valves be installed on any irrigation pipeline.

There are two characteristics of gases that result in the same outcome: an unwelcome build up of gas phases in the process piping. As pressure drops, there is an increased quantity of gas species released from the liquid phase and an increased volume occupied by the gases released. These effects occur consistently as the operating pressures drop as fluid flows through the system during normal operation.

Both Nitrogen and Oxygen, the primary components of atmospheric air, are soluble in water. One can therefore expect irrigation fluids to be multi-phase mixtures, with a certain part of gas dissolved in the liquid phase. Henry's Law, states that the solubility of a gas, C, is directly proportional to the pressure, P, of that gas, where k is a species-specific constant.

$$C = kP_{gas} \quad [12]$$

An increase in the quantity of gas species as fluids flows through a decreasing pressure gradient is expected. Short of significant venturi effects, predicted by the Bernoulli equation, in our closed system, fluid will flow from areas of high pressure to progressively lower pressures until discharge, or re-pressurization. This is a fundamental enabling concept of hydraulic power systems.

The volume occupied by a given quantity of gas species in a mixture is related to the intrinsic properties of that gas mixture, and the temperature and pressure of that mixture. The relationship between the pressure, volume and temperature of a gas mixture is governed by the combined Boyle-Guy-Lussac gas law where a gas constant c, can be determined from experimentation for a given species using the following relationship.

$$c = \frac{PV}{T} \quad [13]$$

For a constant temperature T, as pressure P, decreases, the gas volume V, must increase for a fixed value of c. The volume of gas species is expected to increase as fluid flows through the hydraulic system, following the decreasing pressure gradient. As the volume increases, the gas phase will occupy larger pockets of system piping, displacing liquid volumes, resulting in several unwanted effects.

In the actuators the undesirable effect is a reduction in overall bulk modulus, and in piping systems, it is impeded fluid flow that is of most concern. According to our design principles, this challenge is preferentially addressed via a simple, low-mass and passive design.

As pressure drops, there is a commensurate increase of gas phase species coming out of solution which occurs as the flow passes through primary actuator control valve. This creates a continuous source of gas ‘production’ on every actuator cycle. These gases migrate and accumulate at the highest points of the enclosed volume. This can be in the actuators themselves, but also anywhere along the process piping. Two key accumulation areas are just after the main inlet pressure reducing value, and directly downstream of the primary actuator control value. If this constantly increasing volume of gas is not removed, a gas build occurs creating an unwanted decrease in bulk modulus. The variation of this key parameter increases the complexity of control, or in the extreme, can result in vapor lock conditions, where compartments of gas impede the desired liquid phase flow.

This issue can be addressed in three ways, with the most robust approach being a combination of all three avenues:

- Limiting gas phase creation,
- removing any gas phases created, or
- accommodating any gas phases produced.

Two key parameters to investigate are pressure and temperature. The design is constrained to use the available irrigation system pressure, and to achieve optimal efficiency, leveraging the entire pressure range is desirable. Increased actuator operating pressures has a positive impact on HAM performance. While increasing the system pressure locally before consumption by the actuators is used in many applications, the inclusion of additional pumping is not desirable owing to significant increases in components and systems design. However, this functionality may eventually be required to meet other design requirements. The additional complexity of a secondary pumping system, midstream, goes against our design guidelines of leveraging passive systems and minimizing complexity.

This is also the case with attempting to control the fluid temperature. While decreasing temperature would reduce overall gas volumes, this would require active temperature monitoring and control elements, resulting a more complex, active system.

Recirculation rate also contributes to accumulation of gas phases. While very uncommon in hydraulic systems, the proposed system specifically avoids (if possible) recirculation. Rather the process fluid is discharged to the environment after a single use. A 100% discharge rate effectively removes any accumulated gases. However, the need to operate the device without discharge is a plausible application scenario. This would necessitate either onboard storage to capture flow at discharge, an onboard recirculation pump or some form of reverse flow back to the supply system.

In the case of single-use-flow and pumped recirculation, a storage tank can be employed with atmospheric venting, eliminating the recirculation issue. In the case of reverse flow to the supply system, entrained air could potentially accumulate in locations upstream of the irrigation coupling point. Here the problem is transferred back to the supporting system and can be addressed via existing supply system venting mechanisms integral to irrigation piping systems.

Venting is a removal approach, and can be achieve passively, as in the case of venting to atmosphere from a drain tank, or actively in the case of venting midstream from pressurized systems. There are many options available to achieve venting from high points of gas accumulation in the system. Float valves are commonly employed as a semi-passive system, or solenoid operated valves can also be employed.

In our case, for a mobile device whose configuration and orientation can change during normal operation, minimizing of unvented volumes and creation of a reliable collection points for venting were two high potential methods reviewed. Two design elements using gas removal are proposed to address to this challenge and are presented in the following sections.

Finally, accommodation of gas phases was investigated. While there are some designs in the literature that leverage a hybrid pneumatic/hydraulic system for improved compliance [41], attempting to achieve this by controlling pocket volume would likely create

significant additional design constraints, that would not be required if effective reduction and elimination approaches are implemented. The lower tibia hydraulic cylinders could use this approach to provide cushioning. This approach could be investigated as a backup solution for the HAMs, in the case that the first two approaches are unsuccessful.

3.3.5.1 H.1.2.1A – DESIGNING FOR VERTICALLY ORIENTED ACTUATORS

One must consider and control the orientation of actuators and system components to create consistent locations for air accumulation. The design choice to cluster the long and thin HAMs together was motivated by the need for a reliable venting path. However, the actuator itself must assist in ensuring the orientation approach is successful by venting in as many of the expected actuator positions as possible.

The proposed actuator has a port located at the top of the actuator. Maintaining any position, other than tipped past horizontal, will provide a clear exit path for any accumulated gases, with one caveat. The internal spar removes the central volume but also the ability to provide a simple axial fluid port. Access to the bladder is more complicated than standard HAM configuration. A simple solution is proposed to alleviate this issue.

The fluid port is located on the hollow spar itself, as a series of circumferentially spaced ports penetrating from the open spar volume into the enclosed volume of the bladder. These ports are located as close as possible to the clamping surface that swages the bladder to the spar. Accommodations are required to prevent the bladder from sealing over the port during bladder outflow conditions.

The implementation of a ring of ports alleviates the issue when only a single port is used. When tipped from vertical, if the single port is on the underside of the spar, a high spot is created where gas can become trapped. The ring of ports ensures a venting path is always available, independent of the vertical cant angle of the actuator. A section view highlighting the circumferential locations of the actuator flow ports is shown below.

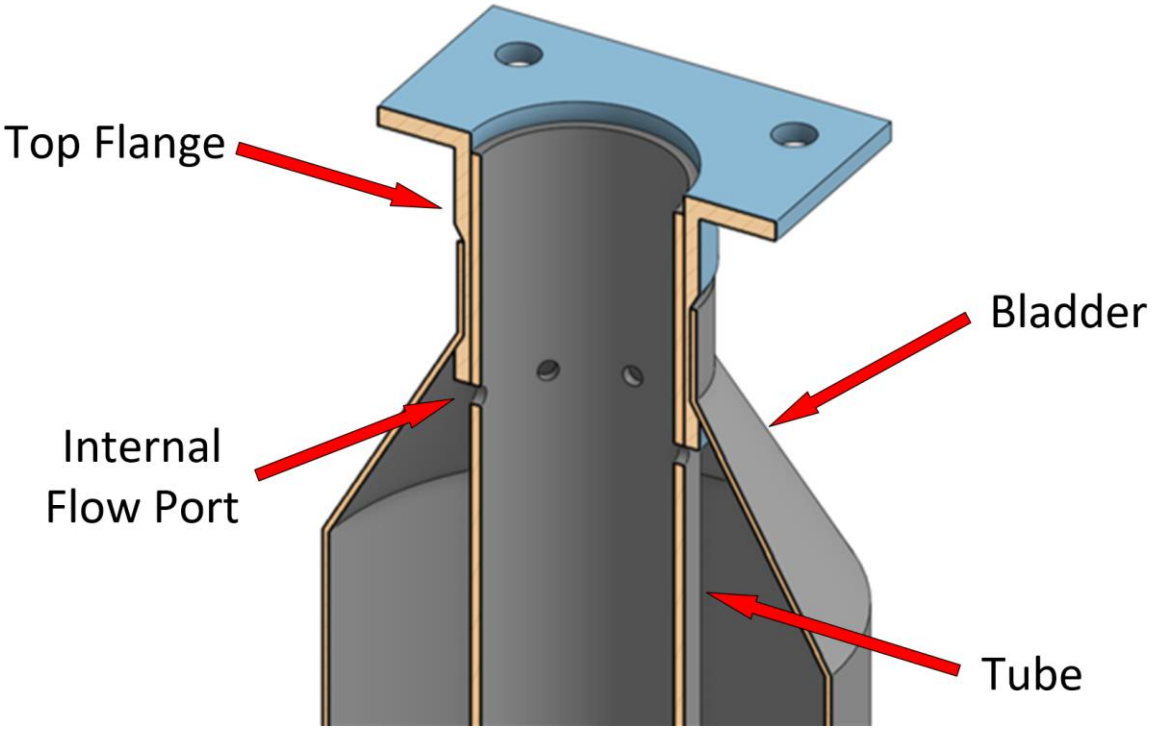

Figure 27 - Section view of actuator showing ring of multiple flow ports

This port configuration, coupled with the vertical orientation enabled by the clustering of actuators on the femur, implements and effective passive collection strategy. However, this open volume would allow for easy passage of gases up and out of the actuator, fluids would tend to run down the inner spar, conflicting with other design elements, namely the tendon attachment hardware. As such a valve stem, located internal to the spar, is proposed in the following section.

3.3.5.2 H.1.2.1B – INTERNAL PROXIMAL CONCENTRIC VALVE STEM

To facilitate the internal ring of fluid ports a concentric valve configuration is proposed. A close tolerance circular fitting is inserted into the top of the spar which contains a servo actuated valve stem. The fitting is sealed via a pair of O-rings, positioned directly above and below the ring of circumferential fluid ports. The fitting has a hollow circular chamber into which a valve stem is inserted. A servo mounted under the valve stem, also inside the spar, drives the valve between its three positions. O-rings seal the valve stem from below at the servo end. A manifold assembly caps the upper section of the value which connects the actuator to the service lines of the leg module.

The valve stem is a three-position device, with flow channels segmented along the top of the stem with O-rings. When the servo holds the valve stem in the middle position, flow is completely blocked. Pulling the valve stem down connects the actuator volume to the LP manifold port of the valve body, pushing the valve stem upwards connects it to the HP manifold of the valve body. In this way the actuator can be filled or drained from the HP an LP manifolds, respectively. The no-flow central position locks the actuator in place, and the compliance of the materials and the bulk modulus of the fluid permit negligible actuator motion.

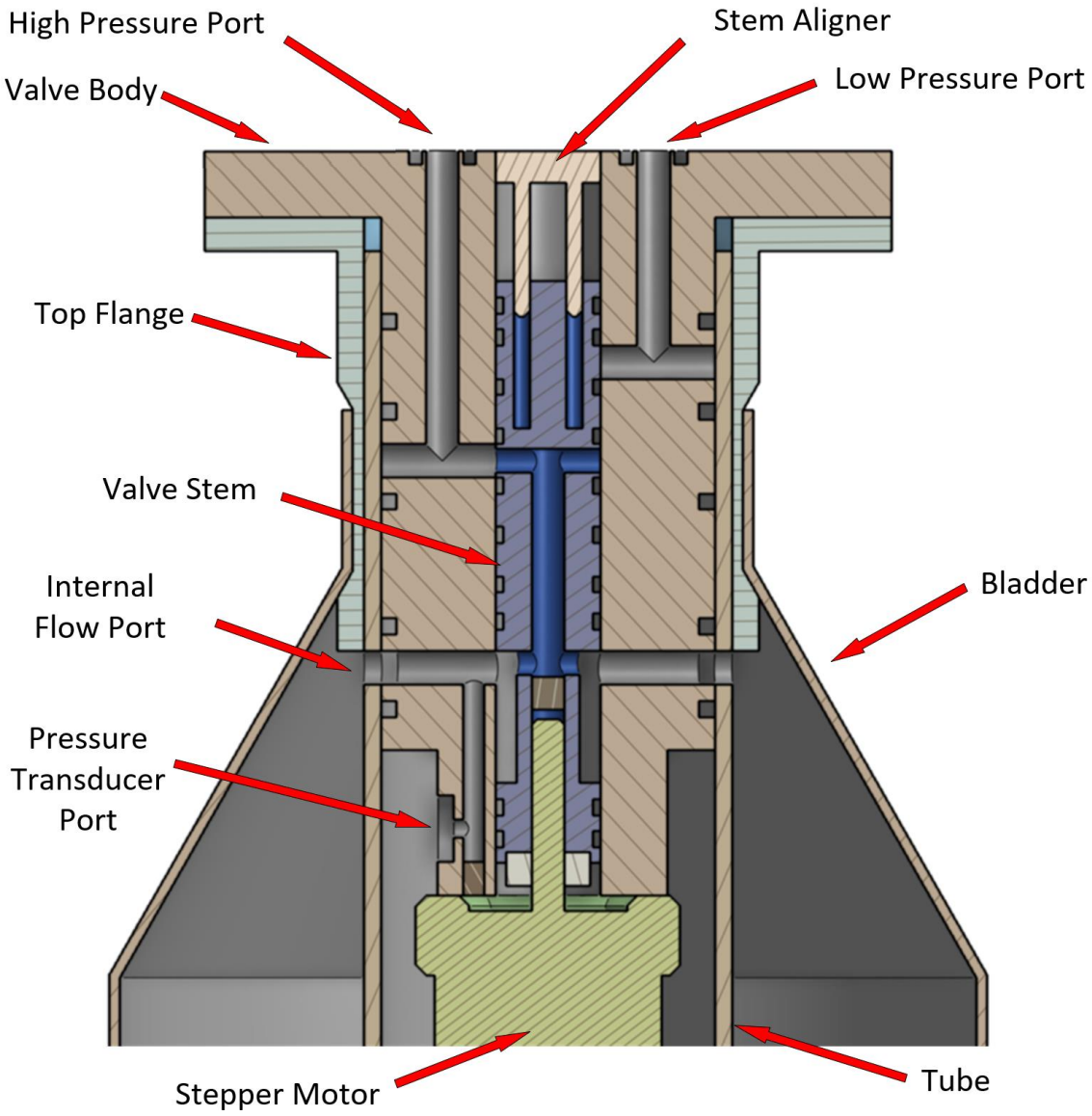

Figure 28 – Section view of proximal concentric valve stem, mounted inside spar. Valve body (pink), valve stem (dark blue and grey) and servo motor (light green)

By proximally locating the control value concentric to the actuator, the dead volume of the actuator is decreased, reducing the impact of bulk modulus effects as the overall active volume in minimized, when compared to a long run of piping between the actuator ports and the control valve. In addition to reduction of dead volume, this configuration also meets the synergy design constraint. The inner spar provides mechanical support, positioning and protection to the delicate value components, repurposing the wetted volume displaced by the spar. The narrow flow port created by this concentric valve design also reduces the axial pushout force on the valve stem and manifold connection. The surface area perpendicular to the longitudinal actuator axis is the small internal flow port, not the entire actuator base surface area, as is the typical case in HAMs, requiring a robust fitting and mounting arrangement.

3.3.6 P.1.2.2 – EXCESSIVE ACTUATOR MASS

The McKibben type actuator was envisioned as a pneumatic device. The mass of the gaseous process fluid comprises a tiny fraction of the overall actuator mass. When used hydraulically, the process fluid mass becomes non-negligible. Inspection of the operating principles of the actuator show that there is a significant volume of unexchanged wetted volume inside the actuator.

There exists some research and patented designs that recognizes this shortcoming and attempts to resolve it. Sato was issued a patent [42] in 1992 for a pneumatic actuator that contains two rigid, internal telescoping members that seeks to reduce the volume of pressurized fluid.

This has positive implications on dynamic response and energy loss between cycles when applied to a pneumatic actuator. Some of the benefits are not applicable in the hydraulic application. However, the decrease in mass that accompanies the removal of some pressurized fluid volume is useful in achieving our design guideline of optimizing material usage. Carrying less volume of water has cascading impacts across the entire device particularly via reduced ground pressure and joint torque requirements.

Our nominal actuator relaxed size is 40 mm diameter, full inflation is roughly 85 mm diameter, the actuator can be overstretched as well, reducing the overall diameter below

nominal value. This leaves 35 mm diameter of fluid volume remaining in the actuator even when at its lowest volume (full extension). This creates two unwanted conditions, inefficient use of mass and increased active volume worsening bulk modulus issues.

The ratio of mass reduction ranges from 18% to 77% from a fully inflated to a fully relaxed actuator. For an actuator at half-stroke, this is a per actuator mass reduction of 28%. Using a nominal 40 x 400 mm actuator and an overall estimated system mass of 300 kg, this results in ~5% reduction in system mass.

Zheng and Shen [43] proposes a double acting actuator design, modelled after Sato's translating sleeve design in a pneumatic application to increase performance. The sleeve reduces the effective end cap surface area at either end of the actuator. This eliminates much of the axial force developed by the bladder pressure that counteracts the tensile forces developed by the contracting outer weave.

Unlike Sato's design, which leaves the displaced volume open to the atmosphere, Zheng and Shen propose filling the volume with pressurized air to create a double-acting actuator. If used as a HAM, this doubling-acting design does not result in any mass reduction. While the tensile forces dwarf the extension forces developed, the author suggests some utility is provided in specific applications.

To guide the search for synergistic uses of the structure required to displace the unused wetted volume, other unrelated actuator characteristics were considered.

- Instrumentation requirements
    - Likely requires pressure, force and position sensors
- Tendon coupling and adjustment requirements
    - Need capacity to adjust the gross tendon length and provide static tension
    - Finite path length to transition from braided tendon to actuator terminus
    - Coupling point for a force transducer
- Valve and flow passage layout requirements
    - Actuator volume port at upper end of wetted volume

    - Minimize wetted volume between actuator port to control valves
    - Manifold attachment point for HP and LP flow lines
    - Three position spool valve (HP, blocked, LP)
    - Valve requires servo actuation
- Actuator load requirements
    - Need structure to support terminuses
    - Must support hydrostatic forces on unused wetted volume displaced
    - Minimize bending and torsional loads created by structure
- Operating requirements
    - Protect sensitive components
- Fabrication, assembly and maintenance requirements
    - Components must be accessible for inspection and replacement

After review of the diverse set of actuator specific requirements, a design hypothesis is proposed. A rigid, load bearing, hollow, tubular member concentrically placed inside the actuator would displace the required volume, provide well aligned axial support as well as create a usable space to mount many of the required ancillary components.

Two groups have worked on this concept in the past. Shen's group provided several papers of the double acting PAM [43]–[45] as well as applications. Cullinan et al. [46], [47] show several examples of using the rigid spar to convey the loads and term their version a Sleeve PAM. An image of their actuator, showing similar slotted arrangement to the proposed actuator is shown below.

Figure 29 - Partially contracted sleeve PAM with central slot and coaxial tendon. Adapted from Cullinan [46]

3.3.6.1 H.1.2.2 – CENTRAL LOAD BEARING SPAR

While an inert low-density space consuming component can be used to reduce the overall mass. A synergistic use of materials is proposed to create this void space and then use the space created to address several other design objectives.

The primary purpose of a HAM is to provide a linear tensile force. Some type of mechanical structure must displace the unused internal volume and withstand the hydrostatic pressure developed in the surrounding bladder. A rigid central spar supplies the structure to support the internally generated loads; compressive axial (tension) and radial compression (hydrostatic).

The proposed hollow cylindrical tube supplies the following functions:

- Displace unexchanged wetted volume
- Carry hydrostatic pressure (in compression)
- Carry axial compressive load generated by sheath contraction forces
- Carry externally applied loads – axial, bending and torsional

A section view of the basic structural spar, with mounting flanges is shown below.

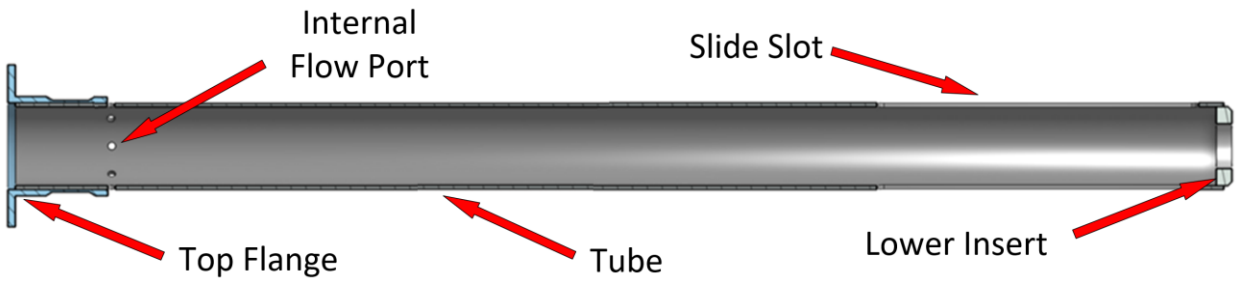

Figure 30 - Section view of proposed inner spar with mounting flanges attached, fluid port holes shown at one end

While these structural functions are helpful in achieving a synergistic design, implementing the central spar also adds to the complexity of the actuator design. A normal HAM is well sealed at both ends, often with a robust standard threaded port used to connect to process piping. The introduction of the central spar creates a sliding seal connection. This introduces a new wear part as well as an additional point of failure.

The section views below shows the layout of the central spar, the flanged ends, as well as the translating components which maintain the seal and transfer the load from the sheath to the central tendon. Also shown are the spool valve, servo, LVDT, force transducer and tendon fixture components.

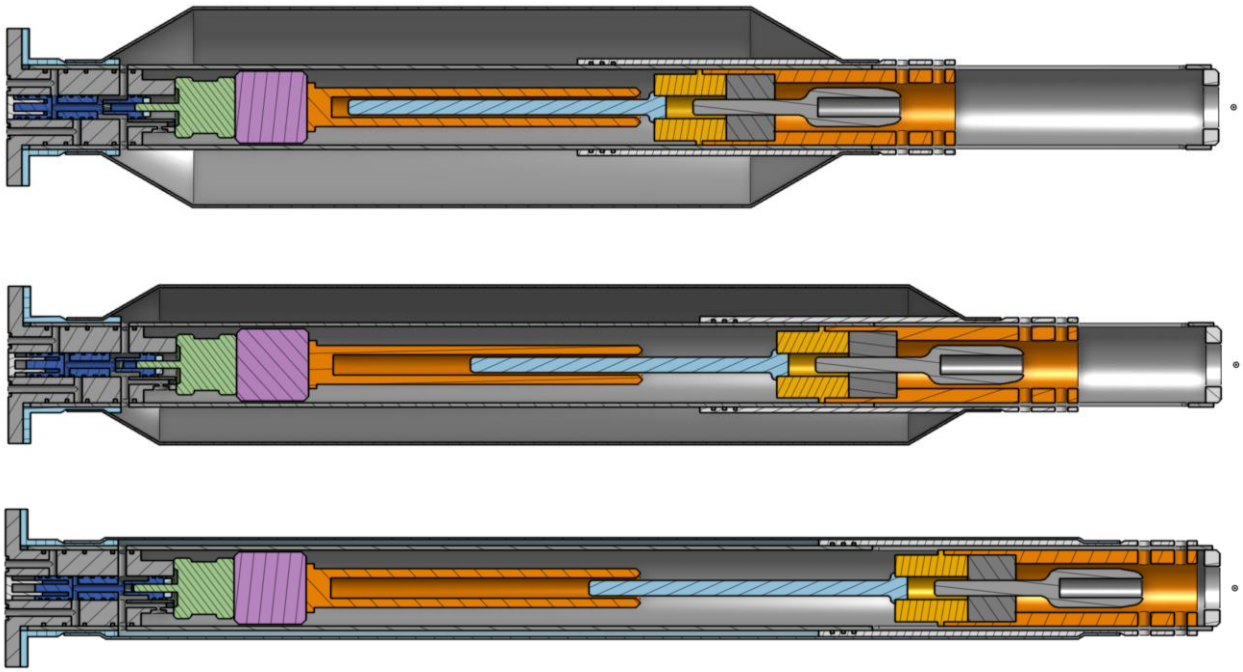

Figure 31 - Section view of proposed actuator showing internal components (top – fully contracted, HP port open; middle – partially contracted, port closed; bottom – relaxed, LP port open)

A standard, freely supported HAM has an unencumbered translating end, allowing tendon coupling directly on the central axis. With the introduction of the spar, this simple axial fixation is not possible and the load is aligned outside of the central axis. To avoid applying unwanted moments to the sliding parts, a symmetric or concentric attachment point is required around the spar circumference. The attachment points must be yoked into a single central tendon aligned with the actuator longitudinal axis. The need for this yoking increases the effective actuator length as the fixed end of the actuator is now positioned further away from the tendon terminus to allow for the finite distance to bridle together the separate tensile members.

To resolve this challenge, the sliding member on the outside of the spar rigidly couples to an inner sliding axial part that carries the central tendon. Fasteners to couple the pair of

sliding components pass through slots cut in the lower section of the spar. The two sliding components move in unison directly coupling the free end of the actuator to the single central tendon.

The outer sliding component is swage-connected to the free end of the bladder and extends up inside the bladder to allow sealing O-rings to be mounted inboard and away from the slots in the base of the spar.

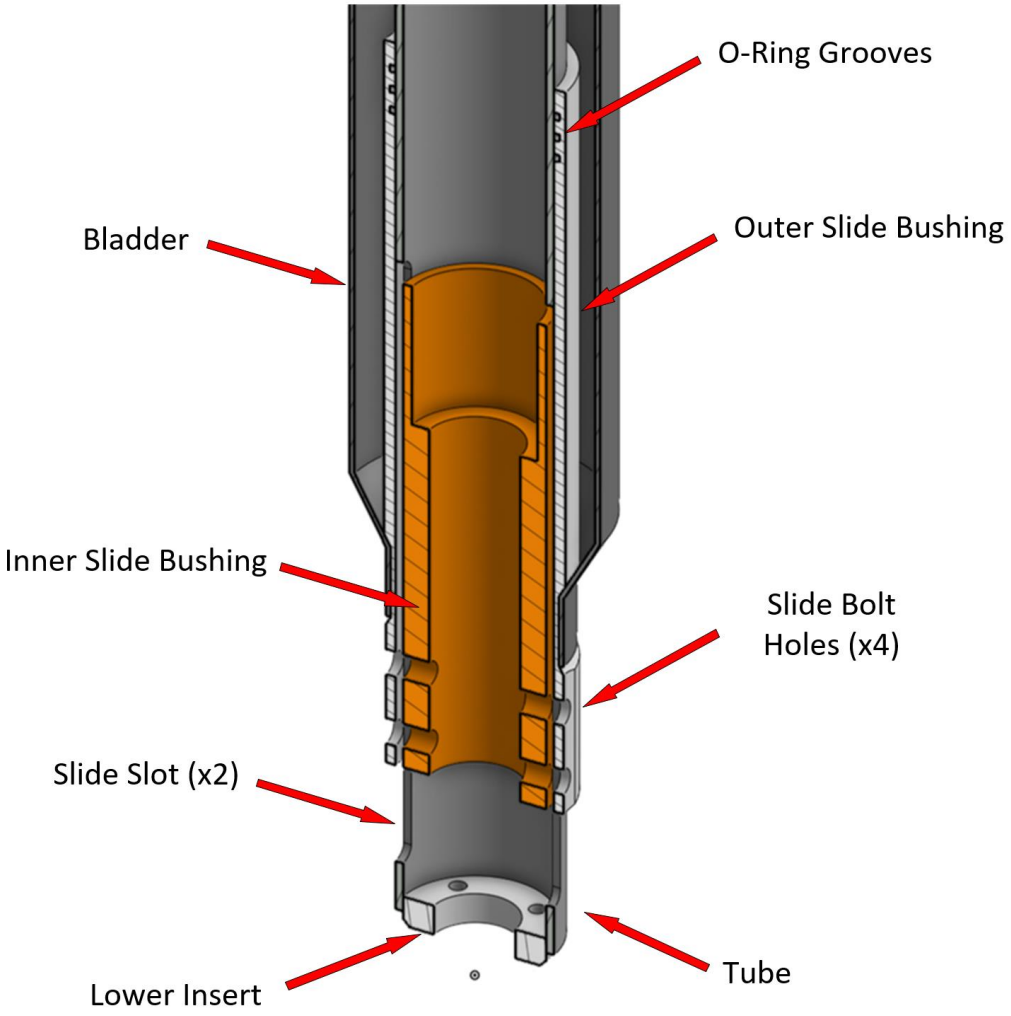

Figure 32 - Section view showing the sliding outer seal part (white) and the sliding inner tendon coupling part (orange)

Like the outer slide, the inner sliding member also extends up into the actuator body, inboard of the swage point. This inverted design creates added space for tendon hardware, making the overall actuator design more compact. This internal locating of tendon hardware is presented in a subsequent section.

The introduction of fluid port holes and slots along the length of the body could potentially compromise the structural integrity of the member. Basic FEA analysis was completed to calculate the Von Mises stresses for the proposed spar design. A design load of 10 kN was used, which corresponds to the peak tensile load of a 40 mm diameter actuator under 0.6 MPa hydrostatic pressure. A commercially available AISI 304 stainless-steel tube material at a nominal thickness of 1.65 mm is proposed.

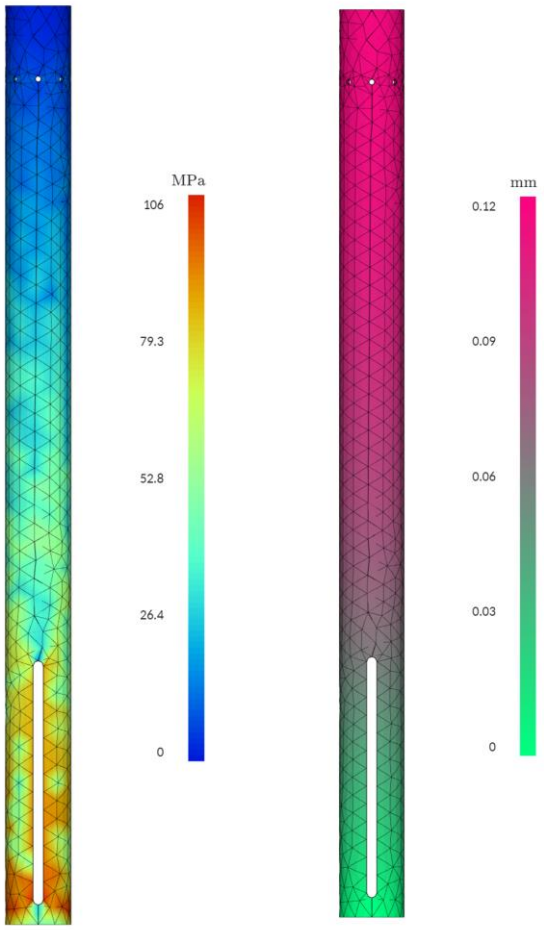

Figure 33 - Von Mises stress and displacement FEA results for AISI Type 304 stainless steel 1.65 mm wall thickness tubing

Von Mises stresses peaked at 106 MPa and a maximum deflection of 0.12 mm was observed. Stress concentrations are visible at the ends of the slots. However, stress levels are well below the yield stress of AISI Type 304 stainless steel (215 MPa) suggesting that this configuration and material selection could support additional externally applied axial, bending and torsional loads. This capacity is increased when several actuators by clustering several actuator spars together with end plates to form a multi-element structure.

This design addresses several other requirements, beyond the ability to carry internally developed and externally applied loads. The hollow internal spar supplies a convenient location for valving components, close to the actuator fluid ports, as well as the capacity to locate the tendon fixation point inside the actuator, reducing the overall actuator length. Synergistic design is realized in multiple areas for a water based HAM via the hollow spar and sleeving approach.

3.3.7 P.1.2.3 – ACTUATOR FORCE TO CONTRACTION INVERSELY PROPORTIONAL

A unique challenge of HAMs, introduced in earlier sections, was the inverse proportionality of contractile force to contraction length. The actuator provides maximum force at full extension, when the braid angle is low (~20°) and when the braid angle reaches 54.4°, the force is reduced to zero as beyond this angle, further radial expansion of the outer braid does not result in further axial contraction

Typical actuator applications do not have a demand profiles that tend to zero at one end of the range of motion. The availability of peak force at any point in the stroke of the actuator is a desirable characteristic. In the proposed device, the parallel nature of the mechanism provides joint actuation redundancy. Either the knee joint, or the hip joint could provide the necessary joint moments in the close chain linkage to support the mass of the thorax. The ability to easily add mechanical advantage at the knee joint motivated an actuation scheme where the dominant knee joint would supply the necessary torques to fully support the static device mass. The hip joints then are required only to stabilize the thorax orientation, supply forces parallel with the ground to affect movement as well as support legs when lifted and repositioned.

A load profile was evaluated for the knee joint, providing joint torque as a function of joint angle. Nominal design dimensions were used to assess the demand across the expected range of motion. A 900 mm tibia, a 600 mm femur, a 300 mm ground clearance and a thorax width of 300 mm were used along with 10 kg tibia mass, 20 kg femur mass, a 60 kg thorax mass and a 60 kg payload, both applied at the center of the thorax. The range of motion of the knee angle, β is between 0 and 90°. In practice 20 - 50° is the expected nominal range during most tasks.

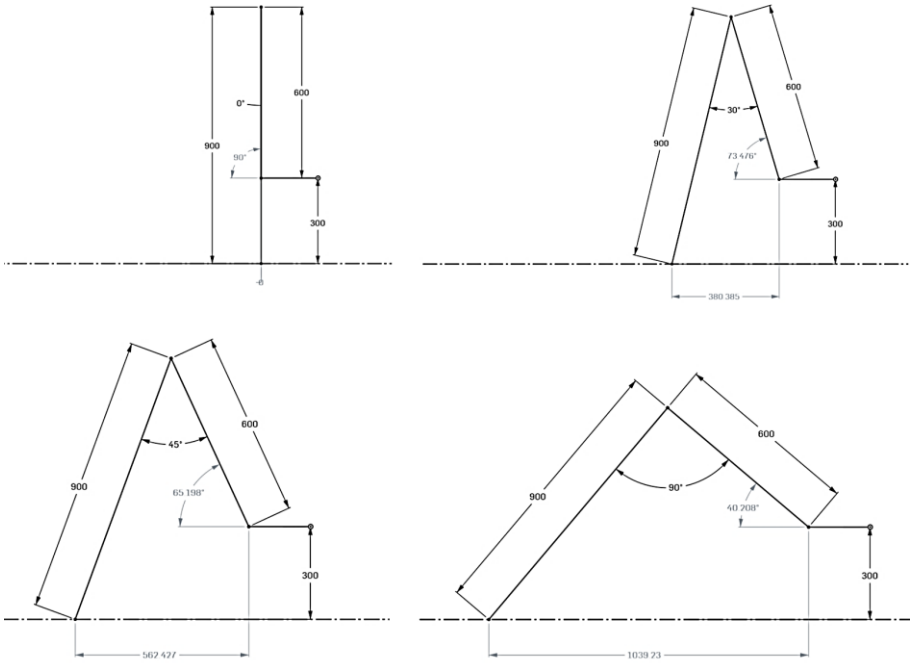

Figure 34 - Potential leg module range of motion. Top Left 0° : Top Right 30° : Bottom Left 45° : Bottom Right 90°

A simplified gait suffices for basic load analysis at the conceptual design stage. In this basic gate, a maximum of two legs are in the air at any given point, leaving four legs to support the thorax mass and the two suspended appendages. The robot moves by transferring weight onto four legs, then lifting and moving the two outboard legs on one side forward. Weight then transfers to other legs and the two outboard legs on the opposing side move forward. Lastly two central legs lift and the robot swings forward on the four outboard, ground-engaged legs and the process repeats.

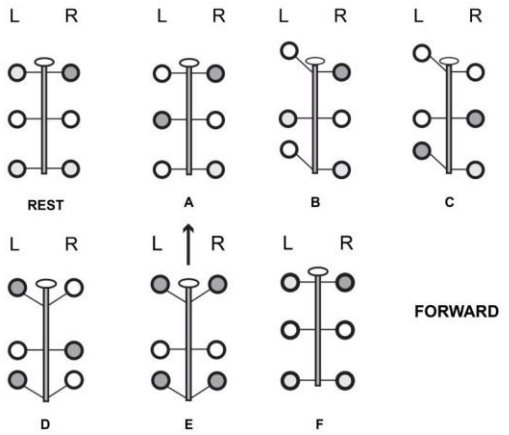

Figure 35 - Simplified hexapod gait – with a minimum of four legs supporting the total device mass

The joint geometry of the proposed device allows for significant range of motion, however, the loads to support the fringes of the available envelope put significant demands on the actuators, resulting in increase sizing to support these peak loads. Gait and load analysis using a reduced range of motion supplies a minimum viable motion. The outer ranges of the joint envelopes are exploitable using higher fluid pressures, either supplied or generated on board via a secondary pump.

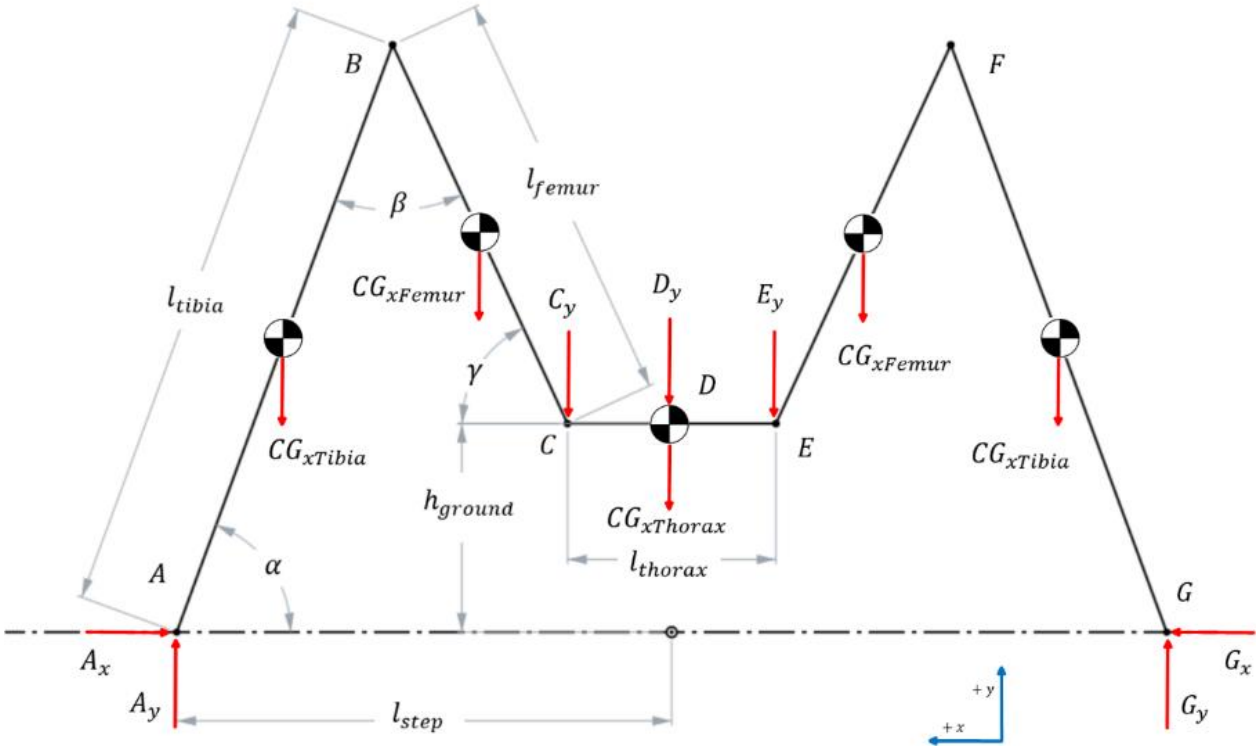

Figure 36 - FBD of the six-link closed actuator linkage, one of three identical pairs

The knee joint angle, β, ranges from zero to 60°, about the *z* axis, with typical operation in the 20 to 50° range. The hip joint has 90° of swing range, about the *y* axis, 60° of lifting motion, γ, about the *z* axis, with vertical being the upper boundary, and +/- 20°, about the *x* axis, the third rotational DOF.

The knee joint torque was evaluated across its range, for the dominant used case opening the knee joint wider (a negative moment about the *z* axis) using the nominal dimensions and mass of the proposed device. The joint torque ranges from 0 to a peak at approximately 70°. See the appendices for supporting calculations.

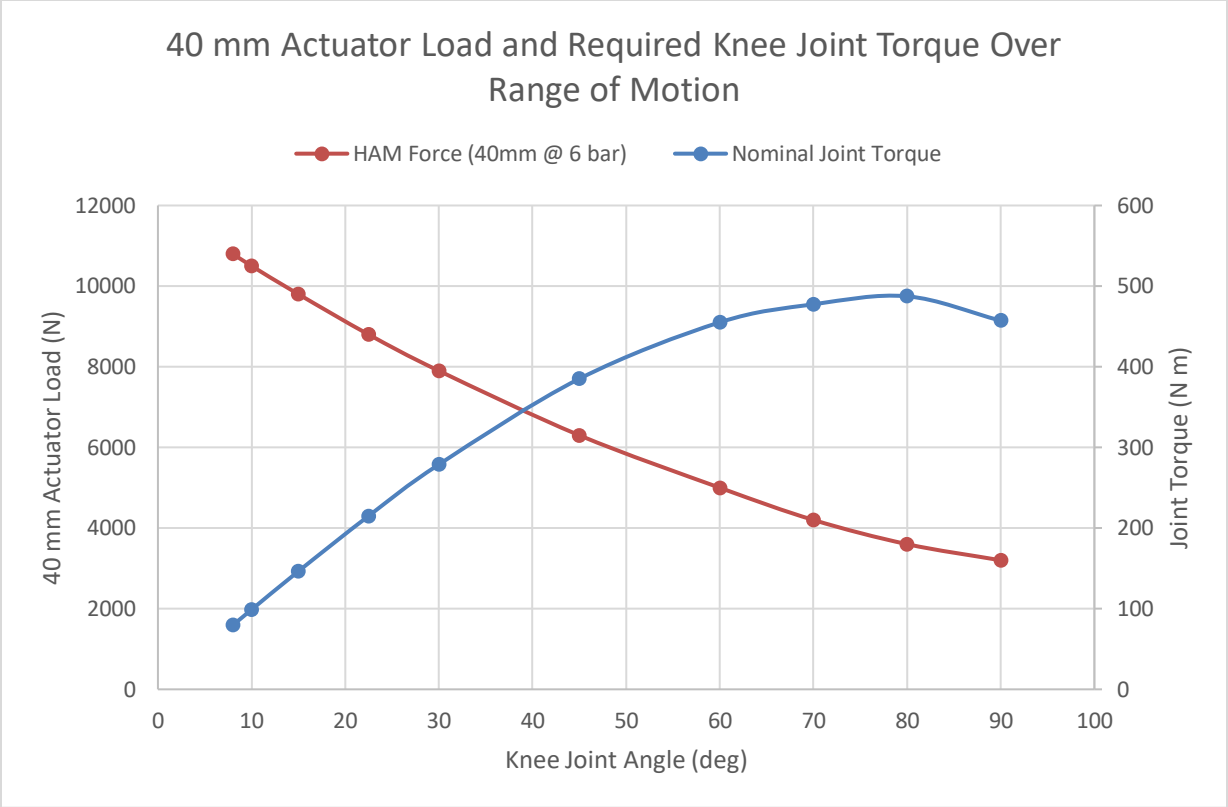

Figure 37 - Actuator Load compared with Joint Torque demand at knee joint

When compared to the load delivery curve of the HAM, the mismatch is obvious. HAM force decreases steadily with contraction as the joint rotates, yet joint torque increases as knee angle increases. To address mismatch a variable rate pulley at the knee joint is proposed and compared against a fixed diameter pulley and a simple lever arm linkage.

3.3.7.1 H.1.2.3 – VARIABLE RATE TENDON PULLEY

The decrease to zero force at full contraction is a challenging attribute of HAMs. To address this challenge, the range of motion of the HAM is limited to 25% strain rate to ensure the actuator can develop tensile forces across its entire range of motion. For the 40 x 400 mm nominal design, there is 100 mm of usable actuator travel. By adding some form of mechanical advantage between the actuator and joint, the applied torque can be varied to match the joint torque demands. Pulleys supply an excellent method to achieve mechanical advantage in tendon-based devices. A fixed-rate pulley was envisioned to supply the required gear ratio. An early stage concept is presented below, with a two-tendon HAM coupling configuration.

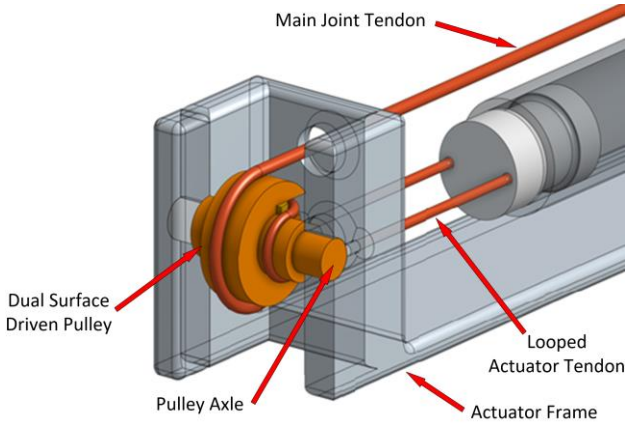

Figure 38 - Early stage integrated actuator pulley design

This composite pulley can couple dual tendons (a coupling technique briefly explored) to a single tendon and providing mechanical advantage at the same time, via the dissimilar running circumferences. However, the fixed gear ratio did not address the mismatch between knee joint torque and actuator load.

Variable rate pulleys could address the knee joint torque to actuator load mismatch. A variable rate pulley could easily be mounted on the knee cross shaft allowing mechanical advantage to be located directly at the joint. This is not workable for the hip joints as the intrinsically fixed radius of the spherical ball limits our ability to achieve a variable rate mechanical advantage; a secondary idler pulley is necessary.

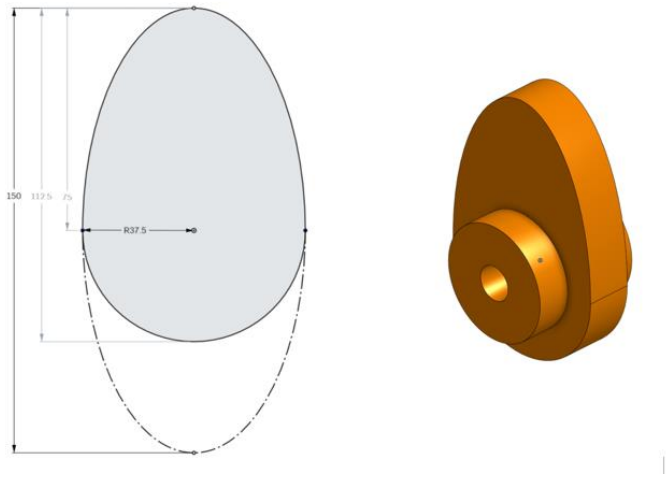

Figure 39 – Early stage lobed pulley design for the knee joint. Profile view (left) isometric view (right)

Initially, a lobed variable radius pulley was envisioned for the knee joint. This provides a smooth transition and tailoring of the mechanical advantage. While providing suitable

variable mechanical advantage, a simple linkage design was preferred to reduce the tendon travel path along the surface of the pulley. This linkage is shown in the image below with the tendon path highlighted in orange.

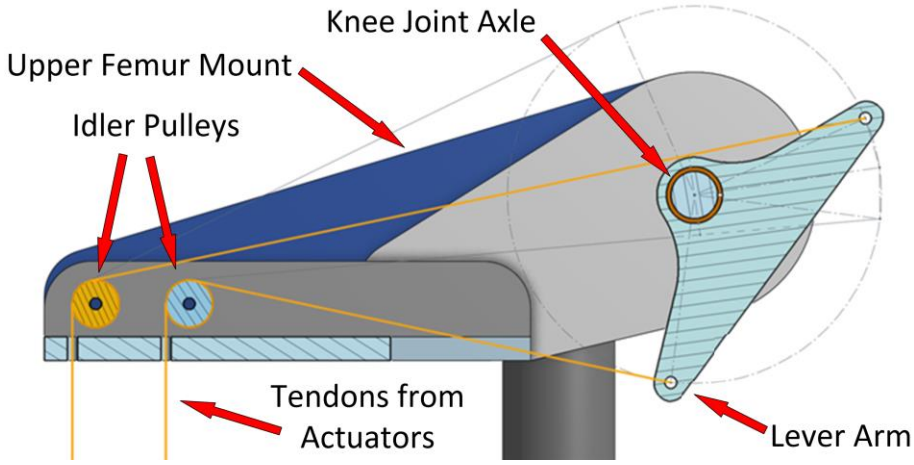

Figure 40 - Section view of the knee axle showing the lever arm linkage, in the fully extended position. Tendon positions for the fully retracted (a CCW rotation of 90°) position shown in grey, with a dashed circular line showing the swept path of the lever arm pin.

A pin linkage on a simple radial lever arm does not require extra tendon length to travel the circumference of the pulley. The need to run the tendon along the circumference of the pulley reduced the maximum radius to below 75 mm whereas the linkage design created a variable lever arm from 0 to 100mm with a matching 100 mm stroke.

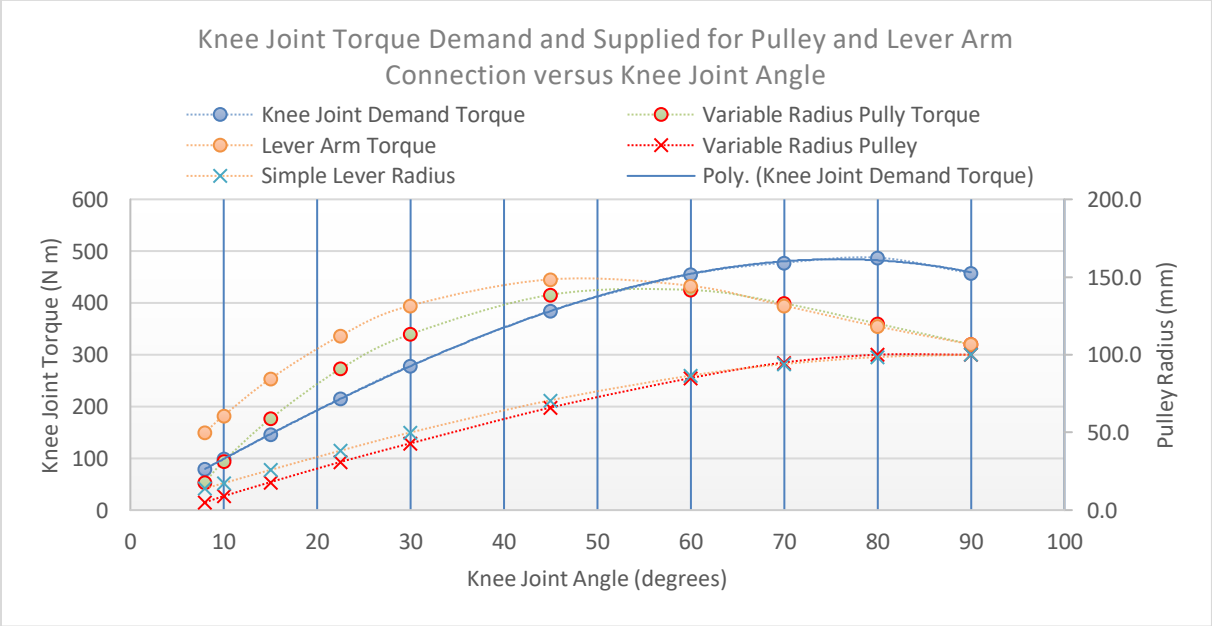

Figure 41 - Knee torque and lever arm length versus joint angle for a vairiety of design options

While the variable rate pulley matched the load profile well across most of the joint range, the lever arm supplies significantly more torque in the lower joint angles which is the higher usage range of the joint. In both cases, torque tapers off significantly beyond 60 degrees. The requirement to supply torque at high knee angles is not critical.

3.3.8 P.1.2.4 – LOW STRAIN RATE

HAMs have a low strain rate when compared to many other flexible actuator types, with only 25% contraction length having practical load generating capacity. However, the effective strain rate must include the overall actuator length, not just the active pressurized zone. Depending on the configuration, ancillary components, like tendon hardware, pulleys and inline instrumentation can add to the overall length of the actuator, without impacting its available contraction length.

To address unwanted increases in effective actuator length, the tendon mounting hardware is located inside the actuator spar, inboard of the free end of the actuator. This is presented in the following section.

3.3.8.1 H.1.2.4 – INTERNAL TENDON COUPLING HARDWARE

The low strain rate of HAM's mandates a search to reduce the effective actuator length. To couple the tendon to the actuator, there is a finite distance that is required for the termination hardware. Additionally, a method is needed to provide length adjustment during assembly and commissioning as well as the likely requirement for an inline force transducer to provide feedback for joint control purposes.

A tendon driven design can use a range of tendon materials. There are many commercially available options using a variety of materials, stainless steel, nylon, Kevlar and polyethylene to name a few. Woven, ultra-high molecular-weight polyethylene rope is a lightweight, high-strength, low-stretch material for tendon driven robots. Common commercial brands are Dyneema and Amsteel Blue. Both are used extensively in marine applications as these ropes are hydrophobic and float in water. For our application, the high strength to weight ratio, resistance to water ingress, ability to withstand harsh environmental conditions and recyclability motivated its selection.

To couple the woven tendon to the rigid inner slide mechanism an interfacing component is required, ideally with some length adjustment capacity. These are commercially available in the form of splice style terminus with a threaded rod. Additionally, an inline force transducer is required at this location and the connection wiring is run up inside the spar and joins the communication bus of the actuator module.

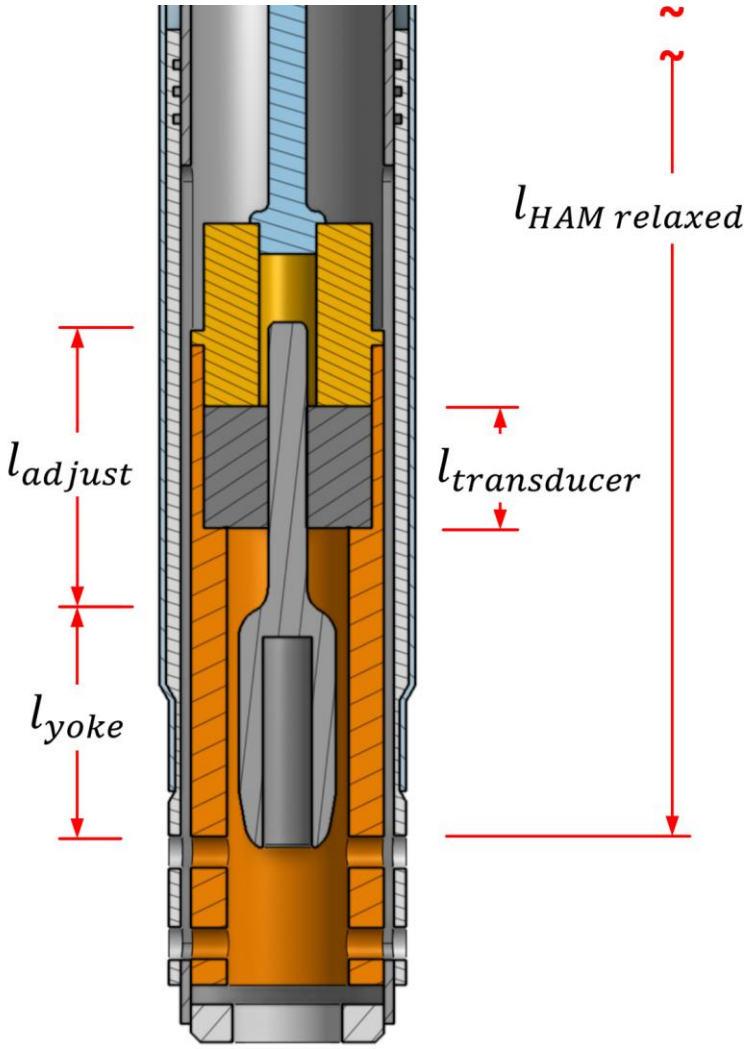

Figure 42 – Section view of proposed actuator, showing inner slide (orange), outer slide (white), tendon termination (light grey), force transducer (dark grey), transducer cap (yellow) and LVDT core (light blue)

When fixed to the terminus of the HAM in series, these elements add to the effective length. The area inside the spar supplies an excellent opportunity to synergistically eliminate this unwanted decrease in effective strain rate and also provides both protection for the components, but also provides a mount for the LVDT and cabling can run from the force transducer up the inside of the spar and connect to the controller block.

The reduction in the overall length, when these components are placed inboard of the actuator terminus is presented below.

$$\varepsilon_{effective} = \frac{l_{HAM,relaxed} - l_{HAM,contracted}}{l_{overall}} \quad [14]$$

$$l_{overall,norm} = l_{HAM\ relaxed} + \left(l_{yoke} + l_{adjust} + l_{transducer} \right) \quad [15]$$

$$l_{overall,internal} = l_{HAM\ relaxed} \quad [16]$$

$$\varepsilon_{effective,internal} < \varepsilon_{effect,norm} \quad [17]$$

The hollow spar design allows the coupling point to move inside and inboard of the free end of the HAM which allows the connection of the tendon termination, adjustment screw and force transducer in series without impacting the effective length of the actuator. The tendon axis is supported directly in the center of the spar, eliminating unwanted moments about the sliding components.

4 DISCUSSION

The primary research objective was to propose and vet the conceptual design of an autonomous device that increases both irrigation and operational efficiencies. Additionally, the conceptual design could potentially address some of the needs of both small- and large-scale agricultural operations. This primary objective was partially achieved, in that a viable conceptual design was realized which can effectively improve irrigational efficiency, however improvements in operation efficiency require further validation. Two technologies (3DOF compact spherical joint and HAM) were implemented together, in a unique approach that uses water pressure as the working fluid to actuate the combination.

The ability of the actuators to provide sufficient joint torques was evaluated and the actuators as sized provide adequate tensile forces to support the mass of the robot as well as lift and reposition legs as required. Some areas of the workspace would require increased pressures above the 6-bar upper range, and at the lower end of the pressure range motion is significantly limited reducing the feasibility of operating on low pressure.

There is significant potential for improvement in this area, specifically by improving the force to pressure ratio of the actuator. Novel origamic McKibben type actuators offer on promising avenue to explore. Additionally, specifying higher pressures is also possible, but was specifically avoided in the interest closing on a design that was intrinsically low energy, rather than simply rely on an assumption of abundant power.

The capacity of the robot to provide effectively provide irrigation services requires an assessment of the flow demands of the device and a comparison to the irrigation volumes required. An estimation of the unoptimized flow rate showed a close match with expected areal inflows or existing irrigation systems. However, the ability to disperse the rate flowing to the robot over a suitable area requires further investigation.

Specifically, irrigation efficiency is best when discharged over a small area, versus spraying the discharge stream over a broad area. A broad discharge area may be required to effectively disperse the flow rates required to operate the machine. Additionally, the requirement to allow device motion without discharge creates a significant challenge requiring on board pumping or various flow line configurations.

Lastly the device must support travel speeds that mesh with the travel velocity of various irrigation supply points (pivots and laterals). The constraining of the ability of the robot to operate in a slow, quasi-static state is necessary to limit the mechanical assessment to static analysis during the conceptual design phase. Low operating speeds address some applications, like the slow moving irrigation pivots. However, to improve upon operational efficiency, the need to increase ground speed is obvious. While not investigated directly in this work, additional research into wheeled or tracked implementations is a promising avenue to address this limitation and is left as future work.

The coupling of many parameters mandated the recursive design approach. To reduce the design space, a set of design constraints were established, and components sized against that baseline. While the final design constraints may not be fully valid for the applications intended, they supply a framework to evaluate the interplay between components and systems.

The intended application was irrigation of small- and large-scale agricultural operations. However, at this early stage of development, the ground speed limitations make this device most suitable to niche applications, for example, the protection of humans from harm, like the proposed firefighting application, or cases where slow-speed pervasive plant study in research applications match the proposed devices current operational characteristics. Added research is required to provide the ability to meet many higher speed applications.

4.1 DESIGN PROBLEMS SOLUTION SUMMARY

This section collects all the various design problems identified throughout the work and presents the solution proposed for each and the method of address.

Table 7 - Design Solution Summary

Design Element – Solution	Design Problem Addressed	Method of Address
Type of hip joint – 3DOF compact spherical joint	• Series revolute joints require structural support • Offset in joints requires more complex control algorithms and transformation calculations	• Compact spherical joint has common point of rotation for all three axes, rather than offset joints • No need to transfer orthogonal joint torques across disparate revolute joints

	• Complexity of passing high load tendons across revolute joints • Need for tarsus dexterity to avoid crop damage • Desire to explore creative gaits for optimal efficiency	• 3rd DOF allows z-axis pivot to move contact point forward while conserving rotational inertia when compared to a leg swing type gait
Type of linear actuator – McKibben with water as process fluid	• Synergistic use of irrigation pressure to actuate robot • Simple, robust compliant actuator • High strength to weight ratio • Zero actuator backlash when used in antagonistic pairs	• Synergistically use irrigation water as working fluid • Use of reasonably incompressible working fluid allows actuator control to be flow based rather than pressure based • Allows variable joint stiffness to be achieve by for identical joint positions
Coupling of actuators to joints – Tendons with agonist/antagonist actuator pairs	• Need to de-couple actuator orientation from joint orientation	• Tendons with directional idler pulleys allow flexible load paths • Agonist/antagonist pairs to eliminate backlash (2 for 1 DOF joint, and 4 for 3DOF joint)
McKibben embodiment – Internal load bearing spar	• High actuator mass when using water as working fluid • Passive entrained air release in actuators	• Spar passes through entire actuator • Displaces unexchanged water volume • Provides load bearing structural members • Reclaims previously underutilized space at critical location
Actuator location and Orientation – Actuator cluster on femur	• Passive entrained air release in actuators • Passive entrained air release in HP and LP supply lines • Complex piping and electrical connection • Need for synergistic use of materials	• All actuators remain vertically oriented • Common location allows manifold porting • Joint location on femur end positions creates high point at top of manifold for HP and LP air venting • Allows grouping of spars to share handling of external loads passed through femur
Tibia morphology – Twin stanchion prismatic joint	• High bending moments on tarsus • High bending moments on knee joint • Need for neutral stance • Need to vary thorax clearance to ground • Need to accommodate uneven terrain	• Twin cylinders provide two chambers for increased surface area compared to one large cylinder • Dual stanchion design created stiffer prismatic joint and transfers load to wide knee joint, reducing need for excessive structure • Space between tibia members allows ground contact point to directly below knee (or even inboard) allowing for neutral pose
Knee joint mechanical advantage – Variable radius knee pulley	• McKibben actuator force is inversely proportional to strain rate	• By varying the pulley radius, actuator force can be decreased at beginning of stroke and increased at end of stroke, flattening the force to linear displacement curve
Tendon fixation – Internal tendon connection	• Central spar forces line of action of actuator away from primary longitudinal axis	• Slotting the spar and passing the actuator tensile load to tendon on the longitudinal axis • Extra space to allow the connection point to be inverted and placed inside the actuator, allowing for decrease overall length • Tendon to actuator gross linear adjustment occurs at this connection point • This length allows the insertion of FT and LDVT internal to the actuator, recapturing this space and protecting sensitive devices

Actuator valving – 3 position, servo driven spool valve located inside the spar	• Need to minimize dead volume between active actuator volume and control valves • Need to access bladder volume from inside spar • Need to protect and house servo valve and PT	• Valve stem is co-axial with the actuator spar, located directly adjacent to the bladder ports, inside the spar • Servo is located below the spool with manifold connections at the top of the spar • Pressure transmitter is located within the spar between the bladder ports and the spool • Electrical connections passed through the manifold and down into the spar to connect to the servo, PT, FT and LDVT

4.2 CONSUMPTION RATES

To determine the viability of the HAM and the proposed conceptual design, an evaluation of the consumption rate of water was undertaken. The basic four supported leg-swing gate identified earlier was used for this process. A full travel cycle of a leg was composed of three stances. Using the nominal design parameters, the motion of knee and hip actuators was estimated for a leg cycle. Actuator displacements for these joint positions were calculated, and differential volumes determined for each transition between the three distinct leg positions.

Table 8 - Actuator Displacement Single Leg Module for PEP, SEP and AEP Leg Positions

	Variable	Postion 1 (PEP) Parameters	Postion 2 (SEP) Parameters	Postion 3 (AEP) Parameters
Hip Joint Angles	$\vartheta 1^\circ (x)$	0	0	0
	$\vartheta 2^\circ (y)$	-5	-15	-5
	$\vartheta 3^\circ (z)$	45	0	-45
Knee Joint Angle	β°	45	30	45
Neutral Actuator Postion	(mm)	350	350	350

Joint	Tendon Number	Length Change (h)	Actuator Position (L)	Volume at Position (V)	Length Change (h)	Actuator Position (L)	Volume at Position (V)	Length Change (h)	Actuator Position (L)	Volume at Position (V)
		(mm)	(mm)	(mL)	(mm)	(mm)	(mL)	(mm)	(mm)	(mL)
Hip Tendons	1	-31.54	318.46	1488.96	-8.77	341.2	1287.44	8.99	359.0	1095.29
	2	18.73	368.73	974.65	9.31	359.3	1091.53	-29.02	321.0	1468.82
	3	-29.02	320.98	1468.82	9.31	359.3	1091.53	18.73	368.7	974.65
	4	8.99	358.99	1095.29	-8.77	341.2	1287.44	-31.54	318.5	1488.96
Knee Tendons	1	-20.00	330.0	1392.49	0.00	350.0	1196.76	-20.00	330.0	1392.49
	2	0.00	350.0	1196.76	-37.00	313.0	1530.97	0.00	350.0	1196.76

Table 9 - Basic Gait Walking Cycle - Total Volume Consumption for Full Robot

Volume Δ from 1 - 2	Volume Δ from 2 - 3	Volume Δ from 3 - 2	Volume Δ from 2 - 1	Total Volume Inflow per Leg Cycle
(mL)	*(mL)*	*(mL)*	*(mL)*	*(L)*
~~-201.52~~	~~-192.15~~	~~-192.15~~	~~-201.52~~	
116.88	377.28	377.28	116.88	
~~-377.28~~	~~-116.88~~	~~-116.88~~	~~-377.28~~	
192.15	201.52	201.52	192.15	
309.03	**578.80**	**578.80**	**309.03**	**1.78**
~~-195.73~~	195.73	195.73	~~-195.73~~	
334.21	~~-334.21~~	~~-334.21~~	334.21	
334.21	**195.73**	**195.73**	**334.21**	**1.06**
Total Inflow Volume for Full Leg per Cycle				**2.84**
Number of Legs				6
Total Inflow Volume for Robot per Cycle				**17.01**

Using the nominal leg module dimensions, a 40 x 400 mm sleeve HAM, the proposed lever arm mechanical advantage for the knee joint, and a 50 mm hip joint ball diameter, a fluid consumption rate of 1.06 L per cycle for the two the knee joint actuators was found. This resulted from a simple knee swing angle from 30 to 45° across the leg cycle. The four hip joint actuators consumed a total of 1.78 L per cycle. The femur lifted from 65 to 75° during the lateral swing action at the hip, which spanned 90° of horizontal rotation. The equations in Section 4.22 were used to determine the tendon differential lengths for a given *zyx* rotation matrix for the sphere. Tendon motions was no more than +/- 40 mm from the neutral pose.

This resulted in a combined consumption of 2.84 L per leg, per step cycle. For all six legs this summed to 17.0 L per step. For the nominal design dimensions, this resulted in an approximate step length of 0.75m. This is an effective consumption rate of 22.5 L per meter of distance travelled. If a slow travel rate of 0.1 m/s is selected, this would result in a flow rate of 2.25 L/s or roughly 35 GPM. For a 4-meter-wide local irrigation zone, this amounts to approximately 5 mm of irrigation in a single pass. This is within the range of normal irrigation processes. The step length used was the minimum possible for estimation, however a longer step length can be achieved by extending the lower slide joint and increasing the lift angle at the hip. This would allow for either faster ground speed at the same consumption rate, or a decreased consumption rate for and identical travel speed.

However, this rate of application might result in local surface pooling, flow and erosion. To mitigate this, increasing the area covered by the device would reduce the depth of water applied per unit area, at the cost of irrigation efficiency as dispersal via spray heads would be required to reach further from the device. This is not desirable from a design perspective. A wide spray bar added to the device would reduce dispersal issues, at the expense of a cumbersome addition to the device payload.

If a 10 m delivery line is assumed, at this flow rate a 1” diameter hose would be required to keep pressure losses below 1 bar. For 100 m, a 1.5” diameter hose is required. The mass of these irrigation lines would be between 0.5 and 1.0 kg per meter. This is also within the payload allotment of 60 kgs for the device. 50 m of hose would result in a hose mass of 25kg – 50kg at the thorax. This does not include the containment structure nor the reeling mechanism. It is clear from this early analysis that optimizations in mass and fluid consumption will prove critical in future design work.

Greater overall mass of the device requires larger actuators, with higher flow rates, which increases pressure drop, requiring larger hoses, which again increases mass. The recursive intercoupling of mass was a key factor in the desire to reduce the overall mass, starting with the individual mass of the actuators.

The novel origamic actuator, that provides significant improvements in force for equivalent pressures would be an ideal candidate to achieve this reduced mass as a smaller actuators would be required to produce similar joint torques Unfortunately, the pressure regime of these actuators is not sufficient for this application. Further refinement and modelling of the overall device may yield the required mass reductions. A mass reduction of 50% would bring the demand and therefore mass of the stored water down significantly.

Another area where optimization could occur is leveraging the third DOF of the hip joint to facilitate a reduced required joint range of motion. Once a higher fidelity dynamic model is established, an optimization study could be undertaken to find an optimal gait, that reduced the displacement required per stroke. This is left as future work.

Another avenue to reduce the required flow rates, which are based on actuation from 6 bar source then vented to the environment, would be to chain pressure drops between actuators

that have differing pressure requirements. In this way, flow can be routed between actuators, reducing the overall flow rate required to service the cluster. This could be achieve at the leg module level, or implemented across the entire device via a series of descending pressure rails and various actuators operated across these banded pressure differentials depending on their needs. This would have the effect of reusing the same volume of fluid, but exploiting smaller pressure drops to achieve the joint motions required.

4.3 ZERO DISCHARGE OPERATION

While the original intent was to provide a device that can autonomously irrigates, continuously discharging, the capacity of the device to operate without discharge is desirable, if not a requirement. This introduces significant complexity in the device.

For a nominal flow rate, q of 2.25 L/s at field pressure, p of 6 bar and a pump with efficiency, η of 0.5, the shaft power, P in kW required to provide this hydraulic supply can be determined.

$$P = \frac{q \cdot p}{\eta} = \frac{(2.25\ L/s)(6\ bar)}{0.5} = 2.7kW \qquad [18]$$

A pump of this size would add additional mass to the device, likely in the 10^1 kg range. Additionally, a power source must be provided to drive this unit. This quantity of power could be provided via the tether, or from onboard battery with an additional weight penalty.

In a battery powered scenario 2 – 4 kg of lithium ion batteries (0.250 kWhr/kg) would be required to provide 10 minutes of independent operation. This could be significantly higher for various ambient temperatures to maintain healthy discharge rates and duty cycles. Even with a tethered connection to an electrical power source, a battery is still required to permit periodical decoupling from the tether to move to another coupling point.

Without a tethered power supply, it would be difficult to outfit the device with effective power generation equipment on board, without having to resort to hydrocarbon fuel-based engine. Solar panels would be impractically large. It is possible that surplus energy could be harvested using the same electric rotary machine that drives the pump. During periods of discharge, some of the flow energy could be harvested to provide recharge capacity. Duty

cycle would be an important parameter to control to ensure enough fluid power was available for locomotion and electrical power generation demands.

When operating in zero discharge mode, fluid heating could begin to impact performance as the system is designed for-flow through conditions. The recirculation pump would continuously add heat to the process fluid. There may be sufficient surface area available to radiate this heat, however thermal modelling is required to assess the viability of the operating mode. This is left as future work.

Another potential method to provide zero discharge operation is a cyclic reverse flow procedure. This fully tethered operating mode requires an onboard tank to capture discharged water. The robot would move under zero discharge mode filling the tank until full. At this point it would signal the supply system to depressurize and reverse flow from the onboard tank back into the piping system. Once empty, the system would re-pressurize and return to normal operation.

While possible, this may not be a desirable operating mode. Specifically, the mass of the onboard storage quickly dwarfs the payload capacity. It would take only 10 or 15 seconds at 2.25 L/s to reach the payload mass of 60 kg. Then it would take another, likely longer period of time for this quantity of water to be suctioned out of the device back into the supply system. During the return flow phase, motion would not be possible, and any irrigation devices coupled to the locally depressurized pipe network would require reverse flow protection and obviously would be unable to irrigate.

By specifying a supply and return service line, a return-flow system is also possible. Each line would need to accommodate the full flow rate, doubling line losses. To provide the recirculating flow, a powered pump is mounted at the supply point, or could use the existing pumping station, after considerable piping system modifications. While possible, this operating mode is marginally desirable as the hose handling issues double. Running power to an onboard pump is more efficient from an operations perspective.

There is one divergent option for zero-discharge operation; the conversion of the device to operate pneumatically rather than hydraulically. While the design intent was to operate hydraulically, there is nothing preventing the system from being drained of water and the

service lines delivering pneumatic power rather than hydraulic. This could be a manual process, allowing the device to be converted and redeployed seasonally, or it could be a dynamic and frequently used capability of the device. In either case a method for draining the water is required, as well as a pneumatic supply and control system modifications.

Of these three requirements, the draining of the system presents the greatest challenge, particularly if this was to be a dynamic or autonomous process. One method of draining would be to use gravity with the existing air venting system. This would require a significant increase to both the knee and joint angle ranges allowing inversion of the both the tibia and femur actuators. Without inversion capabilities, a system of relief valves, mounted at the base of each actuator is required. Automating another 8 valves per leg adds to the device complexity.

Owing to the passive air purging design, reversing the system back to hydraulic operation would be less challenging. However, for larger volumes of gas, vapour lock could prevent effective refilling. While not insurmountable, dynamic or autonomous conversion between pneumatic and hydraulic would impose a challenging set of additional requirements. Whereas seasonal conversion would offload this complexity to human operators.

4.4 DEVICE APPLICATIONS

While the design exercise was instructional, the ability of the device to meet application requirements is paramount. This application discussion aligns with the two persona specific requirements. The small-scale farmer needs a device to enable autonomous irrigation while the large-scale application is coupling to larger semi-autonomous irrigation systems. Additionally, a high potential application outside of the agricultural domain is also proposed; autonomous forest-fire fighting.

4.4.1 LEVERAGING THE FUNCTIONALITY OF THE DEVICE

While irrigation is the primary objective of the device. Once a fully autonomous robot, capable of operating on a small farm is enabled, there are a myriad of other potential use cases that could leverage the intrinsic capabilities of the device. The overall weight of the device and the power of the actuators is enough to allow ground engaging activities to be

undertaken. While significant soil tillage is outside of the operational capacity, many other agriculturally relevant tasks are not. Specifically, the following capabilities could be enabled via specification of added sensors, tooling and likely would also required increasing the operational ground speed.

- Seeding: plant a variety of raw seeds at precise depth, location and time. The ability of the device to frequently visit any location in the parcel would allow the seeds to be tended to, specifically to apply low volume, but frequent irrigation events.

- Weeding: mechanical weed suppression on every step. The device could choose foot placement locations to avoid crops of interest and repeatedly target weed varietals without any added tooling. For more comprehensive weeding, hoeing action could be used to disrupt the weed root systems. More advanced techniques of using high pressure water jets, steam or even laser ablation are also possible. These techniques would use the sensors and computational power that comes with an autonomy package. This includes machine vision and advanced data processing.

- Integrated pest management: intervene at the plant scale to disrupt pest growth cycles at the most effective time. Similar to the weed application, the ubiquitous presence of the robot allows for early interventions resulting in highly efficient use of resources.

- Soil parameter assessment: carry a variety of sensors to evaluate soil parameters beyond local moisture levels. The multiple ground contact points could provide proximal soil sensing, using electrical, radiographic or optical properties. This operation would use the existing processing and data collection capacities.

- Crop health assessment: carry proximal sensors (visible/hyperspectral image capture or lidar instrumentation) to evaluate plant parameters. This ability again requires existing onboard data processing capacity.

- Data logging for research support: operate as a full research platform, rather than an agriculture service robot. The pervasive presence on a parcel of land allows the

collection of data sets that would either require intensive human labor, or extensive installation and operation of fixed data collection systems.

These additional applications are relevant for the small- and large-scale applications. The flexibility for the robot to complete a host of unique tasks is a feature of value for the small-scale operator. Whereas the ability to do a single, homogenous and repetitive task at scale is of greater value to the large-scale operator. Future research in this area would move the design closer to being able to realize these advanced applications.

In the small-scale application, a single unit completes a variety of dissimilar tasks over the seasons of operation. For large-scale applications, many devices complete the same task at scale. Reconfiguring the devices for another unique task would likely follow seasonal variations.

4.4.2 SMALL SCALE AUTONOMOUS IRRIGATION PROCESS

The small-scale autonomous irrigation application was the original target for this device. The primary utility to the farmer is the ability the offload the responsibility of establishing and maintaining an optimal irrigation schedule. This was a common pain point expressed during the farmer interview process – “I know when I should irrigate, but often it is a challenge to execute on that knowledge in a timely fashion”. Transfer of these tasks to the robot optimizes irrigation efficiency. The robot can sense soil conditions, monitor for weather changes and irrigate without intervention. The ability to control critical irrigation tasks while being able to attend to other priority tasks, improves operational efficiencies. However, there may be many new and cumbersome tasks created by the use of the proposed device that could easily negate the advantages stated. Added assessment and review would be required to validate that the net operational efficiency is actually.

For the device to be effective for the smaller operator, fully autonomous operation is required. This includes the ability to independently couple and decouple to various irrigation points as well as deployment and retrieval of the tethered service lines. While complex, autonomy, coupling and tether control are all assumed to be tractable problems and left as future work and addressed once the application use case is more fully defined.

The simplified mode of operation for the device, once deployed and commissioned on a given parcel of land would be as follows:

- Device deployed with a stated mission – irrigate a given parcel of land
- Walk to the first selected irrigation coupling point
- Couple to the irrigation system
- Move about the reachable workspace, deploying tether as it moves
- Sense soil moisture conditions and irrigate to achieve desired saturation
- Retrace path back to coupling point, retrieving tether along the way
- Decouple from the irrigation point and walk to the next coupling point

The capacity to monitor soil moisture conditions is essential to optimize irrigation efficiency. Local soil moisture conditions are evaluated before application and afterwards, as the robot retraced its steps to the irrigation coupling point. This supplies multiple data points for the same geolocation; before, during and after application of a known volume of water. This information provides a closed loop irrigation process that is well aligned with the optimization of irrigation efficiency.

While operating an irrigation program, the device could concurrently execute one or more of the services presented above, depending on the need and the capabilities installed on the device. The ability to run without discharge is key for these ancillary operations, particularly for shoulder season operations where irrigation is not required.

4.4.3 LARGE SCALE IRRIGATION SYSTEM COUPLED APPLICATIONS

Pivots and lateral move irrigation systems match well with the capabilities and operating requirements of the proposed robot. In the small-scale application, the robot must carry enough hose and the necessary hose-handling machinery to allow it to effectively span and traverse between fixed coupling points. Pivots and lateral moves offer a mobile coupling point, but also mechanical structure to support the ‘last-mile’ of hosing between the coupling point and the robot. This can mitigate the need for extensive onboard hose-handling.

The discussion is constrained to center pivot systems. While the operation is very similar between devices, the flexibility and diversity of configuration options of lateral move systems create added operating parameters to address. However, similar approaches are applicable for both types of mobile irrigation systems.

There are three primary operating locations for the robot:

1. Full traversal: the robot can traverse the entire length of the pivot, and therefore the entire envelope covered by the pivot. This would require either service hose festooning to allow the robot to move radially, or a hose reel system and multiple coupling points along the pivot length. This second mode of operation is similar to the small-scale operating mode, with the exception of coupling to a mobile pipeline from above rather than to ground laid networks.

2. End operation: the robot couples to the end of the pivot and supplies service to a band outside the pivot covered area, or into the irregular corners unreachable by the pivot radius. This would require hose handling in the form of onboard reel system, or an overhead cantilevered boom and a smaller hose supplying from above.

3. Band operation: the robot couples to a fixed point somewhere along the pivot and can only traverse a certain radial band, within the constraints of the coupling hose. Again, hose handling is configurable in a myriad of ways highlighted above.

As the robot operates more efficiently on higher pressures, it may be most advantageous to install and use the robots at the end of the pivot. Due to system pressure drops that increase with distance from pressure source, the ends of a pivot are often outfitted with a booster pump to provide the additional pressure to service a sprinkler at the end of the pivot commonly called an end gun. An end gun extends the range of irrigation at the expense of decreased irrigation efficiency. Mounted high on the end of the pivot, it sprays onto a ring area surrounding the pivot.

The end gun, while effective at distributing water to an area outside the normal circular working envelope of the pivot, the irrigation efficiency is lower than the drop tube application method used across the main pivot. This is an ideal use case for irrigation robot.

The robot would traverse the radial band covered by the sprinkler gun. However, as the discharge is at ground level, application is more precise and less losses occur. This extends the high irrigation efficiency of the pivot. With hose-handling, the robot can traverse a larger area that an end gun, especially into the irregular shaped corners of square fields that often forgo irrigation. In this case, the robot would be a direct replacement the complex lateral move booms that operators append to the end of the pivot to reach into odd shaped field corners.

4.4.4 FORREST FIRE FIGHTING APPLICATION

One ancillary application is worth mentioning. There are few applications where it is possible to use the power fluid external to a hydraulic system. Forest fire fighting and agriculture have some key similarities. Both are rugged, unstructured outdoor applications. Both use large quantities of water and distribute it directly onto the land.

However, the operating pressures found in fire fighting applications are significantly higher, with common forestry hose specifications are service tested to 300 psi. This service pressure drastically increases the actuator forces possible. The range of motion of the joints is greatly increased which results in a larger working envelope, greater appendage power and dexterity.

In this use case, consistency of application over the landscape is not a concern, nor is efficiency of application. Concentration of supply to critical areas to control wildfires is the application goal. The task meets the dull, dirty and dangerous characteristics suitable to robotic systems. Rather than put humans at risk, the robot is coupled to a hose and commanded into dangerous areas that would otherwise be unreachable, or too risky to enter.

With a robust bi-directional on-board pump, electric motor-generator and batteries, they could traverse complex paths with hoses deflated, then when in position, pressurize the hose to engage a fire front. The overwhelming surplus of hydraulic power available during water flow can rapidly charge batteries for the next duty cycle. The high power of the appendages also provides sufficient strength to allow hauling of filled hoses, to move and engage fires simultaneously.

The onboard automation equipment and processing power is ideally suited to supplying real time fire sensing. Adding thermal imaging is easy and would be the equivalent to the soil moisture sensing ability in the irrigation application. This closed loop control would make the device and effective autonomous fire fighting asset.

Beyond direct fire engagement, multiple robots can couple together in series, to create autonomous supply and relay hose networks, effectively allowing fire fighters to pre-position supply networks and hydrants without risking human lives or over-extending resources. The device can additionally supply field power, charging stations, or command and control relay points.

This application certainly requires additional investigation as the necessity for improved forest-fire fighting equipment is increasing as climate fueled wildfires increase in frequency and intensity globally.

5 CONCLUSIONS

The initial objective of this research was to develop a viable autonomous irrigation device that could attend to both small- and large-scale applications. A tethered, legged, human scale, water-powered device was developed and investigated for feasibility. Irrigational efficiency was improved, however, further research is required to validate the potential increases in operational efficiency identified.

Key areas of research were potential joint configuration and actuator selection. Unique challenges associated with using water as a process fluid were identified and design solutions proposed. Critical challenges were dealing with entrained air in the system, matching actuator power to joint torque demands and mitigating the low strain rate available from the selected actuator.

A bio-inspired insect morphology was adopted, using a modular leg design. A dual-stanchion prismatic cylindrical joint was implemented to allow variation is ground clearance. A simple revolute knee joint with a variable lever arm linkage was used to couple the joint to a pair of antagonistic water filled McKibben style actuator (HAM). The hip joint was implemented using a compact 3DOF spherical joint coupled to four counter opposed HAMs. 6 modular legs were coupled to a payload carrying thorax with a total design mass of 300 kg.

Actuators were co-located as much as possible, in a vertical configuration to allow for passive air venting and simplified service provisioning. The HAMs were implemented as sleeve type allowing loads to be passed through a central spar. The spar served to contain many critical components, including a simple integrated flow control valve as well as all the tendon coupling hardware, reducing the effective actuator length.

The device performance was assessed and the selected actuator size was found to be adequate for the majority of the range of motion for a simplified gait. However, optimization of the actuators and the pressure and flow controls may provide the necessary improvements. Larger actuators or smaller overall geometry could be specified to address this mismatch.

Flow rates for a nominal gait were calculated and these matched well with typical irrigation rates expected in agricultural applications. Additional matching of discharge rates, operating speeds and patterns will be required to ensure effective irrigation operation.

The device is suitable for use in the small-scale farm, operating across a range of tasks, as well as being suitable to coupling to pivot or lateral move irrigation systems in a variety of capacities. Additionally, the device could make a capable forest fire-fighting device owing to the higher service pressures and application requirements that closely match the irrigation task. Constraints in the operational speed of the conceptual device limit its capacity to address many of these additional applications proposed. The device is currently best suited for niche applications where slow speed operation is acceptable or desirable. Protecting humans from harm or long-term, pervasive in-field agricultural research missions are key examples in contrast to the fast-paced operating environment found in the modern agricultural domain.

This work forms the conceptual design to constrain the application and determine feasibility. Subsequent to this work, full static and dynamic modelling of the robot must be undertaken, a study of the control strategy completed as well as the implementation of systems that support the complex tasks of hose-handling, autonomous navigation and application specific optimization.

5.1 FUTURE TASKS

The following list highlights the ongoing development path, to be complete as future work:

- Higher fidelity actuator modelling (static, dynamic, stiffness, control)
- Higher fidelity 3DOF joint modelling (static, dynamic, stiffness, control, stability)
- Dynamic model of overall device
- Gait analysis
- Tooling and sensor outfitting
- Autonomy integration
- Full robot simulation
- Develop and execute SIL/HIL testing

- Complete detailed beta prototype design
- Fabricate and test beta prototype of leg module
- Fabricate and test beta prototype of full device

REFERENCES

[1] A. Boretti and L. Rosa, “Reassessing the projections of the World Water Development Report,” *npj Clean Water*, vol. 2, no. 1, Dec. 2019.

[2] A. K. Biswas and C. Tortajada, “Changing Global Water Management Landscape,” in *Water Resources Development and Management*, Springer, 2009, pp. 1–34.

[3] J. Chenoweth, “Minimum water requirement for social and economic development,” *Desalination*, vol. 229, no. 1–3, pp. 245–256, Sep. 2008.

[4] M. Rodell *et al.*, “Emerging trends in global freshwater availability,” *Nature*, vol. 557, no. 7707, pp. 651–659, May 2018.

[5] Y. Wada, I. E. M. de Graaf, and L. P. H. van Beek, “High-resolution modeling of human and climate impacts on global water resources,” *J. Adv. Model. Earth Syst.*, vol. 8, no. 2, pp. 735–763, Jun. 2016.

[6] G. Leng, L. R. Leung, and M. Huang, “Significant impacts of irrigation water sources and methods on modeling irrigation effects in the <scp>ACME</scp> <scp>L</scp> and Model,” *J. Adv. Model. Earth Syst.*, vol. 9, no. 3, pp. 1665–1683, Jul. 2017.

[7] R. E. Sojka, D. L. Bjorneberg, and J. A. Entry, “0-7 0 IRRIGATION: AN HISTORICAL PERSPECTIVE.”

[8] S. Trimble, *Encyclopedia of Water Science, Second Edition (Print Version)*. CRC Press, 2007.

[9] B. E. Graeub, M. J. Chappell, H. Wittman, S. Ledermann, R. B. Kerr, and B. Gemmill-Herren, “The State of Family Farms in the World,” *World Dev.*, vol. 87, pp. 1–15, Nov. 2016.

[10] A. Stephanie Tam and A. Petersen, “BC Sprinkler Irrigation Manual.”

[11] V. Shiva, *Monocultures of the mind : perspectives on biodiversity and biotechnology*. Zed Books, 1993.

[12] J. Lipiec and W. St e pniewski, “Effects of soil compaction and tillage systems on uptake and losses of nutrients,” *Soil Tillage Res.*, vol. 35, no. 1–2, pp. 37–52, 1995.

[13] L. Alakukku *et al.*, “Prevention strategies for field traffic-induced subsoil compaction: A review Part 1. Machine/soil interactions,” in *Soil and Tillage Research*, 2003, vol. 73, no. 1–2, pp. 145–160.

[14] R. J. Wootton, “Invertebrate paraxial locomotory appendages: design, deformation and control,” *J. Exp. Biol.*, vol. 202, no. 23, 1999.

[15] N. I. Platnick and S. M. Manton, “The Arthropoda: Habits, Functional Morphology, and Evolution.,” *Syst. Zool.*, vol. 27, no. 2, p. 252, Jun. 1978.

[16] “Control of swing movement: influences of differently shaped substrate.: EBSCOhost.” [Online]. Available: http://web.b.ebscohost.com.ezproxy.library.uvic.ca/ehost/pdfviewer/pdfviewer?vid=1&sid=fd979058-d079-4ed9-baa8-c2417ce96cae%40pdc-v-sessmgr04. [Accessed: 29-Jan-2020].

[17] D. Tanaka, D. Kamo, M. Maehara, and T. Nakamura, “Development of two types of 2-DOF wrist joint driven by pneumatic artificial muscles,” in *2013 IEEE International Conference on Mechatronics, ICM 2013*, 2013, pp. 471–476.

[18] K. Shimamoto, D. Suzuki, and K. Ohnishi, “Bilateral control for 4-DOF manipulator with a tendon-driven spherical joint mechanism,” *Int. Work. Adv. Motion Control. AMC*, pp. 290–295, 2014.

[19] H. Wang, W. Chen, Y. Lei, and S. Yu, “Kinematic analysis and simulation of a 7-DOF cable-driven manipulator,” in *2007 IEEE International Conference on Control and Automation, ICCA*, 2007, pp. 642–647.

[20] S. K. Mustafa, G. Yang, S. H. Yeo, W. Lin, and C. B. Pham, “Development of a bio-inspired wrist prosthesis,” in *2006 IEEE Conference on Robotics, Automation and Mechatronics*, 2006.

[21] K. Koganezawa, M. Yamazaki, and N. Ishikawa, “Mechanical Stiffness Control of Tendon-Driven Joints.,” *J. Robot. Soc. Japan*, vol. 18, no. 7, pp. 1003–1010, 2000.

[22] M. L. Guckert and M. D. Naish, “A Compact 3 Degree of Freedom Spherical Joint,” *J. Mech. Robot.*, vol. 3,

no. 3, p. 031005, 2011.

[23] M. L. Guckert, “Design and Control of a Miniature Robotic Manipulator,” The University of Western Ontario, 2009.

[24] M. Focchi *et al.*, “Water/air performance analysis of a fluidic muscle,” *IEEE/RSJ 2010 Int. Conf. Intell. Robot. Syst. IROS 2010 - Conf. Proc.*, no. September, pp. 2194–2199, 2010.

[25] C. Xiang, M. E. Giannaccini, T. Theodoridis, L. Hao, S. Nefti-Meziani, and S. Davis, “Variable stiffness Mckibben muscles with hydraulic and pneumatic operating modes,” *Adv. Robot.*, vol. 30, no. 13, pp. 889–899, Jul. 2016.

[26] H. D. Yang, B. T. Greczek, and A. T. Asbeck, “Modeling and Analysis of a High-Displacement Pneumatic Artificial Muscle With Integrated Sensing,” *Front. Robot. AI*, vol. 5, Jan. 2019.

[27] R. Niiyama, X. Sun, C. Sung, B. An, D. Rus, and S. Kim, “Pouch motors: Printable soft actuators integrated with computational design,” *Soft Robot.*, vol. 2, no. 2, pp. 59–70, Jun. 2015.

[28] H.F.Schulte, D.F.Adamski, and J.R.Pearson, “Characteristics of the Braided Fluid Actuator,” *Technical Report No.5*. 1961.

[29] R. M. Robinson, C. S. Kothera, and N. M. Wereley, “Quasi-static nonlinear response of pneumatic artificial muscles for both agonistic and antagonistic actuation modes,” vol. 26, no. 7, pp. 796–809, 2015.

[30] N. Tsagarakis and D. G. Caldwell, “Improved modelling and assessment of pneumatic muscle actuators,” *Proc. - IEEE Int. Conf. Robot. Autom.*, vol. 4, pp. 3641–3646, 2000.

[31] C. Chou and B. Hannaford, “Measurement and Modeling of McKibben Pneumatic Artificial Muscles.”

[32] B. Tondu and P. Lopez, “Artificial Muscle Robot Actuators,” *Control Syst.*, vol. 20, no. 2, pp. 15–38, 2000.

[33] T. Vo-minh, S. Member, T. Tjahjowidodo, H. Ramon, and H. Van Brussel, “A new approach to modeling hysteresis in a pneumatic artificial muscle using the Maxwell-slip model,” *IEEE/ASME Trans. Mechatronics*, vol. 1, no. 1, pp. 1–10, 2009.

[34] S. Davis, N. Tsagarakis, J. Canderle, and D. G. Caldwell, “Enhanced modelling and performance in braided pneumatic muscle actuators,” *Int. J. Rob. Res.*, vol. 22, no. 3–4, pp. 213–227, 2003.

[35] G. K. Klute and B. Hannaford, “Fatigue characteristics of McKibben artificial muscle actuators,” *IEEE Int. Conf. Intell. Robot. Syst.*, vol. 3, no. October, pp. 1776–1781, 1998.

[36] B. K. S. Woods, M. F. Gentry, C. S. Kothera, and N. M. Wereley, “Fatigue life testing of swaged pneumatic artificial muscles as actuators for aerospace applications,” *J. Intell. Mater. Syst. Struct.*, vol. 23, no. 3, pp. 327–343, 2012.

[37] R. W. R. W. R. W. R. W. R. W. Colbrunn, G. M. G. M. G. M. Nelson, and R. D. R. D. R. D. Quinn, “Modeling of braided pneumatic actuators for robotic control,” *Proc. 2001 IEEE/RSJ Int. Conf. Intell. Robot. Syst. Expand. Soc. Role Robot. Next Millenn. (Cat. No.01CH37180)*, vol. 4, pp. 1964–1970, 2001.

[38] B. Tondu, “Modelling of the McKibben artificial muscle: A review,” *J. Intell. Mater. Syst. Struct.*, vol. 23, no. 3, pp. 225–253, 2012.

[39] J. Yi, X. Chen, C. Song, and Z. Wang, “Fiber-Reinforced Origamic Robotic Actuator,” *Soft Robot.*, vol. 5, no. 1, pp. 81–92, 2018.

[40] S. Davis and D. G. Caldwell, “Braid effects on contractile range and friction modeling in pneumatic muscle actuators,” *Int. J. Rob. Res.*, vol. 25, no. 4, pp. 359–369, 2006.

[41] C. Xiang, M. E. Giannaccini, T. Theodoridis, L. Hao, S. Nefti-Meziani, and S. Davis, “Variable stiffness Mckibben muscles with hydraulic and pneumatic operating modes,” *Adv. Robot.*, vol. 30, no. 13, pp. 889–899, Jul. 2016.

[42] T. Sato, “Pneumatic actuators for manipulators,” 5,165,323, 1990.

[43] H. Zheng and X. Shen, “Double-acting sleeve muscle actuator for bio-robotic systems,” *Actuators*, vol. 2,

no. 4, pp. 129–144, 2013.

[44] T. Driver and X. Shen, “Sleeve Muscle Actuator: Concept and Prototype Demonstration,” *J. Bionic Eng.*, vol. 10, no. 2, pp. 222–230, 2013.

[45] T. A. Driver and X. Shen, “Design and control of a sleeve muscle-actuated robotic elbow,” *J. Dyn. Syst. Meas. Control. Trans. ASME*, vol. 136, no. 4, pp. 1–10, 2014.

[46] M. F. Cullinan, E. Bourke, K. Kelly, and C. McGinn, “A mckibben type sleeve pneumatic muscle and integrated mechanism for improved stroke length,” *J. Mech. Robot.*, vol. 9, no. 1, pp. 1–9, 2017.

[47] M. F. Cullinan, C. Mcginn, and K. Kelly, “Sleeve pneumatic artificial muscles for antagonistically actuated joints,” *Proc. - IEEE Int. Conf. Robot. Autom.*, vol. 2019-May, pp. 8360–8366, 2019.

[48] M. Schumm and H. Cruse, “Control of swing movement: Influences of differently shaped substrate,” *J. Comp. Physiol. A Neuroethol. Sensory, Neural, Behav. Physiol.*, vol. 192, no. 10, pp. 1147–1164, 2006.

APPENDIX A – GROUND PRESSURE

Ground pressure is assessed by determining the supporting members contact patch surface area versus the supported mass. The geometry of the robot supporting member is a bent round tube that is designed such that as it sinks into the soil the effective contact patch area increases to a maximum when the penetration depth equals the tube bend radius. The supported mass is determined from the overall device mass constraint and the expected least number of supporting legs in the gait. A framework is required to evaluate if the round tube foot design will provide a sufficiently large enough contact patch to ensure for a given supported mass that the ground pressure remains below the application constraint of 50 kPa.

Assumptions:

1. Mass is a fixed parameter $m_{overall}$, which is supported by a minimum of legs $n_{supporting}$.
2. The contact patch is defined as the external dimension of the tube when sectioned parallel to the ground plane and is defined for any given depth of foot penetration into soft soils. While this contact patch is in reality an elliptical profile, it can be approximated by a rectangular section capped by semicircles on the shorted ends, as shown in the image below.

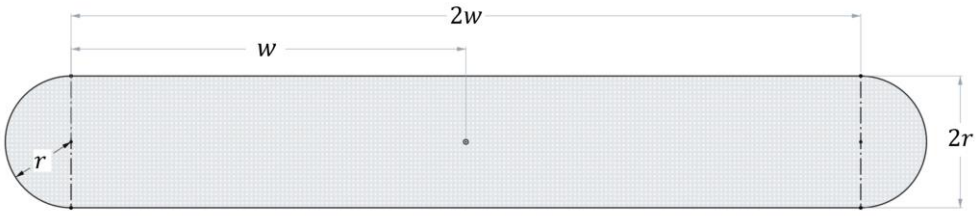

Figure 43 - Plan view of a generalized approximated contact patch for a given penetration depth

The area of the contact patch area, $A_{contact}$, is determined by the following relationship.

$$A_{contact} = \pi\, r^2 + 4rw \qquad [19]$$

This simplifies the analysis and provides sufficient fidelity for conceptual validation. When the depth of penetration d, is zero, the contact patch is at its minimum and is approximated by

a circle of radius r. The contact patch reaches its maximum when the depth of penetration equals the tube bend radius R.

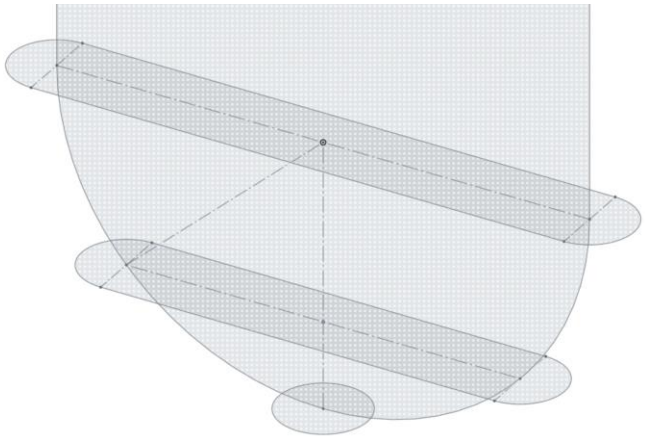

Figure 44 - Isometric view of sectioning estimation, showing the smallest and largest contact patches (bottom and top profiles) and an intermediate (middle profile) against the silhouette of the bent tube leg

The contact patch area can be expressed in terms of the fixed part dimensions, tube outer radius r, tube bend radius R, and the variable parameter penetration depth d by using the geometric relationship shown in the diagram below.

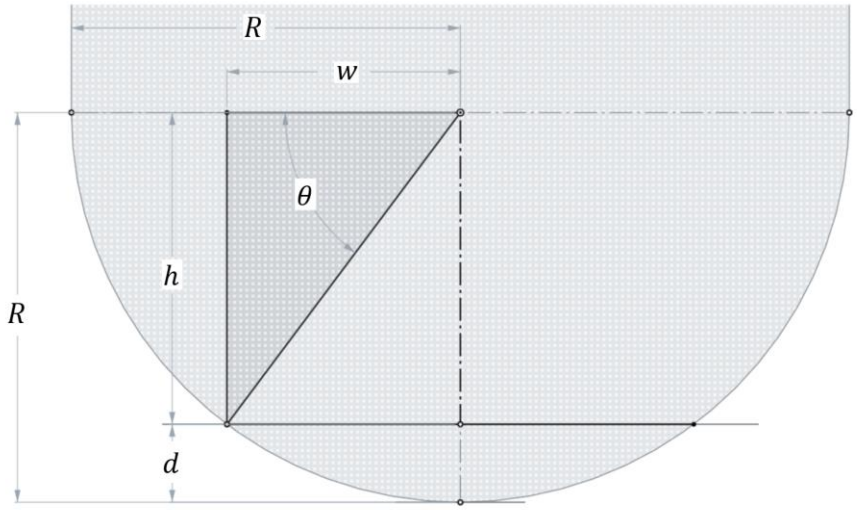

Figure 45 - Front view of the bent tube leg, showing relationship between width of contact patch and penetration depth

$$w = R\cos\theta \quad [20]$$

$$h = R\sin\theta \quad [21]$$

$$h = R - d \quad [22]$$

Combining the three above equations forms an expression for w in terms of the two fixed and one variable parameter.

$$w = R\,cos\left(sin^{-1}\left(1 - \frac{d}{R}\right)\right) \quad [23]$$

Substituting it into the previous expression for contact area results in the following expression.

$$A_{contact} = \pi\, r^2 + 4rR\,cos\left(sin^{-1}\left(1 - \frac{d}{R}\right)\right) \quad [24]$$

The total device mass $m_{overall}$, is determined by summing the components:

$$m_{overall} = m_{thorax} + m_{payload} + n_{legs} \cdot \left(m_{tibia} + m_{femur}\right) \quad [25]$$

Where:

$$\begin{aligned} m_{thorax} &= mass\ of\ the\ thorax \\ m_{payload} &= mass\ of\ the\ payload\ (carried\ at\ the\ thorax) \\ m_{tibia} &= mass\ of\ the\ tibia\ (lower\ leg\ section) \\ m_{femur} &= mass\ of\ the\ femur\ (upper\ leg\ section) \\ n_{legs} &= total\ number\ of\ legs\ for\ the\ device \end{aligned}$$

The applied force for a single leg at the foot $F_{leg,foot}$, is given by:

$$F_{leg,foot} = \left(\frac{m_{overall}}{n_{supporting}}\right) \cdot g \quad [26]$$

Where:

$$\begin{aligned} g &= force\ due\ to\ gravity \\ n_{supporting} &= number\ of\ legs\ supporting\ the\ device\ in\ the\ limiting\ case \end{aligned}$$

Finally, an expression for the ground pressure P_{ground}, in terms of the geometric parameter and the penetration depth is created. This equation is used to evaluate various combinations of tube diameter and bend radius to ensure that the ground pressure is within bounds for a given mass and maximum soil penetration depth constraint.

$$P_{ground} = \frac{F_{leg}}{A_{contact}} \quad [27]$$

$$P_{ground} = \frac{\left(\frac{m_{overall}}{n_{supporting}}\right) \cdot g}{\left(\pi\, r^2 + 4rR\, cos\left(sin^{-1}\left(1 - \frac{d}{R}\right)\right)\right)} \quad \blacksquare \quad [28]$$

APPENDIX B – KNEE JOINT TORQUE

The knee joint and connected antagonistic actuators are required to support the entire mass of the device when only four of the six total legs are ground engaged. To validate the actuator and supporting tendon mechanisms, a relationship between the geometric and mass parameters of the leg module and the supporting knee torque is required.

The leg module is modelled with two masses located at the center of gravity of each of the leg segments, which is assumed to be located at the given leg segment's midpoint. The remaining mass of the robot (thorax, payload and lifted legs) is evenly distributed among the supporting legs and applied directly at the hip joint (point C or E below). This is a reasonable assumption when a symmetric 6-link planar leg configuration is modelled such that the commanded knee angle of all legs, for a device standing on flat and level ground, is identical. The simplified symmetric planar two-leg mechanism, with the thorax constrained as level with the horizon, is shown below.

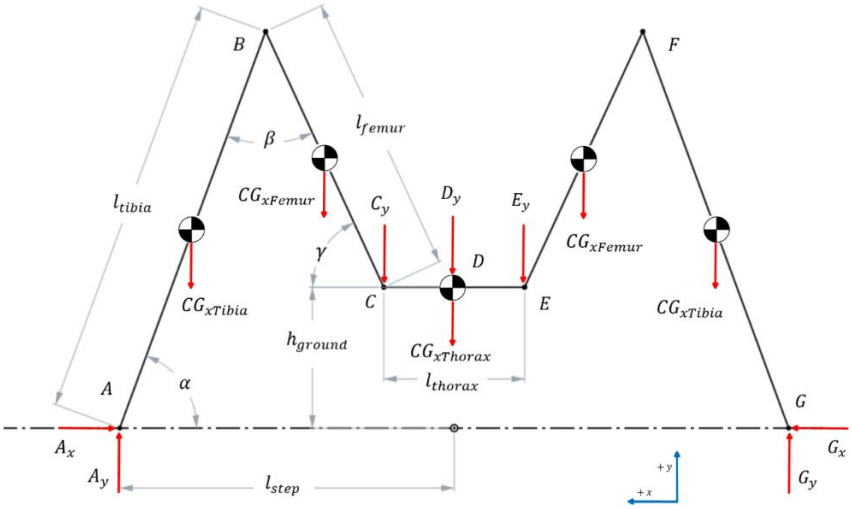

Figure 46 - FBD of the six-link closed actuator linkage, one of three identical pairs

The applied load C_y, due to the combined mass of the thorax, payload and the two raised legs at the hip joint C, is determined as follows:

$$C_y = \left(\frac{m_{thorax} + m_{payload} + (n_{legs} - n_{supporting}) \cdot (m_{tibia} + m_{femur})}{n_{supporting}} \right) \cdot g \qquad [29]$$

The force due to gravity of the two leg segments is defined below.

$$CG_{x,tibia} = m_{tibia} \cdot g \quad [30]$$

$$CG_{x,femur} = m_{femur} \cdot g \quad [31]$$

To determine the moment required to support the thorax, the leg module is modelled as shown below, with a 1DOF revolute (pin) joint at both A and B. Point C is constrained by a control parameter such that it can be modelled as a rolling surface in the y-axis. Restoring forces exist in the x and y-axis at A, but only in the x-axis at C. There is no applied moment at A or C, rather an actuated moment is supplied only via the knee at point B. The FBD for this arrangement is shown below.

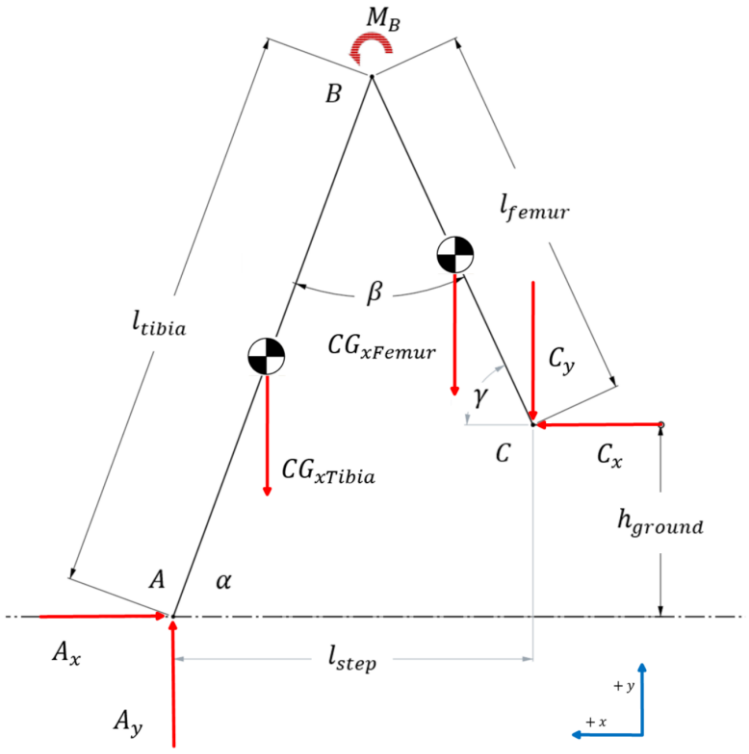

Figure 47 - FBD of a single leg module with pin joints at A and B, and a sliding surface at C such that point C is free to move in the vertical y-axis only

The joint angles are dependent on the lengths of the leg segments l_{tibia}, l_{femur} and the height of the hip joint h_{ground}.

$$\gamma = sin^{-1}\left(\left(\frac{sin\,\alpha}{l_{femur}}\right) \cdot \left(l_{tibia} - \frac{h_{ground}}{sin\,\alpha}\right)\right) \quad [32]$$

Additionally, the three internal angles are related as follows,

$$2\pi = \alpha + \beta + \gamma \quad [33]$$

The equations of static equilibrium are generated for the structure, summing the forces in the x and y-axis and taking the moments about point B, the following system of equations is generated, which can be solved to provide the restoring forces A_x, A_y and C_x. Note that C_y is an applied force, not a restoring force as this joint is modelled as a sliding interface in the y-axis.

$$0 = A_x + C_x \quad [34]$$

$$0 = CG_{x,tibia} + CG_{x,femur} + A_y + C_y \quad [35]$$

$$0 = \left(\frac{l_{tibia}}{2} \cdot cos\,\alpha\right) \cdot CG_{x,tibia} + \left(l_{tibia} \cdot cos\,\alpha + \frac{l_{femur}}{2} \cdot cos\,\gamma\right) \cdot CG_{x,femur} + \left(l_{tibia} \cdot cos\,\alpha + l_{femur} \cdot cos\,\gamma\right) \cdot C_y + h_{ground} \cdot C_x \quad [36]$$

After solving the internal angles for a known knee angle β, the above system of three equations, can be solved for the restoring forces A_x, A_y and C_x.

Once the restoring forces are calculated, the method of sections is used at the knee joint to determine the moment at B required to support the load condition for any value in the range of knee angles. The forces in the x and y-axes are summed and the moments again taken at B, this time with a moment M_B, applied at B. We introduce a normal force N_B and a shear force V_B at B.

$$0 = N_B + C_x \quad [37]$$

$$0 = V_B + CG_{x,femur} + C_y \quad [38]$$

$$0 = M_B + \left(\frac{l_{femur}}{2} \cdot cos\,\gamma\right) \cdot CG_{x,femur} + \left(l_{femur} \cdot cos\,\gamma\right) \cdot C_y + \left(l_{femur} \cdot sin\,\gamma\right) \cdot C_x \quad [39]$$

These three equations, can then be solved together for any given internal knee β, using the outputs from the previous solution for α, γ and C_x, to determine moment M_B, required at B for static equilibrium.

The outputs of the static analysis were used to create a plot of joint torque demand to support the robot mass and its payload across the range of motion of the knee joint. From this set of

data, a third-order polynomial is fit to the data points to provide a continuous function of joint torque to knee angle, for a given geometry and mass distribution.

Next the extension of the HAM was considered across the knee joint range of motion. The actuator is geometrically modelled as a cylinder of length L and diameter D. Wall thickness of the bladder is assumed to be zero and the outer braided threads inextensible. The system constants are the thread length b, the number of turns a single thread makes about the cylinder and the interweave angle θ, between the thread and the longitudinal actuator axis. This relationship is presented below.

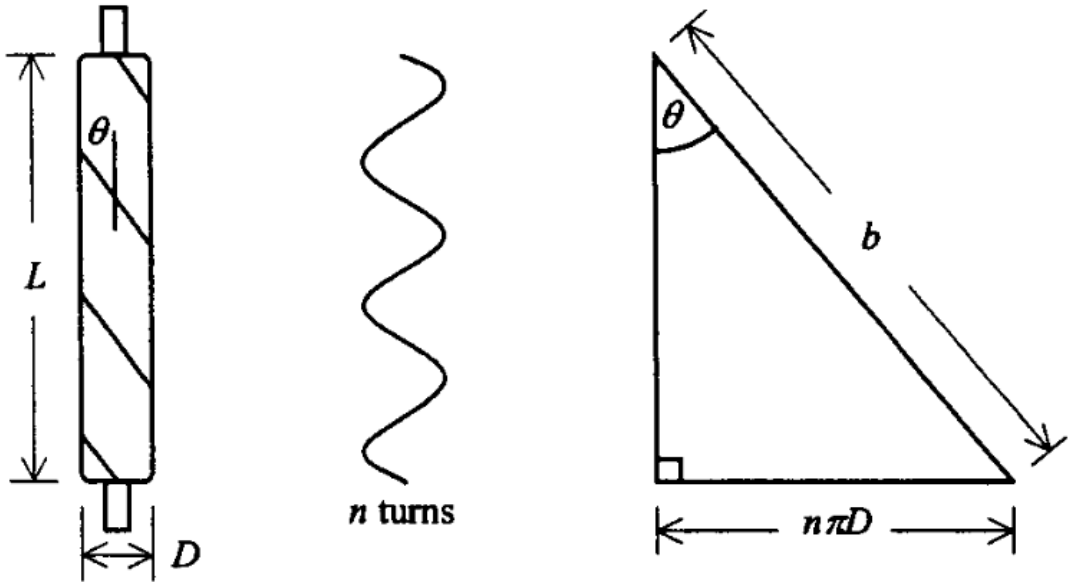

Figure 48 - Geometric relationship of a simple McKibben type actuator. Adapted from Colbrunn [37]

The relationship between the geometric parameters shown above, is given below.

$$L = b\cos\theta \quad [40]$$

$$D = \frac{b\sin\theta}{n\pi} \quad [41]$$

The strain rate of the actuator, ε is defined below, where L_0 is the initial actuator length and L is the contracted length.

$$\varepsilon = \frac{L_0 - L}{L_0} \quad [42]$$

Using the relationship presented by Tondu [38] that expresses an idealized actuator force $F_{actutor,}$ as a function of bladder pressure P and strain rate ε, for a given actuator design with initial sleeve diameter d_0, and initial thread angle θ_0 (typically 20° for most woven sheaths).

$$F_{actutor} = \left(\frac{\pi}{4} \cdot d_0^2\right) \cdot P \cdot \left(\left(\frac{3}{tan{\theta_0}^2}\right) \cdot (1-\varepsilon)^2 - \left(\frac{1}{sin\ {\theta_0}^2}\right)\right) \quad [43]$$

The knee joint is modelled as a pin joint, with a HAM coupled to the axle via a linkage arm of radial length l_{arm}. The critical case is the knee joint supporting the mass of the body. The agonistic actuator that supports this load is modelled across its stroke length and compared to the demand curve generated using the previously described process. The antagonistic actuator provides only enough force to keep the tendon running in the correct path, but without adding any reversing torque to the knee joint.

The relationship of the effective moment arm of the axle linkage is given by the cosine of the knee axle rotation angle φ, with respect to the neutral centerline. The range of pulley motion is between 15 and 105°, to achieve an angular rotation range of 90° and allow for tendon hardware to clear the central axle.

$$l_{leverarm,effective} = l_{arm} \cdot sin\,\varphi \qquad (15° < \varphi < 105°) \quad [44]$$

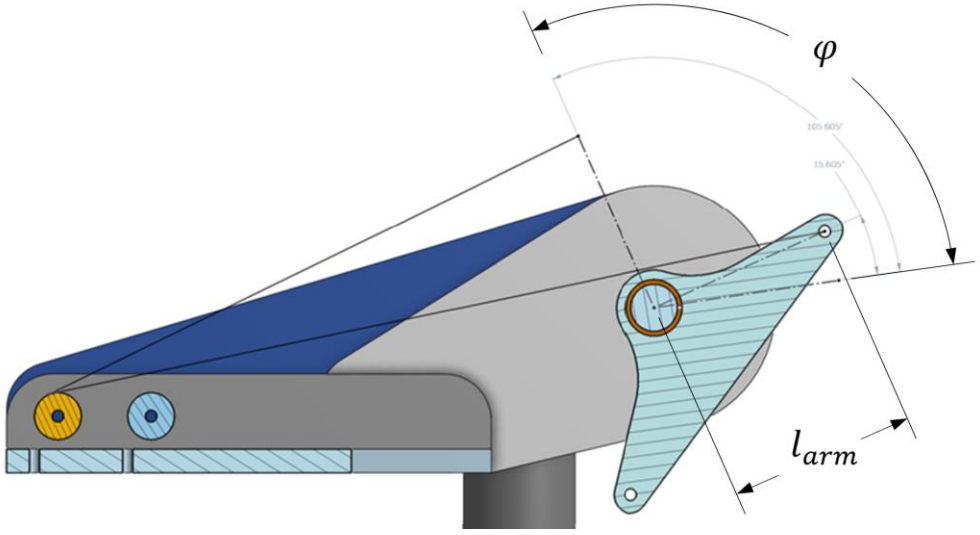

Figure 49 - Knee joint showing range of motion of the lever arm. Angle ψ is shown ranging from 15 to 105°

Practically the range of motion may be limited below this range, for concept validation a simplified relationship between rotation angle and tendon length is modelled as follows;

$$\varphi \cong \beta \qquad (for\ all\ \varphi < 90°) \tag{45}$$

$$(L_0 - L) \cong l_{arm} \cdot cos\,\beta \qquad (0° < \beta < 90°) \tag{46}$$

The available joint torque is given by the following expression.

$$M_B = (l_{arm} \cdot sin\,\beta) \cdot \left(\left(\frac{\pi}{4} \cdot d_0^2 \right) \cdot P \cdot \left(\left(\frac{3}{tan\theta_0{}^2} \right) \cdot (1 - (\varepsilon))^2 - \left(\frac{1}{sin\,\theta_0{}^2} \right) \right) \right) \tag{47}$$

Where:

$$\varepsilon = \frac{l_{arm} \cdot cos\,\beta}{L_0} \qquad (0° < \beta < 90°)\ \blacksquare \tag{48}$$

APPENDIX C – HIP JOINT TORQUE

The spherical hip joint is actuated by four antagonistic HAM's. The knee joint actuators are meant to support the mass load of the robot and the hip joint actuators are primarily used to provide stabilizing torques as well as swing the leg modules laterally to support gait motions. The highest load condition occurs when lifting a leg during a gait step.

The relative tendon motion is determined by the initial geometry and the 3D rotation commanded. The critical geometrical inputs are the radius of the ball and the positions of the tendon insertion and origin points, located on the sphere. The optimal insertion and origin points that provide the maximum joint mobility were determined by of Guckert and Naish [22]. These locations were used to create a similar joint structure for this review.

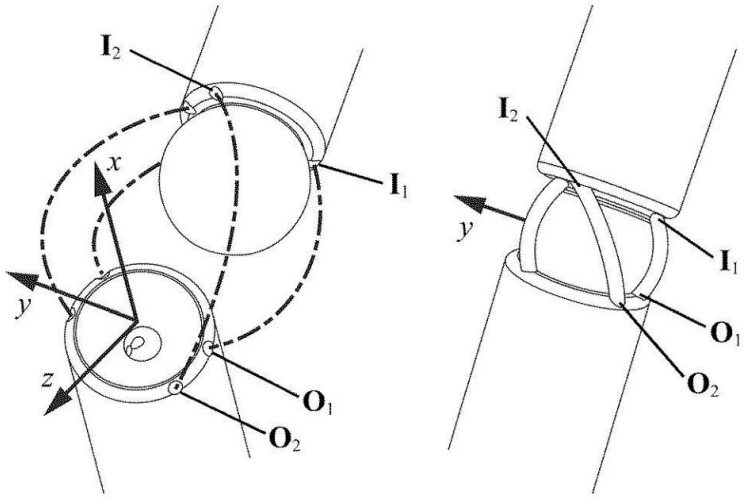

Figure 50 - Compact 3DOF ball and socket joint showing 4 tendons with insertion and origin points. Adapted from Guckert [23]

A hip joint specific co-ordinate system, identical to the arrangement presented by Guckert and Naish, is established at the spherical hip joint, centered on the ball, as shown below.

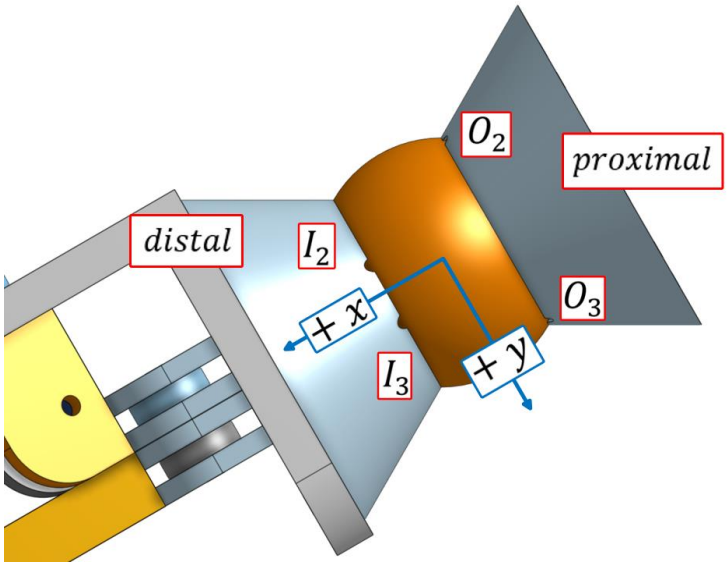

Figure 51 - Cartesian co-ordinate frame with visible insertion and origin points, shown in neutral position which is canted 30 degreed downward in the vertical plane (about the z-axis). Tendons not shown.

Guckert and Naish's optimal origin and insertion points for a ball of radius $r_{gukert} = 3mm$ are shown below. Each column is an xyz cartesian co-ordinate of the points $\boldsymbol{O}_1 - \boldsymbol{O}_4$ and $\boldsymbol{I}_1 - \boldsymbol{I}_4$ respectively.

$$\boldsymbol{O}_{gukert} = \begin{bmatrix} -1.95 & -1.95 & -1.95 & -1.95 \\ -2.55 & -2.55 & 2.55 & 2.55 \\ -1.05 & 1.05 & 1.05 & -1.05 \end{bmatrix} mm$$

$$\boldsymbol{I}_{gukert} = \begin{bmatrix} 1.95 & 1.95 & 1.95 & 1.95 \\ -1.05 & -1.05 & 1.05 & 1.05 \\ -2.55 & 2.55 & 2.55 & -2.55 \end{bmatrix} mm$$

These are normalized by dividing by the scalar radius as follows.

$$\boldsymbol{O}_{norm} = \frac{\boldsymbol{O}_{gukert}}{r_{gukert}} \quad [49]$$

This results in two optimal and normalized sets of insertion and origin points as follows.

$$\hat{\boldsymbol{O}}_{optimal} = \begin{bmatrix} -0.65 & -0.65 & -0.65 & -0.65 \\ -0.85 & -0.85 & 0.85 & 0.85 \\ -0.52 & 0.52 & 0.52 & -0.52 \end{bmatrix}$$

$$\hat{\boldsymbol{I}}_{optimal} = \begin{bmatrix} 0.65 & 0.65 & 0.65 & 0.65 \\ -0.52 & -0.52 & 0.52 & 0.52 \\ -0.85 & 0.85 & 0.85 & -0.85 \end{bmatrix}$$

Joint motion is defined by a zyx fixed-angle rotation matrix $\boldsymbol{R}$, representing the 3DOF rotation of the moving frame (distal, with insertion points $\boldsymbol{I}$) with respect to the fixed frame (proximal, with origin points $\boldsymbol{O}$), where the *x*-axis is aligned with central axis of the fixed frame with the angles of rotation around *z, y* and *x.*

The exposed length between the origin and insertion points of the n^{th} tendon is calculated for a given joint geometry and rotation using the following relationship.

$$L_n = r \cdot \arccos\left(\boldsymbol{R}\hat{\boldsymbol{I}}_{n,optimal} \cdot \hat{\boldsymbol{O}}_{n,optimal}\right) \quad [50]$$

Where L_n is the length of a tendon running across the sphere surface, r is the radius of the sphere, and $\hat{\boldsymbol{I}}_{n,optimal}$ and $\boldsymbol{O}_{n,optimal}$ are the n^{th} column of the $\hat{\boldsymbol{I}}_{optimal}$ and $\hat{\boldsymbol{O}}_{optimal}$ 3 x 4 matrices, respectively . The proximal motion, h_n, of the n^{th} tendon away from the fixed frame, for a given initial and final orientation of the joint, is described by the following expression.

$$h_n = L_{n,initial} - L_{n,final} \quad [51]$$

Additionally, the vector of torques, $\boldsymbol{\tau}_n$, generated by the n^{th} tendon about the fixed frame can be determined as follows.

$$\boldsymbol{\tau}_n = t_n \left(\boldsymbol{R}\hat{\boldsymbol{I}}_{n,optimal} \times \hat{\boldsymbol{O}}_{n,optimal}\right) \quad [52]$$

Where, t_n is the tension in the n^{th} tendon, and $\boldsymbol{\tau}_n$ is the vector of torques generated by the n^{th} tendon about the fixed frame, using the n^{th} column of the $\hat{\boldsymbol{I}}_{optimal}$ and $\hat{\boldsymbol{O}}_{optimal}$ 3 x 4 matrices, relating to the n^{th} tendon under review. From these relationships, the following algorithm was used to calculate the actuator position, tendon loads and overall joint torque for a series of known leg poses that represent start (PEP), intermediate (SEP) and end positions (AEP) of the basic gait.

1. Set the co-ordinate system, determine joint poses and torque use case
2. Determine the fixed angle rotation matrix required for the pose ($\boldsymbol{R}$)
3. Determine the relative tendon motions from the neutral pose ($\boldsymbol{h}$)
4. Determine the actuator strain rate and dimensions (ε, D)
5. Calculate the tendon tensions to achieve the required joint torque ($\boldsymbol{\tau}_n$)

6. Calculate the required actuator pressures (P) to achieve the required tension

For the limiting case when the hip joint must support the entire mass of the leg, the applied torque is considered as a positive moment about the z-axis only.

$$\boldsymbol{M}_C = \begin{bmatrix} M_{x,C} \\ M_{y,C} \\ M_{z,C} \end{bmatrix} \quad [53]$$

$$\boldsymbol{M}_{C,leg\ lift\ case} = \begin{bmatrix} 0 \\ 0 \\ M_{z,C,leg\ lift\ case} \end{bmatrix} \quad [54]$$

This moment is a result of force due to gravity of the tibia and femur, applied at the segment midpoints, at a distance given by the joint pose, as shown below.

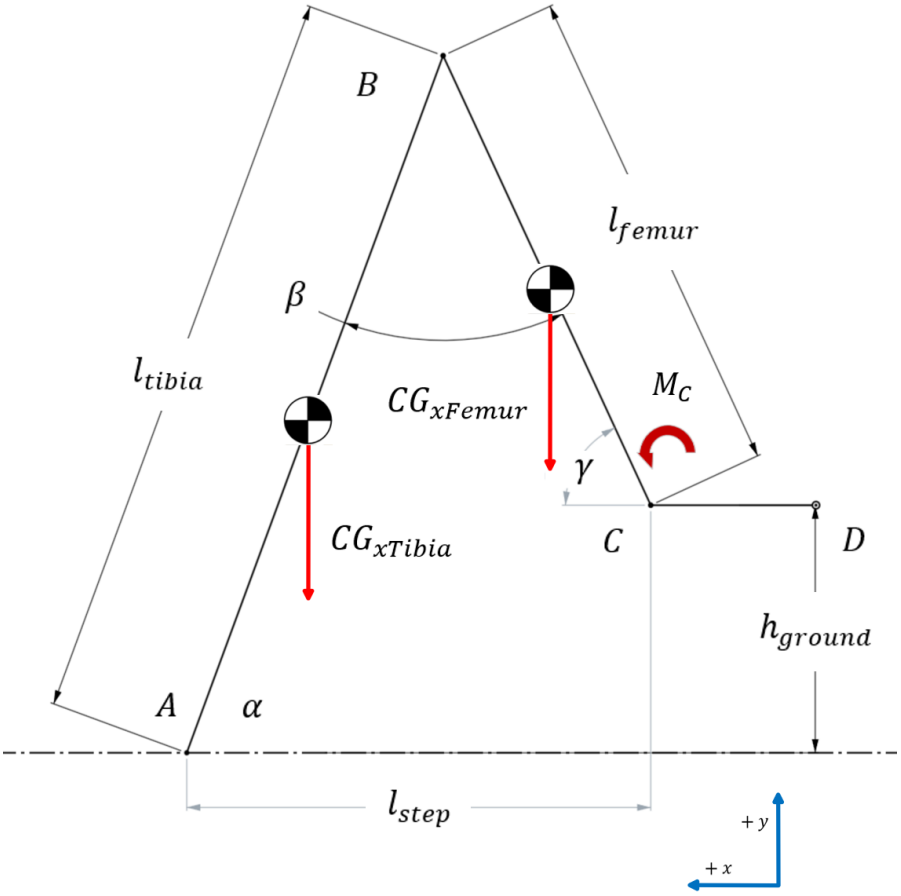

Figure 52 - FBD of a single leg module during a leg lift event. A moment about the z axis is generated in the hip joint at C from the force due to gravity at the center of gravity of the two leg segments.

This moment is required to support the leg in this configuration and is shown below.

$$M_{z,C,leg\ lift\ case} = \left(\frac{l_{femur}}{2} \cdot cos\,\gamma\right) \cdot CG_{x,femur} + \left(l_{femur} \cdot cos\,\gamma + \frac{l_{tibia}}{2} \cdot cos\,\alpha\right) \cdot CG_{x,tibia} \blacksquare \quad [55]$$

APPENDIX D – FLUID CONSUMPTION RATE

To determine the consumption rate of the device for a given gait, the various poses of the leg are determined for a full cycle. There is motion at the knee joint, as well as rotation about the hip joint. A simplified gate comprised of three poses is used, which assumes negligible clearance of the foot during the free swing motion. Where the arc PEP-SEP-AEP, shown in the image below, is approximated as a straight line, in both forward and reverse directions.

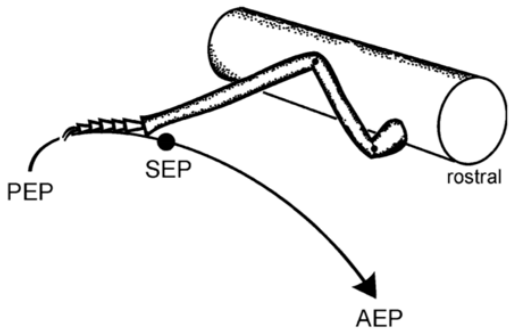

Figure 53 - Schematic of leg morphology showing PEP: posterior extreme, SEP: swing extreme position, and AEP: anterior extreme positions. Adapted from Schumm [48]

The consumption rate is determined by:

1. Determine the leg poses required to complete a full stepping cycle
2. Determine the joint angles (knee and hip) for each of the leg poses
3. Determine the six actuator displacements/strain rates for each pose
4. Calculate the six actuator volumes for each pose
5. Determine the differential volume between each pose for each actuator
6. Sum the volume of fluids ***added*** to each of the six actuators throughout the cycle
7. Multiply this per leg cycle volume by the number of legs ($q_{cycle,robot}$)

This algorithm generates a total flow to all the actuators on the entire robot to complete one full leg cycle, which results in a distance travelled determined from the leg geometry (l_{femur} and l_{tibia}), height of the thorax above ground (h_{ground}) and joint angles at PEP and AEP.

Fluid flow rate is calculated as follows:

$$\dot{q} = \frac{q_{cycle,robot}}{z_{cycle,robot}} \cdot \dot{z}_{robot} \qquad [56]$$

Where:

$$\dot{q} = volume\ flow\ rate\ of\ robot$$
$$q_{cycle,robot} = total\ actuator\ volume\ demand\ per\ step\ cycle$$
$$z_{cycle,robot} = total\ distance\ travelled\ in\ the\ horizontal\ z\ direction\ per\ step\ cycle$$
$$\dot{z}_{robot} = travel\ speed\ in\ the\ horizontal\ z\ direction \quad \blacksquare$$

APPENDIX E – DIMENSIONAL DRAWINGS

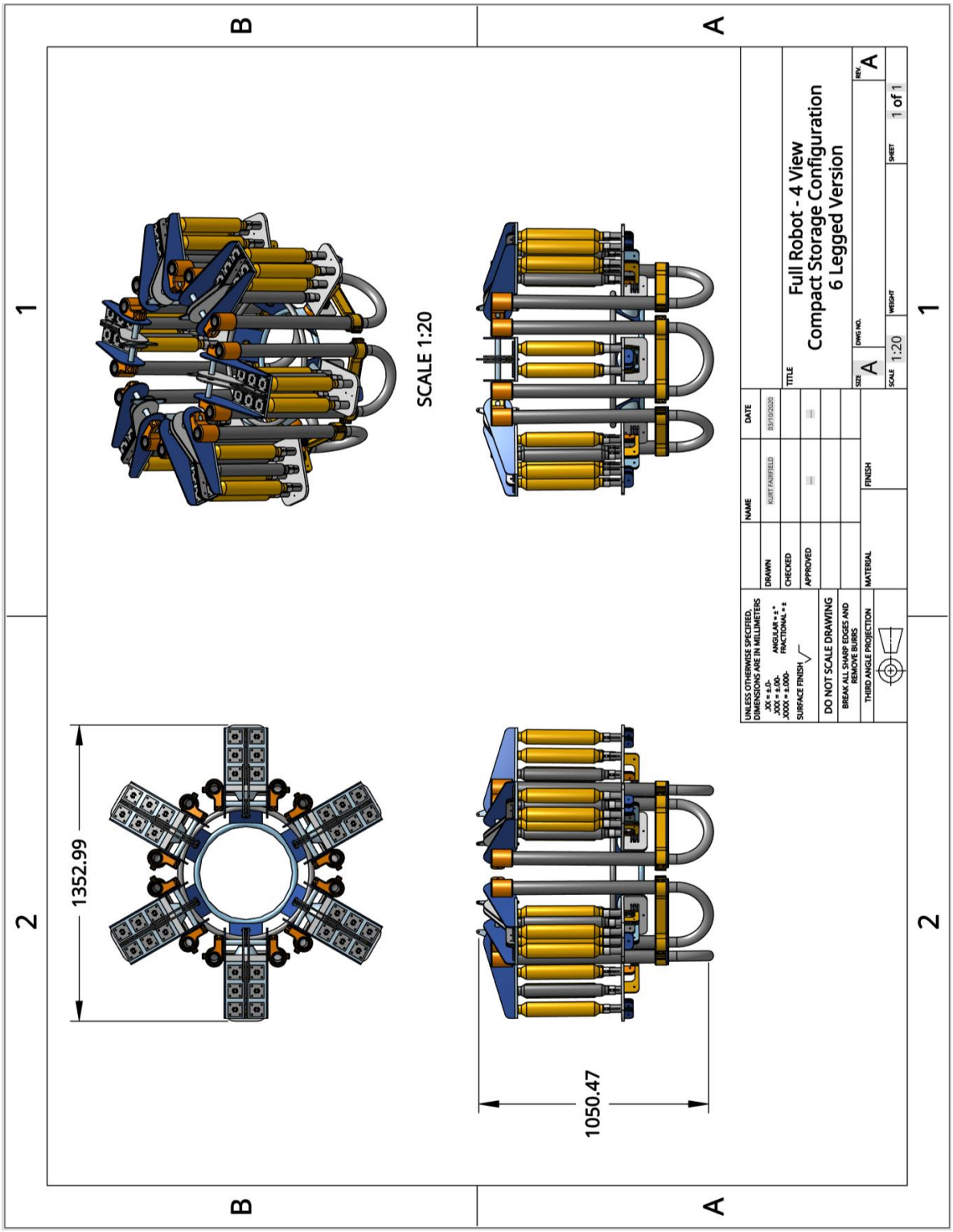

Figure 54 - 4 view drawing of full robot in compact storage configuration, showing maximum envelope dimensions

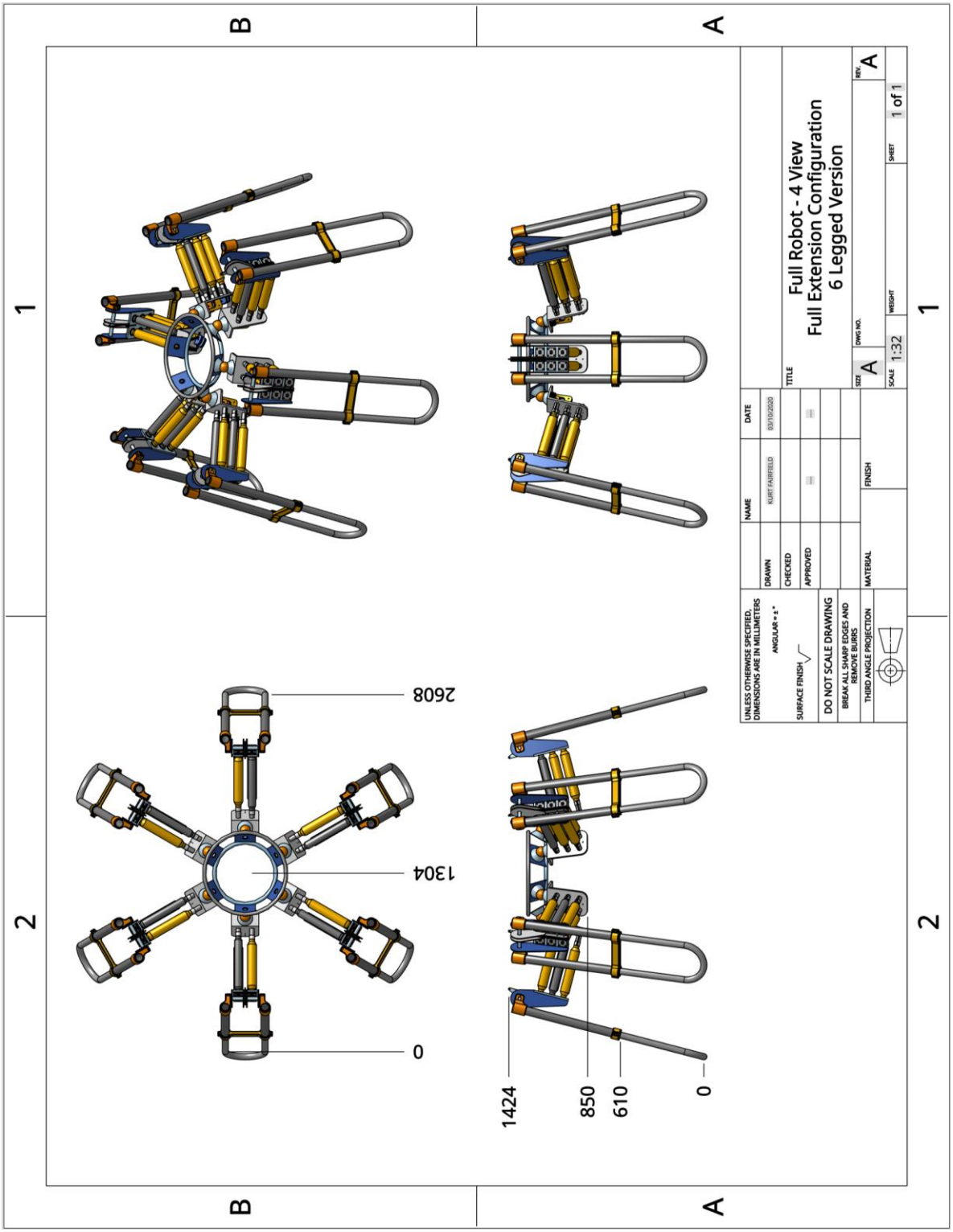

Figure 55 - 4 view drawing of full robot in full extension configuration, showing maximum envelope dimensions

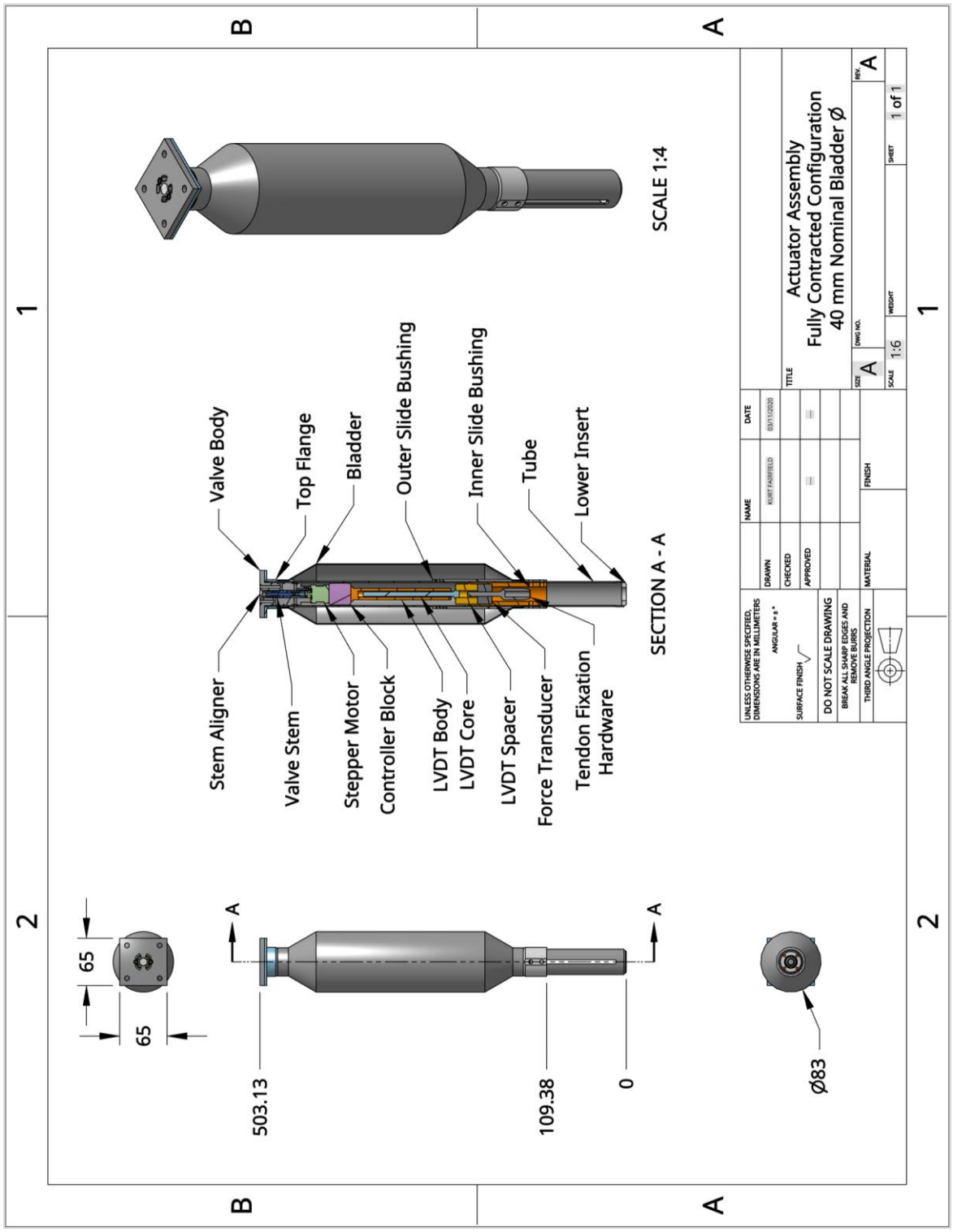

Figure 56 - 4 view drawing of actuator assembly with labelled section view